TWO-DIMENSIONAL INFLATED BUILDINGS IN A CROSS WIND

BY

D. GOLAND

A Thesis submitted to the Faculty of Graduate Studies and Research in partial fulfillment of the requirements for the degree of Master of Engineering.

Department of Mechanical Engineering

McGill University

Montreal, Quebec, Canada

March, 1980

SUMMARY

The purpose of this work was to investigate the behaviour of long quasi-two-dimensional inflated buildings in a cross wind. The study was both theoretical and experimental.

A numerical solution based on ideal-flow theory was developed. A streaming flow of uniform vorticity was superimposed on a surface distribution of sources and sinks, and the shape of the surface was corrected in an iterative manner to satisfy pressure — tension equilibrium of the membrane forming the building. The theoretical streaming flow was then matched to a wind velocity profile as represented by a power law.

The experimental work included wind-tunnel measurements at model scale of tension in the membrane, external pressure distribution, flow separation and reattachment, and model stability, for a wide range of inflation pressures, for various height-to-chord ratios, and for two different wind profiles.

Comparison was made between the theoretical and the experimental results. The comparison gave good agreement for the tension, and in the case of low buildings, good agreement for the pressure distribution. It is concluded that the results are useful as an aid in designing inflated buildings subjected to a cross wind.

RÉSUMÉ

Le but de ce travail était d'étudier le comportement de bâtiments longs, gonflés presque bidimensionels soumis à des vent transversaux. L'étude a été à la fois théorique et expérimentale.

On a établi une solution numérique fondée sur la théorie de l'écoulement d'un fluide parfait. On a superposé un écoulement à vecteur tourbillon constant à une répartition superficielle des sources et des puits, la forme de la surface étant évaluée par itérations de façon à satisfaire aux conditions d'équilibre des forces de pression et de tension de la membrane composant le bâtiment. On a ensuit déterminé l'écoulement théorique de façon à obtenir un profil de vitesse du vent représenté par une fonction puissance.

Les essais incluaient des mesures en soufflerie, à l'échelle du modèle, de la tension de la membrane, de la distribution de la pression extérieure, des points de séparation et de réattachement de l'écoulement ainsi que la stabilité de modèle, pour une gamme étendue de pressions de gonflage, pour divers rapports hauteur - corde, et pour deux différents profile de vitesse du vent.

La comparaison des résultats théoriques et expérimentaux est bonne pour la tension, ainsi que la disribution de la pression dans le cas des édifices des faible hauteur. Il s'ensuit que les résultats peuvent être utilisés pour aider à la conception de bâtiments gonflés assujettis à des vents transversaux.

ACKNOWLEDGEMENTS

I would like to express my gratitude to Professor B.G. Newman for initiating this project and for providing helpful guidance, encouragement and constructive criticism throughout the course of this work.

I also thank Mr. J. Dubik for the construction of the experimental apparatus and for many practical suggestions concerning its operation, and Mr. G. Dedic for his help with the operation of the instrumentation.

This work was supported financially by the Natural Science and Engineering Research Council, grant number A-7096 awarded to Prof. B.G. Newman.

TABLE OF CONTENTS

	Page
SUMMARY	i
RÉSUMÉ	ii
ACKNOWLEDGEMENTS	iii
TABLE OF CONTENTS	iv
NOMENCLATURE	vi
1. INTRODUCTION	
1.1 PNEUMATIC STRUCTURES	1
1.2 AIR STRUCTURE DEVELOPMENT	1
1.3 PREVIOUS WORK ON WIND LOADS	2
1.4 TWO-DIMENSIONAL INFLATED BUILDINGS	3
1.5 THE PRESENT WORK	4
2. THEORY	
2.1 THE PROBLEM	5
2.2 DIMENSIONAL ANALYSIS	5
2.3 IDEALIZATION OF THE PROBLEM	7
2.4 A TWO-DIMENSIONAL RIGID BODY IN A FLOW	11
2.5 A FLEXIBLE BODY IN A FLOW	24
3. EXPERIMENTS	
3.1 GENERAL DESIGN OF THE EXPERIMENTS	28
3.2 EXPERIMENTAL APPARATUS	29
3.3 CHECKS AND CALIBRATIONS OF THE APPARATUS	35
3.4 EXPERIMENTAL PROCEDURE	38
3.5 MEASUREMENT ERRORS	41

Page

4. RESULTS AND DISCUSSION

4.1 THEORETICAL RESULTS 45

4.2 EXPERIMENTAL RESULTS 47

4.3 COMPARISON BETWEEN THEORY AND EXPERIMENT 53

5. CONCLUSIONS

5.1 EVALUATION OF THE RESULTS 58

5.2 PRACTICAL USE OF THE RESULTS 59

5.3 SUGGESTION FOR FURTHER WORK 60

REFERENCES 61

APPENDIX I Approximation of a Power Low Profile by a Streaming Flow of a Uniform Vorticity 64

APPENDIX II The Computer Program 66

APPENDIX III Design of the Spires 77

TABLES

FIGURES

PLATES

NOMENCLATURE

a	The inverse of the slope of a uniform-shear onset-flow.
A_{ij}	Matrix of coefficients of influence: outward-normal-velocity.
c	Building chord length: the building width.
C_d	Drag coefficient of a two-dimensional plate.
C_f	Local skin friction coefficient = $df/\frac{1}{2}\rho U^2 ds$.
C_F	Total skin friction coefficient = $f/\frac{1}{2}\rho U^2 \ell$.
C_{Ph}	Inflation pressure coefficient = $(P-p_\infty)/\frac{1}{2}\rho U^2$.
C_{Th}	Tension coefficient = $T/\frac{1}{2}\rho U_h^2 c$.
C_{ps}	External pressure coefficient = $(p-p_\infty)/\frac{1}{2}\rho U_s^2$.
C_{Ts}	Tension coefficient = $T/\frac{1}{2}\rho U_s^2 c$.
$C_{p\tau}$	External pressure coefficient = $(p-p_\infty)/\frac{1}{2}\rho U_\tau^2$.
C_{p_τ}	Inflation pressure coefficient = $(P-p_\infty)/\frac{1}{2}\rho U_\tau^2$.
$C_{T\tau}$	Tension coefficient = $T/\frac{1}{2}\rho U_\tau^2 c$.
d	Spacing between spires.
f	Skin friction force per unit span.
F	Horizontal force acting on a pair of flexures.
h	Height of the building.

$\hat{i}$	Unit vector in the x direction.
$\hat{j}$	Unit vector in the y direction.
k_s	Equivalent sand roughness.
k_1	Hot wire longitudinal correction coefficient.
K	Local drag coefficient of a spire.
K_1	Coefficient of pressure drop across a row of spires.
ℓ	Membrane length from leading to trailing edge.
L	Span of the building.
n	The inverse of the power of the wind profile (=1/α).
$\bar{n}$	A unit vector pointing outwards.
N	Number of discretization points.
p	Local external pressure acting on the building.
Pa	Pressure upstream of spires.
p_∞	Atmospheric pressure.
P	Inflation pressure.
q	A point on a closed surface.
r	Distance from a source or a sink.
R	Local radius of curvature of the membrane.
Re	Reynolds number = $U_e \ell/\nu$.
Re_τ	Reynolds number = $U_\tau c/\nu$.
R_1, R_2	Distance of flow reattachment points from the model edge (Fig. 4).
s	Coordinate along the membrane.
S	Local ratio of solid area of spire to the total area.
S_1, S_2	Distance of flow separation points from the model edge (Fig. 4).

T	Tension per unit span in the membrane.
u	Velocity in the x direction.
u_e	Velcoity in the x_e direction.
u'	Fluctuation in the x direction of a turbulent flow.
U	Local velocity of a wind in the x direction.
U_a	Wind tunnel velocity upstream of the spires.
U_e	Free stream velocity.
U_s	A theoretical slip velocity at ground level for the uniform vorticity flow.
U_h	Approaching velocity at the top of the building.
U_τ	Skin friction velocity of the boundary layer.
U_{10}	Wind velocity at a height of 10 m above the ground.
v	Velocity in the y direction.
v'	Fluctuation in the y direction of a turbulent flow.
v_e	Velocity in the y_e direction.
$\bar{v}$	A disturbance velocity.
V	Onset flow in the y direction.
$\overline{V}$	Velocity field.
$\overline{V}_i$	Local velocity at the surface.
$\overline{V}_{ij}$	Velocity induced by the i-th element at the j-th element.
$\overline{V}_\infty$	Onset flow field.
w	Weight per unit area of the membrane material.
W	Local width of a spire.
x	Coordinate along the chord of the building profile.
x_e	Coordinate parallel to a surface element.

y	A coordinate in the vertical direction.
y_e	A coordinate normal to a surface element.

Greek Symbols

α	The power of a power-law wind-profile (=1/n).
β	~~A variable in the~~ onset-flow profile-~~matching (=h/a).~~
δ	Boundary layer thickness.
θ	Leading or trailing edge angle.
ν	Kinematic viscosity.
ρ	Density of air.
σ	Source-sink distribution intensity per unit length.
τ_w	Wall shear stress.
ϕ	Potential function.
ψ	Stream function.
ω	Vorticity component normal to the x and y plane.

1. INTRODUCTION

1.1 PNEUMATIC STRUCTURES

A pneumatic or air structure consists of a flexible membrane which may form a complete surface, such as a balloon, or a partial surface attached to a rigid frame or base, such as an inflatable building. The membrane assumes its shape and tension due to the action of the pressure of a fluid, pressure which may be of a static or of a dynamic nature or both.

In nature structures occur in animals which might be described as pneumatic structures. Examples are the wings of bats and insects, and, more generally, lungs and air sacks.

1.2 AIR STRUCTURE DEVELOPMENT

Man-made structures such as sails, kites and floats made from inflated animal skins are mentioned in very early recorded history. Whereas for most of man's history the technology of air-structures remained restricted to these examples, in the sixteenth century new ideas began to emerge: a wind wheel with flexible surfaces to catch the wind, the parachute, and later on, the balloon.

In 1783 the first hot air balloon, made by the Montgolfier brothers, rose in the air over France. Hydrogen balloons and flexible airships soon followed. By the twentieth century the technology of producing flexible impervious membranes was well developed.

In 1917 the British engineer, F.W. Lanchester, obtained a patent for his design of an inflatable building, a multi-purpose tent that was made of a flexible surface supported soley by compressed air (ref. 1). In his survey on tensile structures Otto (ref. 2) investigated the membrane theory and the construction of pneumatic structures. Actual production of inflatable buildings on a large scale began after World War II, first by Walter Bird in the United States, and later by many firms, such as Birdair, Schjeldahl, Irving, U.S. Rubber, Goodyear, Texair, Stromeyer, Krupp, Seattle Tent and Awning, and CID Air Structures (ref. 2).

An international symposium on pneumatic structures was held in Stuttgart, Germany in 1967, and a second one in Delft, Netherlands in 1972.

The wide variety of uses for inflatable buildings, their relatively low cost, their light weight and ease of erection made them popular among architects and construction engineers for the design of structures such as exhibition pavilions, temporary shelter for outdoor workers, and covers for athletic events.

1.3 PREVIOUS WORK ON WIND LOADS

When wind blows over an inflated building, it affects the external pressure, which may result in changes in the membrane tension and also possibly in the shape.

Wind tunnel tests for a spherical building were conducted in 1956 (ref. 3), and the pressure distribution, drag and lift forces

were measured. In 1967 E. Berger and E. Macher (ref. 4) presented their results of wind tunnel measurements of pressure distribution for various values of internal/stagnation pressure ratios on spherical and cylindrical models. The cylindrical model was three-dimensional with an aspect ratio of L/c=3. It was a semi-cylinder with quarter spheres attached to its ends. H.J. Niemann (ref. 5) reported in 1972 pressure distribution measurements for different buildings for a full range of wind velocity at both cross and angular flow.

A theoretical solution for design use, and results of tests on shallow cylindrical model buildings in uniform flow were presented in 1979 by B.G. Newman and M.-C. Tse (ref. 6). The tests were done on an inflated lenticular aerofoil which could represent such buildings.

In all these investigations the earth's boundary layer was not correctly represented.

1.4 TWO-DIMENSIONAL INFLATED BUILDINGS

For long buildings it is attractive to consider the possibility of assuming that they may be treated as quasi two-dimensional when in a cross wind.

Such a two-dimensional cylindrical inflated building, with no wind load, assumes the shape of a circular arc. The difference between the internal pressure and the external pressure, which are both uniform, is balanced by the tension in the membrane. When wind blows over the building, the internal pressure remains uniform, but the external pressure does not. This causes the shape of the

building, as well as the tension in it, to change. The new shape causes a new external pressure distribution and so on, till the building assumes a shape and tension that are in equilibrium with the pressure distribution.

1.5 THE PRESENT WORK

Experiments were made on two-dimensional models of inflated buildings, immersed in a thick boundary layer. The flow was at a right angle to the building and simulated the earth's boundary layer.

Two different wind profiles were represented in the experiments. It was intended that flow over countryside and over sparsely wooded country would be simulated, but it turned out that the first case more accurately represented flow from open sea. The wind profiles were generated in a wind tunnel using spires and appropriate roughness as artificial boundary layer thickeners.

The models tested ranged between 0.18 and 0.33 height-to-chord ratio and were inflated with a wide range of pressures.

The measurements included membrane tension, external pressure distribution, flow separation and reattachment, and observations of model stability for low inflation pressures.

An idealized theoretical solution was devised to predict the experimental data. The solution is based on potential flow theory. A streaming flow of uniform vorticity was superimposed on the flow field of a surface source and sink distribution, and the shape of the surface was corrected in an iterative manner to satisfy pressure -- tension equilibrium.

2. THEORY

2.1 THE PROBLEM

The purpose of the theory is to predict the behaviour of a quasi-two-dimensional cylindrical inflatable building in a cross wind where, because of the boundary layer structure of the wind, the flow may separate.

The tension in the membrane forming the building is of considerable practical importance and clearly must not exceed the failing strength of the material. It depends on the membrane length ℓ, the building width in the wind direction c, the inflation gauge pressure $P-p_\infty$, and the wind velocity profile. The latter is sufficiently well represented by a power law profile (Fig. 1a, ref. 7).

$$\frac{U}{U_e} = \left(\frac{y}{\delta}\right)^{1/n} \tag{1}$$

2.2 DIMENSIONAL ANALYSIS

The tension T at a particular position s, measured from the leading edge along the membrane, depends on ℓ, c, $P-p_\infty$, a velocity characteristic of the wind, the power 1/n (eq. 1) which is determined by the terrain, and the air density ρ and kinematic viscosity ν. The characteristic velocity was chosen to be the skin friction velocity U_τ, which is defined as $U_\tau = \sqrt{\tau_w/\rho}$, where τ_w is the wall

shear stress. This is a characteristic velocity for the present problem, since a typical inflated building, having a height of about 1/30 of the average earth's boundary layer thickness (ref. 1, 7), is well within the law of the wall region of the boundary layer where phenomena are characterized by the skin friction velocity rather than by the free stream velocity U_e or the boundary layer thickness δ.

The preceding concept can be summarized as follows:

$$T = f(\ell,\ c,\ P-p_\infty,\ n,\ U_\tau,\ \rho,\ \nu,\ s,\ w) \tag{2}$$

where w is the weight per unit area of the material of the membrane. The tension does not depend on the mass of the material as such, because oscillations of the membrane are not being considered.

There are 9 independent parameters and 3 basic units that determine T, there are therefore 6 non-dimensional criteria for the problem.

Non-dimensionalization of eq. (2) gives

$$\frac{T}{1/2\rho U_\tau^2 c} = f\left(\frac{\ell-c}{c},\ \frac{P-p_\infty}{1/2\rho U_\tau^2},\ n,\ \frac{cU_\tau}{\nu},\ \frac{s}{\ell},\ \frac{w}{P-p_\infty}\right) \tag{3}$$

The tension becomes a tension coefficient $C_{T\tau}$

$$C_{T\tau} = \frac{T}{1/2\rho U_\tau^2 c} \tag{4}$$

The subscript τ indicates that U_τ has been used. Later on other velocities are chosen to define the coefficients. The inflation pressure becomes an inflation pressure coefficient

$$C_{p\tau} = \frac{P-p_\infty}{1/2\rho U_\tau^2} \tag{5}$$

and ν appears in a Reynolds number Re_τ which is associated with the problem. Eq. (3) may be rewritten as

$$C_{T_\tau} = f(\frac{\ell-c}{c},\ C_{p_\tau},\ n,\ Re_\tau,\ \frac{s}{\ell},\ \frac{w}{p-p_\infty}) \qquad (6)$$

Also the external pressure distribution p is reduced to a form of a non-dimensional coefficient based on U_τ

$$C_{p_\tau} = \frac{p-p_\infty}{1/2\rho U_\tau^2} \qquad (7)$$

2.3 IDEALIZATION OF THE PROBLEM

Several assumptions are now made to idealize the problem so that a theoretical solution can be obtained.

2.3.1 The Effect of the Membrane Weight on the Tension

The purpose of this section is to investigate whether the effect of the weight of the membrane may be neglected. Stationary conditions are assumed, i.e. no wind is blowing. Consider an element of the membrane

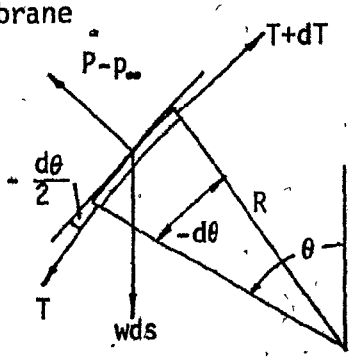

Resolving forces in the normal direction gives

$$(P-p_\infty)\ R\ d\theta = T\ \frac{d\theta}{2} + (T+dT)\ \frac{d\theta}{2} + wR\cos\theta d\theta$$

and the tangential component gives

$$-wR \sin\theta d\theta = dT$$

Neglecting terms of the second order of smallness in the equation for the normal direction and solving for T gives

$$\frac{T_0}{T_1} = \frac{1 - \frac{w}{P-p_\infty}\cos\theta}{1 - \frac{w}{P-p_\infty}}$$

where T_1 and T_0 are the tension per unit span at the leading edge and the top of the membrane respectively.

For the present model scale building $w = 0.245\ N/m^2$ and $P-p_\infty = 30$ Pa so that $w/(P-p_\infty) = 0.008$. For full scale buildings thicker materials are needed and w ranges from 2.0 to 11.8 N/m^2 but $P-p_\infty$ is about 250 Pa so that $w/(P-p_\infty)$ ranges from 0.008 to 0.047.

For $\theta = 60^0$, T_1/T_0 ranges between 1.004 and 1.025 and therefore the change of T along the membrane due to the effect of the weight of the membrane usually may be neglected.

2.3.2 The Effect of the Wind Friction on the Tension

In this section the possibility that the wind friction may be neglected is investigated.

Again consider an element of the membrane.

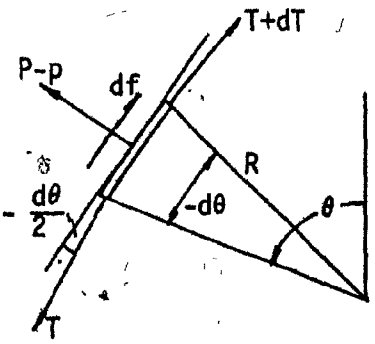

Resolving the forces in the normal direction gives

$$(P-p)\ R\ d\theta = T\ \frac{d\theta}{2} + (T + dT)\ \frac{d\theta}{2}$$

and the tangential component gives

$$df = -\cos\left(\frac{d\theta}{2}\right)\ dT$$

Also

$$df \simeq C_f\ 1/2\ \rho U^2 R d\theta$$

where C_f is the local skin friction coefficient. Neglecting terms of the second order of smallness and assuming that $P-p_\infty$ is of the same order of magnitude as the dynamic pressure, the three equations result in

$$-C_f\ d\theta \simeq \frac{dT}{T}$$

In order to integrate the equation approximately, C_f is replaced by the average skin friction coefficient C_F. Thus the total change in T between leading and trailing edges is

$$\frac{T_2}{T_1} \simeq \exp(-C_F\theta)$$

where T_1 is the tension at the leading edge, and T_2 is the tension at the trailing edge.

For an angle of 1 radian with $C_F = 0.005$, $T_1/T_2 = 1.005$, so that the change in T is very small and may be neglected.

The variation of T along the membrane length with s is caused by the weight of the membrane and by the skin friction. Since they are both neglected, s/ℓ is eliminated from eq. (6).

2.3.3 Assumption of Inviscid Flow

At this point, an assumption is made that the flow is inviscid. Together with the results of sections 2.3.1 and 2.3.2, the conclusion is that eq. (6) may be rewritten as

$$C_{T\tau} = C'_{T\tau}\left(\frac{\ell - c}{c},\ C_{P\tau},\ n\right) \tag{8}$$

To compensate to some extent for the elimination of the boundary layer due to the assumption of inviscid flow, an inviscid streaming flow with a non-uniform profile was used as follows.

2.3.4 Idealization of the Boundary Layer Profile

Instead of the power law profile (eq. 1), a uniform vorticity profile (eq. 9) was matched to the actual profile (Fig. 1, and see section 2.4.2 and Appendix I). This is in order to allow the use of superposition, as will be described in 2.4.1.1.

$$\frac{U}{U_s} = 1 + \frac{y}{a} \tag{9}$$

where U_s is a slip velocity at $y = 0$ and U_s/a is the vorticity.

For the idealized onset flow profile, it is appropriate to base the non-dimensional coefficients on U_s rather than on U_τ, therefore the following coefficients are defined:

Tension coefficient

$$C_{Ts} = \frac{T}{1/2\rho U_s^2 c} \tag{10}$$

Inflation pressure coefficient

$$C_{Ps} = \frac{(P - p_\infty)}{1/2\rho U_s^2} \tag{11}$$

External pressure coefficient

$$C_{ps} = \frac{p-p_\infty}{1/2\rho U_s^2} \qquad (12)$$

In section 4.3 where a comparison between theory and experiment is done, the theoretical coefficients are multiplied by a factor of $(U_s/U_\tau)^2$ in order to compare them with experimental results.

2.3.5 The Required Solution for the Idealized Problem

The tension coefficient C_{Ts}, the external pressure distribution and the shape of the building are to be found for given inflation pressure coefficient C_{Ps}, excess length $(\ell-c)/c$ (Fig. 1) and the power 1/n of the actual profile.

2.4 A TWO-DIMENSIONAL RIGID BODY IN A FLOW

A suitable theory was developed by Hess and Smith for a general three-dimensional incompressible flow (ref. 8). Here it is repeated for the two-dimensional case.

2.4.1 Ideal Flow Theory

Consider the flow about a body bounded by a contour C.

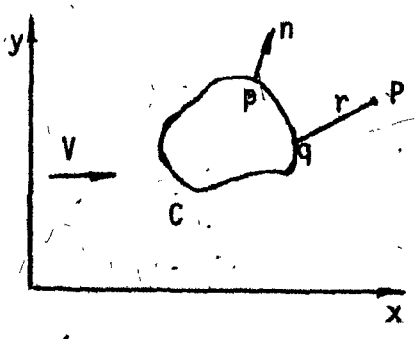

The velocity anywhere in the field is $\overline{V}$.

$$\overline{V} = \overline{V}_\infty + \overline{v} \tag{13}$$

where $\overline{v}$ is the disturbance velocity due to the presence of the body and $\overline{V}_\infty$ is the onset flow which is not necessarily uniform (ref. 8 and section 2.4.1.1).

The case that is presented here is for a disturbance velocity which can be expressed as a gradient of a potential ϕ.

$$\overline{v} = -\nabla\phi \tag{14}$$

The unusual minus sign is according to the convention used by Hess and Smith (ref. 8).

Continuity requires that

$$\nabla \cdot \overline{V} = 0 \tag{15}$$

But also

$$\nabla \cdot \overline{V}_\infty = 0 \tag{16}$$

Hence from equations (13), (15) and (16)

$$\nabla \cdot \overline{v} = 0 \tag{17}$$

which gives together with (14) Laplace's equation,

$$\nabla^2\phi = 0 \tag{18}$$

with a boundary condition which requires that the normal component of the velocity at the boundary will be zero.

$$-\nabla\phi \cdot \overline{n}\Big|_C + \overline{V}_\infty \cdot \overline{n}\Big|_C = 0 \tag{18a}$$

and a boundary condition which requires that the disturbance velocity far from the body will tend to zero.

$$\lim_{r \to \infty} | \nabla \phi | = 0 \qquad (18b)$$

$\bar{n}$ is the unit vector, locally normal to C and positive outward from C.

2.4.1.1 Superposition of a Source Distribution on a Flow with a Uniform Vorticity

Generally speaking a rotational flow ψ_1 cannot be superimposed on an irrotational flow ψ_2. The present method of solution is a special case where such superposition is allowed.

Consider a rotational upstream flow parallel to the x axis

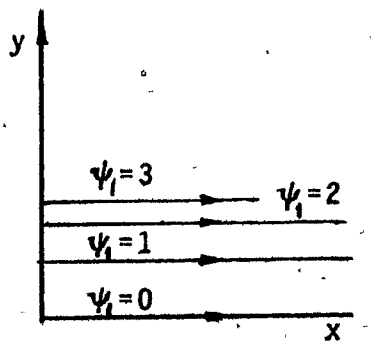

For a steady two-dimensional flow the vorticity ω of a fluid element is constant following the fluid. In a steady flow the streamlines are also pathlines and therefore ω is constant along a streamline and is a function of y only. ω has one component only which is normal to the x and y plane.

$$\omega = \frac{\partial v}{\partial x} - \frac{\partial u}{\partial y} = -\left(\frac{\partial^2 \psi_1}{\partial x^2} + \frac{\partial^2 \psi_1}{\partial y^2}\right)$$

or

$$\nabla^2 \psi_1 = - \omega(y)$$

For a source and sink distribution the flow field is irrotational.

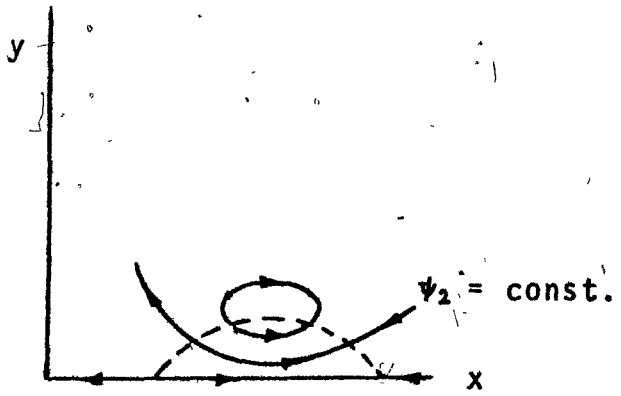

$$\nabla^2 \psi_2 = 0$$

Superposition of both flow fields, if permissible gives

$$\psi = \psi_1 + \psi_2$$

and $$\nabla^2 \psi = - \omega(y)$$

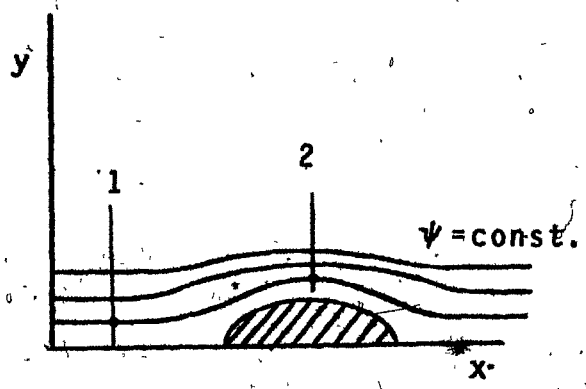

The dividing streamline represents a body surface. The question is: what kind of flow may ψ_1 be?

At station 2, near the body, a particular streamline does not have the same y coordinate as it has at station 1, far from the body. ω can be constant along this streamline only if it is independent of y, i.e. ω = constant.

By the definition of ω:

$$\frac{\partial v}{\partial x} - \frac{\partial u}{\partial y} = \text{constant} \tag{19}$$

Far from the body the onset flow is the only flow, i.e. $v = 0$, and (19) becomes

$$-\frac{\partial u}{\partial y} = \text{constant}$$

u is of the form

$$u = Ay + B$$

and the onset flow $\overline{V}_\infty$ is

$$\overline{V}_\infty = U\hat{i} + V\hat{j} = (Ay + B)\hat{i}$$

which is a uniform shear flow in the x direction.

The legitimacy of superimposing ψ_1 on ψ_2 can also be established in another way. Consider the flow field ψ which is a result of the superposition of ψ_1 the upstream parallel rotational flow with vorticity $\omega(y)$, and ψ_2 an irrotational flow due to singularities representing a body.

$$\nabla^2\psi = f(\psi) = -\omega$$

$$\psi = \psi_1 + \psi_2$$

where $\nabla^2\psi_2 = 0$

From these three equations

$$\nabla^2\psi_1 = f(\psi_1 + \psi_2)$$

This is true for any ψ_2

hence $f(\psi_1 + \psi_2)$ is independent of ψ_2 and is therefore constant,

hence ω = constant.

For a ψ_2 which has a symmetry about the x axis, the onset flow, which is parallel to the x axis, may be reflected in this axis to give

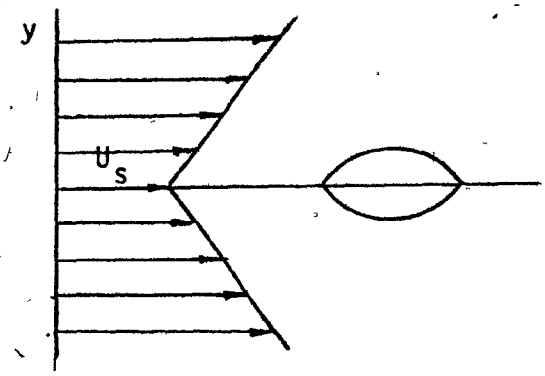

as the flows on either side of the x axis are separate.

2.4.2 Matching Methods for the Onset Flow

Several methods for choosing the slope 1/a and the slip velocity U_s were considered in order to achieve a good approximation of the actual flow. Since there are two unknowns 1/a and U_s, two conditions are needed.

In all the methods the first condition was that the approaching wind velocity at the height of the building U_h would be equal for both actual and idealized profile.

Note that U_e and δ which are used in this section may be a reference velocity and corresponding height on the power-law profile,

and not necessarily the free stream velocity and the boundary layer thickness.

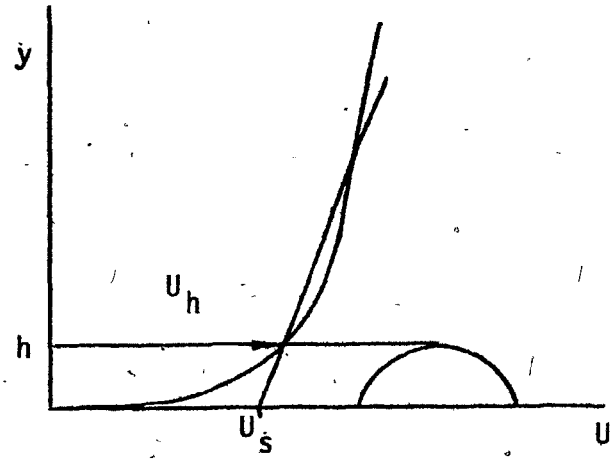

The second condition varies from one method to another:

Method 1: The average dynamic pressure $\overline{q}$ was equated for both profiles.

$$\overline{q} = \frac{1}{h} \int_0^h 1/2\rho U^2 dy$$

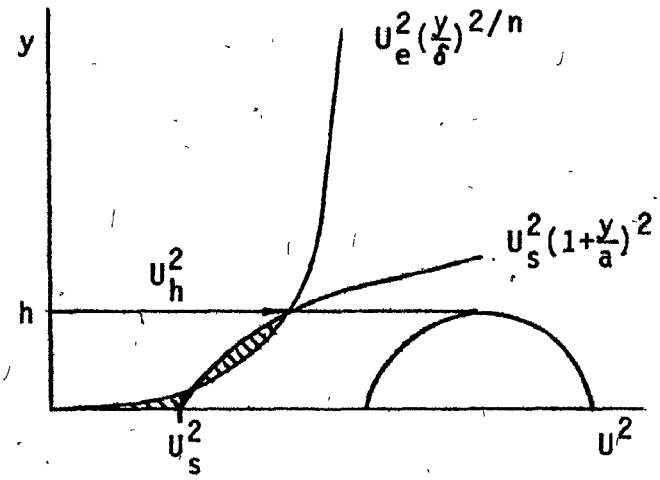

shaded areas: equal

Method 2: The shear (or slope) for both profiles at y = h was equated (see Appendix I). As will be seen later, this method gave the best comparison with experiment (section 4.3.3).

Method 3: The slopes of both profiles at y, corresponding to the average velocity on the actual profile, were equated.

$$y \text{ at } U_{av} = \frac{U_e}{h} \int_0^h \left(\frac{y}{\delta}\right)^{1/n} dy$$

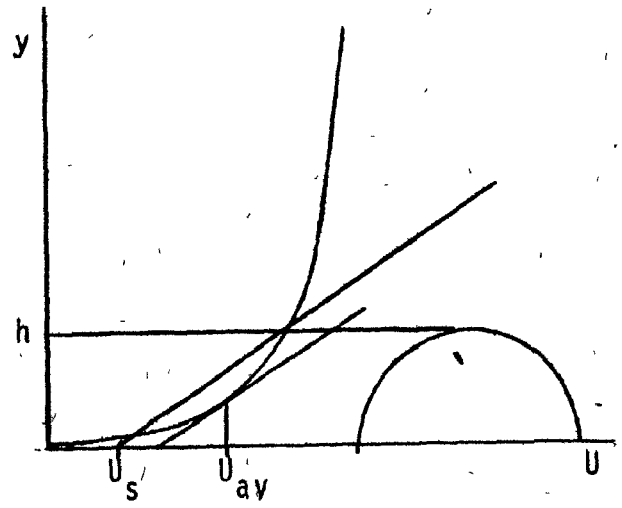

Method 4: The slope of both profiles at y, corresponding to the root mean square velocity on the actual profile, were equated.

$$y \text{ at } U = U_e \left[\frac{1}{h} \int_0^h \left(\frac{y}{\delta}\right)^{2/n} dy \right]^{1/2}$$

Method 5: A uniform flow without vorticity.

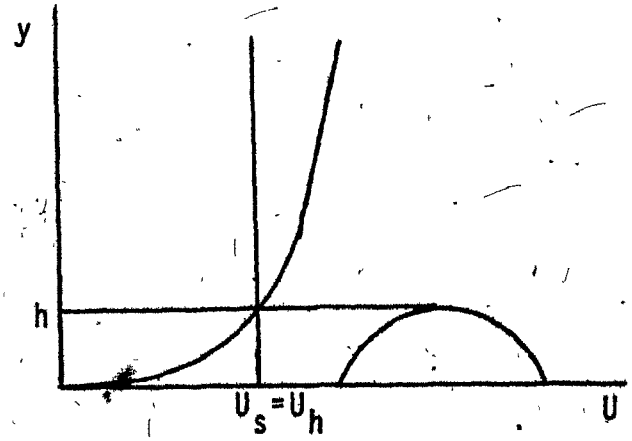

2.4.3 Reduction of the Problem to an Integral Equation

A two-dimensional point source at q causes a potential ϕ at P (see sketch in 2.2.1).

$$\phi = \frac{1}{2\pi} \ell n \frac{1}{r(P, q)} \tag{20}$$

ϕ satisfies eq. (18) and boundary condition (18b) if q is on contour C and P is outside C.

Since the problem is linear, several sources and sinks, including distribution of them, may be superimposed. The potential of a continuous source distribution on C which has the local intensity $\sigma(q)$ per unit length is

$$\phi = \frac{1}{2\pi} \oint_C \sigma(q) \ell n \frac{1}{r(P, q)} ds \tag{21}$$

where s is a coordinate along C.

This potential is differentiated, and boundary condition (18a) is applied by allowing point P to approach point p on C. The result is the equation for $\sigma(q)$ (ref. 9, 10):

$$\frac{\sigma(p)}{2} - \oint_C \sigma(q) \frac{\partial}{\partial n} \left[\ell n \frac{1}{r(p, q)} \right] ds + \bar{n}(p) \cdot \bar{V}_\infty = 0 \tag{22}$$

Each term is an outward normal velocity at point p: The term $\sigma(p)/2$ is the influence of the source at p on itself. The integral term is the influence of the rest of the sources on point p. The minus sign arises from (14). $\partial/\partial n$ denotes differentiation in the direction of the outward normal n at point p. The last term on the left

hand side is the velocity component of the onset flow at point p in the direction of the outward normal.

2.4.4 Discretization of the Problem

It is assumed that the body is rigid and has a known shape. The body is approximated by a polygon (Fig. 5): First, points are chosen on the contour of the closed body, then these points are connected by straight line segments or surface elements. Each of these elements has a uniform distribution of sources or sinks of strength σ per unit length. The value of σ is constant along the element and is unknown. There are therefore a finite number of unknowns, the values of σ for each element. The midpoints of the elements are chosen as control points for the application of equation (22). Velocities and pressure coefficients are calculated at these points.

2.4.5 Calculation of Coefficients of Influence

To begin with a unit strength is assigned to the line sources, i.e. $\sigma = 1$. To calculate the velocity field induced by a single surface element of a unit strength per unit length, consider an element of length Δs.

Consider coordinates x_e coinciding with the element, and y_e perpendicular to it at its midpoint (Fig. 5).

The velocity at point (x_e, y_e) due to an infinitesimally small part of s of a length $d\xi$ at $x = \xi$ is

$$d\bar{v} = \frac{1}{2\pi}\frac{d\xi}{r} = \frac{1}{2\pi}\frac{d\xi}{\left[(x_e-\xi)^2 + y_e^2\right]^{1/2}}$$

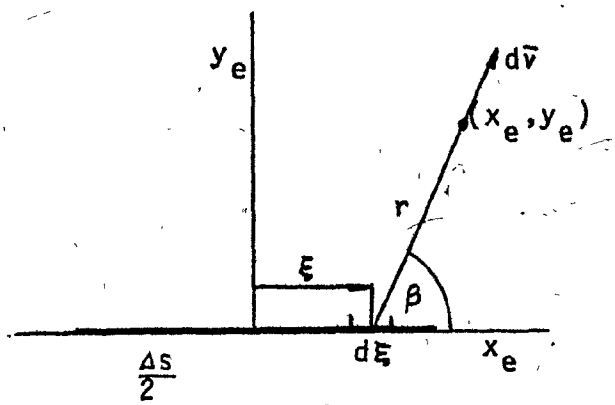

where $d\bar{v}$ is pointing away from $d\xi$ along r, a radius vector from $d\xi$ to (x_e, y_e) forming an angle β with the element.

The components of $d\bar{v}$ are

$$du_e = |\, d\bar{v}\,| \cos\beta = |\, d\bar{v}\,| \frac{x_e-\xi}{r} = \frac{1}{2\pi}\frac{(x_e-\xi)\, d\xi}{(x_e-\xi)^2 + y_e^2}$$

$$dv_e = |\, d\bar{v}\,| \sin\beta = |\, d\bar{v}\,| \frac{y_e}{r} = \frac{1}{2\pi}\frac{y_e\, d\xi}{(x_e-\xi)^2 + y_e^2}$$

Integration over the whole element gives

$$u_e = -\frac{1}{4\pi}\ell n\left[(x_e-\xi)^2 + y_e^2\right]_{-\frac{\Delta s}{2}}^{\frac{\Delta s}{2}}$$

$$v_e = -\frac{1}{2\pi}\operatorname{atan}\left[(x_e-\xi)/y_e\right]_{-\frac{\Delta s}{2}}^{\frac{\Delta s}{2}}$$

hence $$u_e = \frac{1}{4\pi} \ln \left[\frac{(x_e+\Delta s/2)^2 + y_e^2}{(x_e-\Delta s/2)^2 + y_e^2} \right]$$

$$v_e = \frac{1}{2\pi} \operatorname{atan} \left[\frac{y_e \Delta s}{x_e^2 + y_e^2 - (\Delta s/2)^2} \right] \qquad (23)$$

At $x_e = 0$; $y_e = 0$

$$v_e = 1/2$$

At each control point the velocity due to all elements of a unit strength is calculated using (23), and then transformed to the main coordinates x and y. These velocities are denoted $\overline{V}_{ij}$ where $\overline{V}_{ij}$ is the velocity at the i-th point due to the j-th element that has a unit source distribution. i and j correspond to p and q respectively. The x and y components of the $\overline{V}_{ij}$'s are calculated to give two matrices of coefficients of influence. These are used to derive the working matrix A_{ij} which is the outward component of $\overline{V}_{ij}$.

$$A_{ij} = \overline{V}_{ij} \cdot \overline{n}_i$$

Equation (22) can then be replaced by a set of linear equations

$$\frac{\sigma_i}{2} + \sum_{\substack{j=1 \\ j \neq i}}^{N} A_{ij} \sigma_j = - \overline{n}_i \quad \overline{V}_{\infty i} \qquad (24)$$

The terms in this equation correspond to the terms in (22). $V_{\infty i}$ is the velocity that would exist at the location of the i-th control

point if there was not a body in the onset flow and N is the total number of elements.

2.4.6 Calculation of Velocities and Pressures

The set (24) is solved to give σ_i. The velocities $\overline{V}_i$ at the control points are

$$\overline{V}_i = \sum_{j=1}^{N} \overline{V}_{ij} \cdot \sigma_j + \overline{V}_{\infty i}$$

which is the sum of the velocities induced by all the elements plus the onset flow. The pressure coefficients are

$$(C_p)_i = 1 - \left(\frac{\overline{V}_i}{V_{ref}}\right)^2$$

Here the reference velocity V_{ref} is chosen as the slip velocity U_s of the onset flow of uniform vorticity.

2.4.7 Symmetry

In the present problem the body is placed so that its leading edge and trailing edge are on the x axis. The body is reflected in the $y = 0$ plane to give the closed contour C.

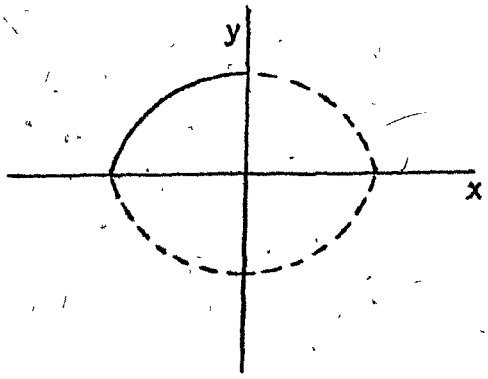

The contour C has another axis of symmetry, and the y axis is chosen so that it is this axis of symmetry. Now the discretization of only a quarter of C is sufficient, and once the $\bar{V}_{ij}$ values are calculated for one quadrant, the quarter body is reflected in the two planes of symmetry to give three images, and the effect of these reflections is added to the $\bar{V}_{ij}$ matrices. This reduces the number of control points to a quarter of their original number, and computation time is saved.

2.5 A FLEXIBLE BODY IN A FLOW

A flexible body in a flow has unknown boundaries, since its shape is affected by the flow. The previous method for a rigid body therefore has to be iterated. A computer program for the complete iteration has been developed and is given in Appendix II. The procedure is as follows.

2.5.1 Calculation Procedure

a) For a given inflation pressure P, tension T, and wind profile n, an initial shape y(x) is assumed. The initial shape was chosen to be a circular arc which corresponds to the wind-off case i.e. the radius of curvature is constant along x and equals T/(P-p).

b) The pressure distribution along the membrane is found by the Hess and Smith method as described in 2.4. The onset flow is a flow with uniform vorticity (eq. 9).

The height of the membrane changes slightly from one iteration to another. Since the velocities are being matched at the top of the building, the slope 1/a of the velocity profile also changes to give a specific wind profile exponent 1/n (see section 2.4.2 and Appendix I).

As an alternative option the computer program can also solve for a fixed uniform vorticity which has no relation to a boundary layer power profile.

c) The local curvature of the membrane under a net pressure P-p is calculated from the relation

$$\frac{1}{R(x)} = \frac{P-p}{T}$$

d) A new shape $y(x)$ is found from the radius of curvature $R(x)$ and the boundary conditions $y(0) = 0$ and $y'(c/2) = 0$, where c is the chord length. The former requires that the membrane is attached to the floor at its leading edge and the latter requires that the membrane is parallel to the floor at the top of the building.

The solution of the equation

$$\frac{1}{R(x)} = \frac{y''}{(1+y'^2)^{3/2}}$$

$$y(0) = 0$$

$$y'(c/2) = 0$$

is complicated even when done numerically and it requires a long computation time. It is more convenient to use the

natural coordinates s and θ. s is a coordinate along the curve and θ is the local angle between the curve and the x axis.

$$\frac{1}{R(x)} = \frac{d\theta}{ds}$$

$$ds = \frac{dx}{\cos\theta}$$

We have now the equation

$$\frac{dx}{R(x)} = d\theta \cos\theta$$

and the boundary conditions

$$\theta(c/2) = 0$$

$$y(0) = 0$$

The solution of this equation gives $\theta(x)$, and $y(x)$ is calculated from

$$\frac{\Delta y}{\Delta x} = \tan\theta(x)$$

e) The new shape is compared with the former shape at $y(c/2)$ within a desired accuracy ($\Delta y/c < 10^{-5}$ in the present work). If the shapes are not equal, the program returns to b) and repeats the calculation until convergence, at which point a solution for y and p has been achieved.

Only the point $y(c/2)$ was checked for convergence. It has been observed that the rest of the shape changes less than the midpoint $y(c/2)$ from one iteration to another and it was verified by printing out in each iteration the whole shape (see computer output in Appendix II).

Note that the role of $(\ell\text{-}c)/c$ and C_{Ts} as independent and dependent variables is switched in the numerical solution, i.e. C_{Ts} is an input and $(\ell\text{-}c)/c$ is an output of the program.

3. EXPERIMENTS

3.1 GENERAL DESIGN OF THE EXPERIMENTS

The purpose of the experiments was to simulate the behaviour of a typical cylindrical inflated building in a cross wind.

The variation of wind speed with height is usually approximated by a power law profile as in equation (1). Values of $1/n = 0.16$ and $1/n = 0.24$ were aimed for. These values correspond to flat open country and to sparsely wooded country respectively (ref. 7, 11).

An average thickness for the atmospheric boundary layer is $\delta = 360$ m (ref. 7), and a typical height of existing inflatable buildings in a shape of a semi-cylinder, is 12 m (ref. 1). With the experimental facilities available it was anticipated that the boundary layer would be about 1 m thick. To keep the same scale as in the actual situation, the height of the model would be 33 mm, which is too small for meaningful measurements. Nevertheless, a larger model with a height of up to 85 mm was used, since the building is well within the law of the wall region and is affected only by the lower region of the boundary layer. A similar approach was used by N.J. Cook (ref. 12).

The recommended inflation pressure needed in a cylindrical building is 0.6 times the dynamic pressure of an approaching wind that blows over it (ref. 4). This was used as a guideline in

identifying 20 Pa gauge as the typical inflation pressure for a nominal wind tunnel velocity of 7.7 m/s.

Only one tunnel speed was used, a speed which was near the maximum possible for the wind tunnel. Any appreciably lower speed would incur inflation pressures, tensions and external pressures which were so low that they could not be measured with sufficient accuracy. Thus any possible change in the tunnel speed would not change the order of magnitude of the Reynolds number and no additional information would be obtained.

The Reynolds number based on a velocity of 7.7 m/s outside the boundary layer and the chord length of the model was

$$Re = \frac{U_e \cdot c}{\nu} \approx 2 \cdot 10^5$$

3.2 EXPERIMENTAL APPARATUS

3.2.1 Wind Tunnel

The 2 m by 1.5 m blower, boundary layer wind tunnel in the Aerodynamic Laboratory of the Department of Mechanical Engineering at McGill University was used. The test section of the tunnel is 10 m long, and the flow is supplied by a centrifugal fan rated at 30 kw. The pressure at the exit from the test section is atmospheric. The roof of the wind tunnel is made of segments that can be lowered or raised. There is a pressure tap in the center of each roof segment. The roof was adjusted so that there was no pressure gradient along the tunnel. The static pressure tap just before the final contraction and downstream of the screens was used as

a wind tunnel reference pressure to establish the tunnel dynamic pressure (Fig. 2).

3.2.2 Spires

An array of 4 spires with splitter plates was placed across the entrance to the working section (Fig. 2 and Plate 1). The spires were 1 m high and spaced at 0.4 m. They were designed to give a boundary layer with a δ = 1 m thickness at a distance of at least six spire heights downstream of the spires (ref. 13, 14 and see Appendix III). However, the actual boundary layer generated by these spires was 1.4 m thick (see section 4.2.1.1).

3.2.3 Roughness

In order to maintain the specific power 1/n for the boundary layer achieved by the spires (eq. 1), roughness was needed on the wind tunnel floor. Two theoretical rectangular roughness arrays were calculated according to Fig. 2 of ref. 15. It was determined that an array of square three-dimensional bars 3 mm high and 30 mm apart would give 1/n = 0.16, and an array of rectangular two-dimensional bars 12 mm high and 250 mm apart would give 1/n = 0.24. The roughness arrays which were actually used were: 1) A commercial plastic mat with cone-shaped protrusions. The cones were 3 mm high, 4 mm base diameter spaced every 28 mm in an hexagonal array (see Plates 2, 3 and 4). This roughness was the best available substitute for the calculated roughness. 2) A canvas carpet with 12 x 12 mm strips of wood attached across it and arranged 250 mm apart to form a two-dimensional roughness as calculated.

The spires gave 1/n = 0.13 with roughness 1, instead of the designed 1/n = 0.16 (see 4.2.1.2). The same spires were therefore used for both profiles.

3.2.4 Pitot Tube Comb for Boundary Layer Survey on the Floor

The comb consisted of a metal bar which could be installed vertically in the wind tunnel in the absence of the model and which held 18 Pitot tubes between the roof and the floor of the tunnel. The lower 9 tubes were 50 mm apart, and the upper 9 tubes were 100 mm apart.

3.2.5 The Model

A schematic diagram of the model is shown in Fig. 3. Pictures of it are shown in Plates 2, 3, 4 and 5. In this section numbers in brackets refer to the part number in Figure 3.

The model was placed in the wind tunnel 1 m from the exit.

The inflatable building model consisted of a membrane with a 650 mm span (1) and a length ℓ which could be varied between 260 mm and 320 mm. The material of the membrane was a flexible impervious light cloth (Stablecote II rip-stop nylon, 25 gr/m^2) which is used for spinnaker sails. The model was inflated with an adjustable supply of air from the blowing side of a 650 W domestic vacuum cleaner. The air was introduced to the inside of the model through a perforated pipe (8) which was calculated to give an even distribution of air.

Both ends of the model abutted on plexiglas plates (2). Four pipes passed through these end-plates: the air supply pipe and three pipes which were open ended pressure tubes (5) for the measurement of the average inflation pressure. The pressure tubes measured the pressure at three equally spaced lateral positions

inside the model and their openings pointed in different directions, so that any significant air flow within the model would have been detected (see Plate 5).

The model and end-plates were held by a rectangular frame (9) that fitted into an opening of the same shape in the wind tunnel floor. The frame held the model horizontally so that its axis was perpendicular to the wind tunnel flow.

A second membrane (6) below the level of the wind tunnel floor (4) was clamped between the leading and the trailing edges of the model, the purpose of which was to seal the inflated model and prevent air from escaping at the edge gaps. Some air escaped inevitably between the model and the end plates, but this was minimized by allowing an extra 5 mm at each end of the cloth where it touched the end plates. This extra cloth was tucked inward to further improve the seal. The model and the seal were connected by two long clamps (7), one on the leading edge of the model and one on the trailing edge. A system of flexures and strain gauges was used to measure the fore and aft force, and ultimately the tension in the membrane. Each clamp was mounted on two flexures (10), one on each end of the clamp. Attached to the four flexures were strain-gauges which measured the strain due to the horizontal force that was applied by the tension in the cloth of both the model and the seal. The dimensions of the flexures were dictated by the 20 Pa gauge inflation pressure, the requirement of 500 micro-strain reading at the maximum pressure and limitation of the

flexure deflection to no more than 1 mm. The dimensions found were 51 x 9.5 mm (2 x 3/8 inch) with a thickness of 0.5 mm.

The seal was designed to have the shape of a semi-circle when the model was inflated, so that it would not apply a horizontal force on the flexures. However this was not exactly achieved and the horizontal force due to deviation from this semi-circular shape was taken in account. The flexures were mounted on the frame (9). The distance between the clamps fixed the chord length c at 250 mm. The height of the model could be varied by changing the length of the membrane of the model clamped between the clamps. The membrane of the seal was not varied.

3.2.6 Rigid Dummies

The length of the model occupied the middle third of the width of the tunnel. In order to complete the model so that it would span the tunnel and achieve a quasi two-dimensional condition, two rigid dummies in a shape of a circular arc with the same chord length as the model were added one on each side between the end plates and the tunnel wall. There were two pairs of rigid dummies, one for each range of model height.

3.2.7 Traversing Static Tube

A static tube was designed to measure the external pressure distribution along the surface of the model. The static tube was designed using a three-dimesional source in potential flow to represent the tube, and a two-dimensional doublet to represent the stem. The surface of the model was not accounted for. The holes of the

static tube were drilled at the location where these two bodies cancel each other's effect. The static tube was tested in the wind tunnel (3.3.1).

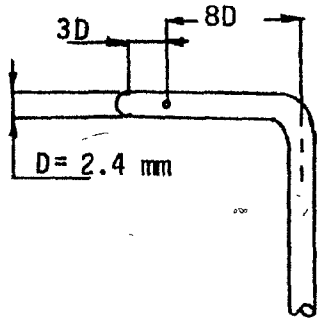

The static tube was mounted on a traversing gear so that it might be aligned with the surface of the membrane. The static tube lay in a vertical plane which is parallel to the flow and passed through the lateral midpoint of the model. It had three degrees of freedom in the above mentioned plane: two linear and one rotational.

Another method of external pressure measurement was tried using pressure taps in the membrane itself as is often done for rigid bodies. The method was abandoned, since it involved attaching rigid washers around the taps and they caused local stiffening of the membrane.

3.2.8 Instruments

1. Manometers: Three Lambrecht type 655 alcohol reservoir manometers inclined at 1:25 were used to measure:

   a) Inflation pressure.

b) External pressure distribution.

c) Tunnel reference pressure.

2. Bruel and Kjaer strain indicator type 1526 which ultimately measured the forces on the flexures.

3. Heathkit IR-18M chart recorder which recorded the strain indicator reading while it fluctuated, for the wind-on case.

4. Precision Tool and Instrument Company cathetometer 2202 (telescope), to measure the angle between the model and the wind tunnel floor at the leading and trailing edges. (see section 3.4.2)

5. DISA hot wire anemometry system:

a) Hot wire anemometer 55D01.

b) Linearizer 55D10.

c) RMS voltmeter 55D35.

d) Slanting hot wire probe 55P12.

to measure Reynolds stresses ($-\rho\overline{u'v'}$) in the floor boundary layer.

3.3 CHECKS AND CALIBRATIONS OF THE APPARATUS

3.3.1 Static Tube Test

The static tube (3.2.7) was tested as follows: A 115 mm rigid rotatable cylinder with a pressure tap on its surface was placed in the tunnel, axis perpendicular to the flow, but in the absence of the model. The pressure from the tap was read for various azimuthal positions and then compared with that of the static tube when held 0.5 mm from the surface, and they compared within 1 per cent of the local dynamic pressure.

3.3.2 Flexure Calibration

The flexures with the strain gauges for tension measurement, were calibrated by loading them with a horizontal force using a

pulley and dead weights and reading the strain from the B & K strain indicator. The flexures were gradually loaded, unloaded and finally reloaded. The calibration showed maximum error of 0.8 per cent due to lack of repeatability and linearity.

3.3.3 Hot Wire Check

The hot wire system (section 3.2.8 No. 5) was tested by measuring the skin friction in fully developed turbulent flow in a smooth pipe, and comparing it with the skin friction found from the pressure drop along the pipe. The 76.2 mm (3 inch) diameter pipe had pressure taps along it to measure the pressure drop.

The single slanting hot wire probe was traversed from near the wall of the pipe to its center. Then the probe was rotated 180^0 and traversed again from pipe wall to center, (ref. 16). The signal from the anemometer was linearized and the mean square of the AC component was recorded. At each point there were two readings: one reading before rotating the probe and one reading after rotating it. The DC component of the signal from the linearizer was checked to verify that the axis of the probe was parallel to the flow.

To find Reynolds stresses, one reading was subtracted from the other and then the result was multiplied by a factor which included the angle and the calibration constant of the slanting wire. Finally, a correction was applied, to account for the longitudinal

cooling of the wire, using a constant of $k_1^2 = 0.04$, according to the aspect ratio of the hot wire used (ref. 16). This procedure gave the time average of the product of the fluctuating components of the longitudinal and lateral velocities $\overline{u'v'}$ as a function of the distance from the pipe wall, non-dimensionalized by the radius of the pipe. The Reynolds stresses $-\rho\overline{u'v'}$ were plotted and compared with those calculated from the pressure drop (Fig. 6). The results agree within a maximum error of 6 per cent. The skin friction velocity U_τ equals $\sqrt{-\overline{u'v'}}$ at the wall and the maximum error in it is therefore 3 per cent. Over most of the range, however, the error is much less than this.

3.3.4 Wind-Off Measurements

The model was placed in the wind tunnel with the wind off. It was inflated at four different pressures and the readings of the four strain gauge bridges were taken for each inflation pressure. The purpose of the wind-off measurements was two-fold: to check the self consistency of the instrumentation and to substantiate the validity of the theoretical correction due to the seal not being truly semi-circular.

The wind-off tests showed also that no detectable extension of the membrane due to the tension in it or deflection of the flexures was present. For a given membrane length the height h and the chord length c remained constant within the accuracy of measurement for different inflation pressures.

The results of the wind-off experiments are given in Fig. 7. The tension in the membrane was calculated in two ways:

from the internal pressure and from the strain measured in the flexures. Ideally all the results should fall on a straight line at 45^{o}. The present results deviate from this line by a maximum of 3 per cent and usually the deviation is much less. This establishes the reliability of the tension measurements for the subsequent wind-on experiments.

3.3.5 The Effect of the Rigid Dummies

The fact that the rigid dummies were not exactly the same shape as the model did not introduce a detectable error. This was proved by removing the dummies entirely while the wind was on, and seeing that the tension and external pressure reading did not change. The deviation due to the removal of the dummies was found to be less than 0.5 per cent.

3.4 EXPERIMENTAL PROCEDURE

3.4.1 Boundary Layer Measurements

With the spires mounted and the model removed the following measurements were made for each roughness.

3.4.1.1 Velocity Profile Measurement

The wind tunnel was set at a nominal value of 7.7 m/s and the comb of Pitot tubes was mounted in place of the model in the tunnel. The 18 readings of the total pressure were taken for the measurement of the boundary layer velocity profile. This was repeated at three spanwise positions: at the center line of the

tunnel, and on both sides of the center line behind the middle spires.

3.4.1.2 Hot Wire Measurements for Skin Friction Velocity

A single slanting hot wire probe was traversed from the wind-tunnel floor up at intervals of 25 mm. The procedure described in section 3.3.3 was used for the calculation of the Reynolds stresses $-\rho\overline{u'v'}$ in the boundary layer.

3.4.2 Model Measurements

The geometry of the model was measured with the wind off. The height of the model h, its chord length c, and its span L between the end plates were measured using a ruler and sighting through the end plates. The length of the model membrane was read directly from the membrane, as it was graduated with centimeter lines. The height and diameter of the near semi-circle of the seal membrane were also measured using a ruler.

The leading edge and trailing edge angles between the model membrane and the wind tunnel floor were measured using the telescope. An oblique sighting of the angle was required since it could not be measured near the end plates where the vertex of the angle was hidden behind the end plate edge (see Plate 4) and the rigid dummy (Plate 2). The angles were measured therefore at the middle of the span (white line in Plates 2 to 4).

With the wind on and the model inflated, the graticule line of the telescope was aligned with the white line near the

vertex of the angle. The model was then deflated and a protractor was placed on the tunnel floor on the white line. The angle indicated by the graticule line was then read off on the protractor.

The height of the model h was varied between 40-85 mm. The inflation pressure P was varied in a range of 0 to 44 Pa gauge. For each combination of h and P the readings of the strain gage bridges were recorded on a chart recorder, since the reading fluctuated too much to be read directly on the digital voltmeter included in the B & K strain indicator.

Since the models had a height-to-chord ratio of up to 0.4, separation bubbles were expected to form at the leading and trailing edges similar to those found near a rigid bluff body in a boundary layer. The two separation and two reattachment points (Fig. 4) were located using a wand with a tuft attached to its end.

The stability of the model for low inflation pressures was investigated. As the inflation pressure was reduced to low values, the model started to oscillate and subsequently collapsed. The values of these critical inflation pressures were recorded.

The pressure distribution outside the model along the center line of the tunnel was measured using the traversing static tube. The static tube was placed 0.5 mm from the surface locally parallel to it. The reading was usually not sensitive to the exact distance of the static tube from the surface. The distance could be increased to about 2 mm from the surface even near the top of the model. Pressure distribution was measured for each height of model for one inflation pressure.

3.5 MEASUREMENT ERRORS

3.5.1 Blockage Effect

The vertical dimension of the cross section of the wind tunnel and the height of the models tested had a minimum ratio of about 18:1, therefore the blockage effect was expected to be small.

A very rough estimate of the blockage effect correction for the coefficients C_T, C_p and C_p was made for an equivalent two-dimensional wing in the center of a wind tunnel of twice the height with a uniform flow (ref. 17). This is an estimate only, because the flow was not uniform. Nevertheless the corrections were assumed to apply proportionally to the skin friction velocity.

The solid blockage corrections for the coefficients $2\Delta U_\tau/U_\tau$ ranged between 0.3 and 0.6 per cent for the various height-to-chord ratios. The wake blockage effect was estimated from Glauert's method mentioned in ref. 17, which does not use a drag coefficient but is stated in terms of the thickness-to-chord ratio of the model. The wake blockage corrections for the coefficients were 1.2 to 1.9 per cent. The total corrections ranged between 1.5 and 2.5 per cent, according to the geometry of the model, and they were applied to all the results (although they should not have been applied to C_p).

3.5.2 Tension

The tension per unit length T in the model was calculated from the horizontal force F applied to the flexures by the model.

$$T = \frac{F}{L\cos\theta} \tag{25}$$

where L is the span of the model and θ is the leading or trailing edge angle.

A correction for the force F was made due to the fact that the seal was not an exact semicircle. Thus an additional horizontal force F_1 was applied to the flexures as shown in the following sketch.

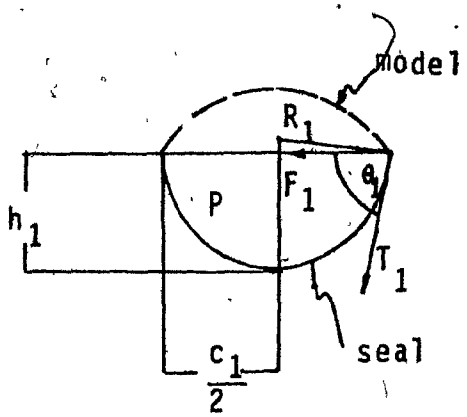

$$F_1 = L_1 T_1 \cos \theta_1$$

where the subscript 1 denotes values for the seal.

Also

$$T_1 = (P-p_\infty) R_1$$

and

$$R_1 = \frac{h_1}{2} + \frac{c_1^2}{8h_1} \qquad (26)$$

From the last three equations

$$F_1 = L_1(P-p_\infty) \left(\frac{h_1}{2} + \frac{c_1^2}{8h_1}\right) \cos \theta_1 \qquad (27)$$

The force applied by the model in eq. (25) is

$$F = F_{read} - F_1$$

The measurement error in T is

$$\frac{dT}{T} = \frac{dF}{F} + \tan\theta \, d\theta - \frac{dL}{L} \tag{28}$$

To investigate the contribution of the error in the additional force F_1 to the error in T, consider the relative error in F_1 calculated from eq. (27).

$$\frac{dF_1}{F_1} = \frac{dL_1}{L_1} + \frac{dP}{P} + \frac{1}{R_1}\left(\frac{1}{2} - \frac{1}{8}\left(\frac{c_1}{h_1}\right)^2\right) dh_1 + \frac{c_1}{4h_1} dc_1$$

$$-\tan\theta_1 d\theta_1$$

where R_1 is given in eq. (26).

The estimated error in measurements of geometry for the model and seal were dc = 0.5 mm, dh = 0.5 mm, dL = 5 mm and $d\theta = 1^o$. The value of dP/P was found from the slight difference between the readings taken from the three inflation-pressure tubes and it was 0.5 per cent.

The error in F_1 could be as large as 20 per cent for the particular geometries in the experiment. However F_1 was only two per cent of the force F of the model, so that $dF_1/F \approx 0.004$, and is therefore negligible. The error in T was therefore calculated from eq. (28) without taking into account dF_1/F_1.

The estimated error in reading strain from the chart-recorder output was 2 per cent, i.e. dF/F = 0.02 and a typical reading of θ was 52^o which gives a possible maximum error of 4 per cent in the tension calculation.

3.5.3 External Pressure Distribution and Boundary Layer Profile

The manometer readings fluctuated more in these measurements than in the inflation pressure measurement. The estimated error was 1 per cent. The hot wire readings had a maximum error of 3 per cent as found in the measurements of the pipe flow.

3.5.4 Separation and Reattachment

The error in determining the distances S_1, R_1, S_2 and R_2 (Fig. 4) is estimated as 10 mm. This is due to uncertainties associated with interpreting the behaviour of the tuft. At the leading edge the separation bubble was typically 20 mm long and the error there was very roughly 50 per cent and therefore large. At the trailing edge the separation bubble was about 200 mm long and the percentage error was therefore much less.

4. RESULTS AND DISCUSSION

4.1 THEORETICAL RESULTS

4.1.1 Program Testing for Rigid Bodies

The computer program was tested by running it for rigid bodies (one iteration) which have a known exact solution.

The chosen bodies all have two axes of symmetry and therefore only one quarter of them needed to be discretized.

a. A cylinder in a uniform flow: The exact solution is found by solving the flow for a doublet in uniform flow. The pressure distribution is given in Fig. 8 for various number of discretization points. The solution for 17 points or more effectively coincides with the exact solution.

b. Rankine oval: The exact solution is found by solving the flow for a source and a sink with an intensity of 2π with a distance of 2 units between them in a uniform flow. This configuration gives a contour defined by

$$\tan y = \frac{2y}{x^2+y^2-1}$$

Results are given in Fig. 9 for 17 discretization points, and again the agreement with the exact solution is very good.

c. Lenticular aerofoil: This is an aerofoil which is composed of two identical circular arcs connected at their ends (ref. 18).

The results given in Fig. 10 give again very good agreement with the exact solution.

A choice of 17 points for discretization per quarter body gave very good agreement with the exact solutions in all cases and this number was therefore chosen in subsequent use of the method.

4.1.2 Results for the Present Problem

Theoretical results for the tension coefficient C_{Ts} and their comparison with experimental results are discussed in section 4.3.1.

Several results for external pressure distribution coefficient C_{ps} and the shape of the building $y(x)$ are given in Fig. 11 to 16.

The higher the building and the lower the C_p the more iterations were needed for the same degree of convergence. For low buildings with high inflation pressure 4 or 5 iterations were needed, and for high buildings as many as 20 were needed.

It appears that for low buildings it is possible to present the results in the compact way using $C_p/\sqrt{(\ell-c)/c}$ as a collapsed parameter. For the cases of buildings with $h/c<10$ per cent, the values of $C_p/\sqrt{(\ell-c)/c}$ were plotted against C_T (Fig. 17). For a constant slope c/a of the idealized onset profile, the results fall on a single straight line with a slope of about 5. Each value of c/a gives a different straight line with the same slope.

It is possible to compare the present theory with the previous approximate theory of Newman and Tse (ref. 6). The case

of $c/a \to 0$ or $a/c \to \infty$ corresponds to a uniform onset flow with no vorticity, and for this case the results in Fig. 17 coincide with the predictions of Newman and Tse.

4.2 EXPERIMENTAL RESULTS

4.2.1 Boundary Layer Results

4.2.1.1 Free Stream Velocity

The free stream velocity was calculated from the stagnation pressure at the top of the boundary layer. Since the measurements were taken near the exit from a blower tunnel, the static pressure was assumed to be atmospheric. The values averaged 7.9 m/s and 7.5 m/s for the roughness (1) and (2) respectively. These values varied by 1.5 per cent as the air density varied between 1.2 kg/m^3 and 1.18 kg/m^3. The boundary layer thickness was 1.4 m, which is well above the design value δ = 1 m, possibly because of additional boundary layer growth along the tunnel, as the measurements were taken at a distance of 9 times the spire height instead of 6 times the spire height and also added roughness was present. Since the phenomena are governed by the flow near the wall only, the boundary layer thickness is not important once it is about four times the height of the model or more.

4.2.1.2 Power Law Exponent

The boundary layer profiles were plotted on a log-log scale: $\log (p_{total}-p_{\infty})$ against $\log y$ (Figs. 18, 19). The power

1/n for the power law profile (eq. 1) was calculated from the slope of the straight line (Table 1). The result for roughness 1 was 1/n = 0.13 compared to the design value of 0.16, probably because a substitute roughness was used (see 3.2.3). Roughness 2 gave 1/n=0.24 as designed.

4.2.1.3 Skin Friction

The skin friction velocity U_τ was found in three ways:

a. The velocity profiles were plotted on coordinates $(P_{total})^{\frac{1}{2}}$ against log y (Fig. 20, 21) to give U_τ from the law of the wall:

$$\frac{U}{U_\tau} = 5.5 \log_{10}\left(\frac{yU_\tau}{\nu}\right) + f\left(\frac{k_s U_\tau}{\nu}\right)$$

The skin friction velocity was calculated from the slope of the graph in the region of $0<y<0.25\delta$.

b. A result of the velocity-defect law is that

$$\frac{U_e - U_{av}}{U_\tau} = \text{Constant}$$

where U_{av} is the average velocity of the wind profile, and the constant is 3.9 (ref. 19) or 4.0 (ref. 20). The value of U_τ was calculated from this relation, using the velocity profiles found in 4.2.1.2, and the results are given in Table 1.

c. The hot wire measurements were reduced to give the Reynolds shear stress (ref. 16) as described in section 3.3.3.

$\sqrt{-\overline{u'v'}}$ was plotted against y (Fig. 22, 23) and was extrapolated to y = 0 to give the wall shear stress τ_w and thus U_τ. The results are also given in Table 1.

The result for U_τ found by hot wire for roughness 1 is much higher than the results obtained from the other two methods, possibly because the roughness was not large enough to eliminate the excess turbulence which is produced by the spires (ref. 13).

Since the mean velocity level is the dominant parameter which determines the shape of the profile and the tension in the membrane, it was decided to use the values obtained from the mean velocity profiles rather than the hot wire readings and the values of U_τ which were used for the coefficients were 0.24 and 0.36 for roughness 1 and 2 respectively.

4.2.1.3 Two-Dimensionality of the Wind Velocity Profile

There was a variation of the wind velocity profiles in the lateral direction across the tunnel, i.e. they were not perfectly two-dimensional. For roughness 1 the power 1/n was 0.13 at the center line, and 0.13 and 0.11 near the ends of the model. For roughness 2 the values were 0.24 at the center line, and 0.23 and 0.20 at the other points. The values at the center line were the ones that were assumed when comparing theory and experiment.

4.2.2 Model Results

4.2.2.1 Tension and Inflation Pressure

The tension per unit length T in the cloth was calculated from the forces on the four flexures, the seal geometry, the inflation pressure and the leading edge and trailing edge angles (see section 3.5.2). The difference between the tensions calculated at the leading edge and at the trailing edge was ± 3 per cent, which is within the range of the measurement error (section 3.5.2). The difference was not attributed to wind friction, because it was not of one sign.

The tension and the inflation pressure were reduced to non-dimensional coefficients as defined in eqns. 4 and 5 using the appropriate U_τ for each roughness. C_T is plotted against C_{P_τ} in Figs. 24, 25. Each curve is for a given membrane length or model height and all are approximately straight lines which do not pass through the origin. The curves are in the consistent order on the graph i.e. the tension is higher for the lower models for a given inflation pressure and each roughness.

Fig. 24, 25 have a lower limit for C_{P_τ} and C_{T_τ} marked by a bold curved line across the C_{T_τ} vs C_{P_τ} lines. The bold line marks the critical inflation pressure coefficient for which the model collapsed. For a pressure slightly above the critical, the models oscillated irregularly and partially collapsed at the leading edge. The critical inflation pressure for the lower

models was somewhat uncertain, since complete collapse was not observed even for zero inflation pressure, and the instability line is therefore shown dashed in this region. This observation agrees with the results obtained by Newman and Tse (ref. 6) for thin lenticular aerofoils; they also did not collapse when the inflation pressure was reduced to zero after the wind was turned on.

The results in Figs. 24, 25 are based on the skin friction velocity U_τ. To make them useful for practical purposes, the data should be related to a wind velocity at a height of say 10 m above the ground U_{10}, where it is usually measured. Table 2, which is based on the work of Davenport (ref. 7), is therefore included. It provides data on winds blowing over various terrains of different roughness, including those represented by the present experiments.

4.2.2.2 An Attempt to Collapse Parameters

It was concluded in section 2.3.3 that the tension coefficient C_{T_τ} is a function of the parameters $(\ell\text{-}c)/c$, C_{p_τ} and n. An investigation is made here, based on the experimental results, whether n is necessarily a parameter of the problem. For the purpose of the investigation, the experimental data were plotted on a graph of C_{T_τ}/C_{p_τ} against $1/C_{p_\tau}$ in two sets of curves (Fig. 26, 27), one for each n.

$$\frac{C_{T_\tau}}{C_{p_\tau}} = \frac{T}{(P-p_\infty)c}$$

and this quotient does not depend on a velocity, a fact which facilitates this investigation. An attempt was made to collapse

the two sets of curves (Fig. 26, 27) onto a single set of curves so that

$$C_T = C_T(\frac{\ell-c}{c}, C_p)$$

without including n, where C_T and C_p are coefficients based on some velocity characteristic of the problem, which is neither U_τ nor U_s.

The collapse of parameters could be done by choosing an appropriate reference velocity to base C_p and C_T on. Such reference velocity was expected to be the velocity of the undisturbed onset flow at a height of a constant fraction of the model for all models and roughnesses which were tested. However, no such constant fraction was found, which proves that the system is characterized by at least three parameters, and is dependent also upon the roughness parameter or wind profile parameter, i.e.

$$C_T = C_T(\frac{\ell-c}{c}, C_p, n)$$

4.2.2.3 External Pressure Distribution

The pressure distribution measurements were reduced to an external pressure coefficient C_p (eq. 7), and were plotted against s/ℓ (Figs. 28 to 37), where s is measured along the surface of the model from the leading edge.

4.2.2.4 Separation and Reattachment

The distances of the separation and reattachment points from the leading and trailing edges (Fig. 4) were plotted against

C_{P_T}. These distances were normalized in terms of the membrane length ℓ, to give s_1/ℓ, R_1/ℓ, S_2/ℓ and R_2/ℓ. Each model gave a separate curve (Figs. 38 to 45).

The locations of the observed trailing edge separation point S_2 were marked on the pressure distribution curves (Fig. 28 to 37). The points are close to the position where the trailing edge pressure becomes constant, as would be expected at separation.

The curves in Figs. 38 and 40 are apparently not self-consistent. This may be attributed to the fact that the relative error in the leading edge separation point was large (see 3.5.4) and Figs. 38 to 41 give only a general idea of the bubble size. The trailing edge separation bubble measurements were much more exact and it is evident from Fig. 42 to 45 that the separation bubble for roughness 1 (open sea) is larger than for roughness 2 (sparsely wooded country). The size of the separation bubble corresponded to the height of the models, and a higher inflation pressure reduced the size of the bubble, probably because it kept the model firmer and closer to a circular arc, whereas a low inflation pressure allowed the shape of the building to become more curved at the trailing edge and cause earlier separation.

4.3 COMPARISON BETWEEN THEORY AND EXPERIMENT

4.3.1 Choice of a Method for Matching Wind Profiles

The choice of the matching method for the wind profile (section 2.4.2) was based on the comparison between the theoretical and the experimental results for the pressure distribution for

the lowest model. The lowest model had a minimal flow separation, and this ensured that the choice of method would not be particularly effected by this source of error. A few results for various matching methods are given in Table 4. The theoretical results are compared with the experimental results for the lowest model and roughness 2 for the extremes of the pressure i.e. at the leading edge and at the top of the model. For the purpose of the comparison, the theoretical coefficients were mutliplied by $(U_s/U_\tau)^2$ so that they were based on the same velocity U_τ as the experimental C_p. The comparison is given in Table 4. Method 2, which matches velocity and slope at the top of the building, gives the best results, followed by method 1.

4.3.2 Tension

All the theoretical results were plotted on a graph of C_{p_τ} against C_{T_τ} and the value of $(\ell\text{-}c)/c$ was noted for each point plotted. Then by interpolation, lines of constant $(\ell\text{-}c)/c$ were plotted. These are compared with the experimental results in Figs. 46, 47. The discrepancy between experiment and theory ranges from ± 2 to ± 15 per cent.

The experimental results were expected to be close to the theoretical results found by Newman and Tse (ref. 6) for the case of small height-to-chord ratio, although in the present work the onset flow was not uniform. The coefficients C_{T_τ} and C_{p_τ} in the present experiment, were changed so that they were based on the onset velocity at the top of the model U_h at $y = h$ for the purpose of comparison.

$$C_{Th} = \frac{T}{\frac{1}{2}\rho U_h^2 c} \quad ; \quad C_{Ph} = \frac{P-p_\infty}{\frac{1}{2}\rho U_h^2}$$

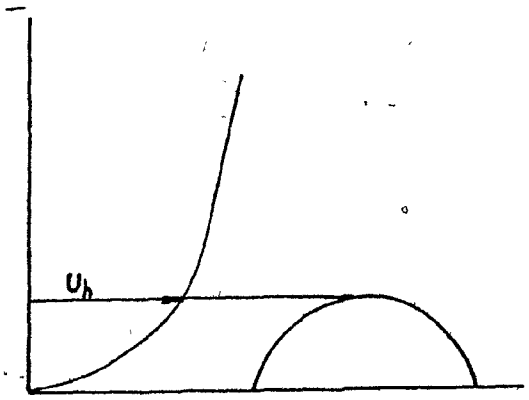

The results are given in Table 3. Comparison between the present experimental results and Newman and Tse's theoretical prediction of C_{Th} shows a 6 to 15 per cent difference for the lowest model and up to 32 per cent for the second lowest model.

The experimental C_{Th} is higher than the one predicted by Newman and Tse, possibly because the onset velocity above the top of the model was greater than U_h and caused the tension to be higher. The velocity below y = h was of course smaller than U_h, but must have had less influence of the tension.

4.3.3 Pressure Distribution

The computer program can only find $(\ell-c)/c$ from C_{Ts} and C_{Ps} and not the other way around (2.5.1). In order to find C_{Ts} for a specific combination of C_{Ps}, $(\ell-c)/c$ and $1/n$, a few runs were needed varying C_{Ts} slightly in each run, until the correct $(\ell-c)/c$ resulted.

For the combinations of C_{ps}, C_{Ts} and $\frac{\ell-c}{c}$ which were found, the pressure distributions are compared in Figs. 48 to 51.

The difference is as low as 5 per cent for the small height-to-chord ratio cases, far enough from the separation zones, for roughness 2. In other cases, the theoretical $C_{p\tau}$ results are a much poorer prediction of the experimental $C_{p\tau}$.

4.3.4 Reasons for the Discrepancies

In the cases where there are discrepancies between the experimental and the theoretical results, they may be attributed to two factors: a. The forming of separation bubbles at the leading and trailing edges. b. The onset flow approximation of the power law profile by a straight line profile.

4.3.4.1 Pressure Distribution

The largest discrepancy for the pressure distribution is near the trailing edge at the location of the larger separation bubble. It is evident from Fig. 28 to 37 that the pressure distribution is greatly affected by the trailing edge separation. Both the smaller separation bubble at the leading edge and the large separation bubble effect the pressure distribution over the whole model. They cause a displacement of the flow, so that the apparent chord is longer, which gives effectively a smaller height-to-chord ratio, thus causing the pressure distribution curve to flatten. Indeed, in Figs. 48 to 51 the absolute value of $C_{p\tau}$ is generally smaller for the experimental results than for the theoretical results.

4.3.4.2 Tension Coefficient

The theoretical C_{T_τ} was expected to be higher than the experimental for given C_{P_τ} and $(\ell-c)/c$, since the matched uniform vorticity profile had velocities which were greater than the actual onset velocities everywhere, as shown in the sketch.

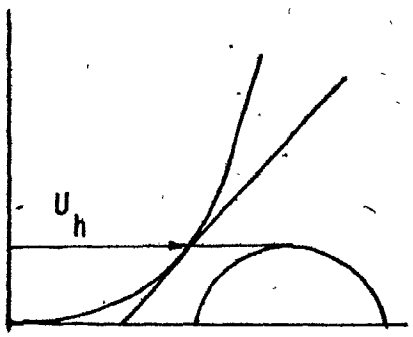

This proved to be true for roughness 1, but not for roughness 2. No explanation was found for the fact that for roughness 2 the theoretical tension coefficient was lower than the experimental tension coefficient, but it is possible that the separation bubbles which were present in the experiments caused somehow a higher tension.

5. CONCLUSIONS

5.1 EVALUATION OF THE RESULTS

Since buildings are typically in the wall-law region of the boundary layer, the tension in the membrane, the inflation gauge pressure and the external pressure distribution, which were measured in the experiments, were reduced to non-dimensional coefficients using the skin friction velocity. The results presented in this way for various height of building are convincing and show a consistent change of tension with height.

The completion of the span of the model using rigid dummies did not introduce a detectable error, and the assumption that the tension does not vary significantly along the membrane due to wind friction was confirmed by the experimental results.

The separation bubble at the leading edge was small and became smaller as the inflation pressure was reduced for a given membrane length. The separation bubble at the trailing edge was large, and it became larger as the inflation pressure was reduced.

Of the various methods which were tried to match a streaming flow with uniform vorticity to a wind profile with a power law, the method which required the slopes of both profiles at the height of the building to be the same, gave the best comparison between experiment and theory. The second best was the method which required the average dynamic pressure over the height of the building to be equal for both profiles.

The present theoretical results give a prediction of the tension within 2 to 15 per cent. The prediction of the pressure distribution for small height-to-chord ratio is fair for the region between the flow-separation zones. In other cases the prediction of surface pressure is less satisfactory.

The present theoretical results are in very good agreement with the previous work by Newman and Tse (ref. 6) for a small height-to-chord ratio, and the experimental results also give good agreement with this previous work.

5.2 PRACTICAL USE OF THE PRESENT WORK

The experimental results are useful for design of long cylindrical inflatable buildings in actual steady cross wind conditions, near open sea or in sparsely wooded country. Data for other types of terrain can be found by interpolation and extrapolation. The present theoretical method is useful for calculation of tension for any wind profile.

An intriguing aspect of the present work is that the internal pressure for low two-dimensional buildings may be decreased with increasing wind speed without encountering instability or collapse. If this behaviour is applied for a real building of finite length, then the membrane tension would be greatly reduced resulting in thinner membranes and reinforcing cables. To obtain these savings, the inflation pressure would be reduced as the wind speed increased, contrary to practice on other building shapes.

5.3 SUGGESTIONS FOR FURTHER WORK

The theoretical solution could be improved by taking into account the separation bubbles. This might be done by adding singularities at or near the leading and trailing edges which would give the separation and reattachment conditions found in the experiments.

Further experimental work could include measurement of the shape of the model and comparison with the theoretical shape. Smoke tunnel tests would give more information on the separation bubbles, and the results could be used in the theoretical representation of the bubbles.

A theoretical solution of a different character could be devised to solve the whole flow field outside the building in the actual onset flow with turbulence and viscosity. This would be a complete solution of the Navier-Stokes equations with a modelling of the turbulence, using a numerical method with iterations for the unknown portion of the boundary, i.e., the surface of the building. The solution would predict the flow separation and the asymmetry of the shape.

REFERENCES

1. T. Herzog — "Pneumatic Structures". Oxford University Press, New York, 1976.
2. F. Otto — "Tensile Structures". MIT Press English translation, 1973.
3. W.W. Bird — "Design Manual for Spherical Air Supported Radomes (Revised)". Cornell Aeronautical Laboratory Inc. Report No. UB-909-D-2.
4. E. Berger, E. Macher — "Results of Wind Tunnel Tests on some Pneumatic Structures". Proceedings of the First International Colloquium on Pneumatic Structures, Stuttgart, 1967.
5. H.J. Niemann — "Wind Tunnel Experiments on Models of Air Supported Structures". International Symposium on Pneumatic Structures, Delft, 1972.
6. B.G. Newman, M.-C. Tse — "Flow Past a Thin, Inflated, Lenticular Aerofoil". Journal of Fluid Mechanics, 1980.
7. A.G. Davenport — "The Relationship of Wind Structure to Wind Loading". Proceedings of 16th Symposium and Structures, National Physical Laboratory, England, 1963.
8. J.L. Hess, A.M.O. Smith — "Calculation of a Potential Flow about Arbitrary Bodies". Progress in Aeronautical Sciences, Vol. 8, Pergamon Press, London, 1967.

9. J.P. Giesing — "Potential Flow about Two-Dimensional Aerofoils". Douglas Aircraft Co. Report No. LB 31946, 1965.

10. T. Seebohm — "The Prediction of Viscous Flow Round Multiple Section Aerofoils". Ph.D. thesis, McGill University, 1972.

11. E.J. Plate — "Atmospheric Boundary Layer". U.S. Atomic Energy Commission, Office of Information Services, 1971.

12. N.J. Cook — "On Simulating the Lower Third of the Urban Adiabatic Boundary Layer in a Wind Tunnel". Atmospheric Environment, Pergamon Press, Vol. 7 pp. 691-705, 1973.

13. S. Campbell, N.M. Standen — Progress report II on "Simulation of Earth's Boundary Layer by Artifically Thickened Wind Tunnel Boundary Layers". N.R.C, Canada, NAE report LTR-LA-37, July 1969.

14. N.M. Standen — "A Spire Array for Generating Thick Turbulent Shear Layers for Natural Wind Simulation in Wind Tunnels". N.R.C. Canada, NAE report LTR-LA-94, May 1972. National Physical Laboratory Aero. Note 1055, May 1967.

15. I.S. Gartshore, K.A. De Croos — "Roughness Element Geometry Required for Wind Tunnel Simulations of the Atmospheric Wind". Journal of Fluids Engineering Vol. 99 Series I, No. 3. A.S.M.E. Publication, September 1977.

16. H.P.A.H. Irwin "The Longitudinal Cooling Correction for Wires Inclined to the Prongs and Some Turbulence Measurements in Fully Developed Pipe Flow". McGill University, Mechanical Engineering TN 72-1, December 1971.

17. R.C. Pankhurst "Wind Tunnel Techniques". Pitman Press, London, 1952.

18. L.M. Milne-Thomson "Theoretical Hydrodynamics". Fifth edition, The University Press, Glasgow.

19. D. Coles "The Law of the Wake in the Turbulent Boundary Layer". Journal of Fluid Mechanics, Vol. 1, 1956.

20. D.W. Smith
J.H. Walker "Skin Friction Measurements in Incompressible Flow". NACA, Technical Note 4231, March 1958.

APPENDIX I

Approximation of a Power Law Profile by a Streaming Flow of a Uniform Vorticity

The approximation was needed for the present method of theoretical solution which can handle a streaming flow with uniform vorticity and not an actual boundary layer of a power law profile.

Two unknowns are to be found: a and U_s (Fig. 1). Two assumptions were made for the matching (method 2):

1. The approaching velocity at the top of the building (y = h) is the same for both actual and idealized profiles.
2. The vorticity (or the slope) of the approaching onset velocity profile at the top of the building (y = h) is the same for both profiles.

The two conditions are expressed by

$$U_a\,(h) = U_b\,(h)$$

$$\left.\frac{dV_a}{dy}\right|_{y=h} = \left.\frac{dU_b}{dy}\right|_{y=h}$$

which results in the following equations:

$$U_e\,(\frac{y}{\delta})^{\alpha} = U_s\,(1 + \beta)$$

$$\frac{\alpha U_e}{\delta}\,(\frac{h}{\delta})^{\alpha-1} = \frac{U_s}{a}$$

where $\alpha = \frac{1}{n}$ and $\beta = \frac{h}{a}$

Simultaneous solution gives:

$$\beta = \frac{\alpha}{1-\alpha}$$

Results for the present experiments are given in the following table:

1/n	h/a
0.13	0.14943
0.24	0.31579

Note that U_e and δ which are used in this section may be a reference velocity and corresponding height on the power-law profile, and not necessarily the free stream velocity and the boundary layer thickness.

APPENDIX II

The Computer Program

I-1. Program notation

A(I, J)	Matrix of coefficients of influence.
AA	A constant in the onset profile VXF(I).
AL	Total length of the curve.
BB	Matching parameter.
CPI	Inflation pressure coefficient.
CP(I)	External pressure coefficient.
CPIL	$CPI/\sqrt{(\ell-c)/c}$.
D(I)	Right hand side of $\bar{A}\bar{x}=\bar{D}$.
DDY(I)	Local curvature.
N	Number of points on a quarter body.
R	Radius of curvature of the wind-off case.
SL(I)	A coordinate along the curve.
SS(I)	Strength of a source or sink element. Note: The strength of a source differs in this program from the conventional notation by a factor of 4π.
T	Coefficient of tension C_T.
VV(I)	Magnitude of the velocity at control point i.
VVX(I), VVY(I)	Components of velocity at control point i.
VX(I, J) VY(I, J)	Components of the velocity induced by the i-th element at the j-th control point.

VXE, VYE	The same as VX(I, J), VY(I, J) but in element coordinates.
VXF(I)	The onset flow velocity profile.
X(I), Y(I)	Coordinates of the control points (Fig. 5).
XI(I), YI(I)	Coordinates of the surface points (Fig. 5).
XE, YE	Coordinates in a system attached to an element.
XN(I), YN(I)	Components of a unit vector normal to the i-th element.
YC(I)	The sine of the angle between an element and the chord (sin θ).

I-2. Notes

1. Lines 21 to 30

Choice of points. Starting at the leading edge, the points are concentrated. Continuing to the next points, the length of the elements increases by a factor of 1.5. Ending at the centerline of the building, the points are sparse and the elements are of equal length.

2. Lines 42 to 54

Control points, length of elements, total length of curve, unit vectors normal to the elements and onset uniform shear flow are calculated.

3. Lines 60 to 64

The body has two axes of symmetry, therefore only a quarter of the body is considered and then reflected in the planes of symmetry to give three images.

4. Lines 84 to 86

Values are assigned to the matrix of coefficients of influence A_{ij} and the system of algebraic equations is solved, using a library subroutine, to find the strengths per unit length of the sources and sinks.

5. Lines 101, and 136 to 158

The local curvature is found by integration. First $\sin\theta$ is found and later y is found from θ. Subroutine ANTGL finds the area under a curve by approximating each three adjacent points by a parabola and by smoothing. The subroutine is good also for unequal increments of x.

6. Lines 102 and 105

The boundary conditions are incorporated into the result of the integration to give a new shape.

```
$WATFIV ,TIME=60,PAGES=60
C THE PREGRAM SOLVES THE PROBLEM OF AN  INFLATABLE EUILDING
C OPTION 1: IN A FIXED UNIFORM SHEAR FLOW
C OPTION 2: IN A FLOATING UNIFORM SHEAR FLOW WHICH MATCHES A GIVEN POWER PROFILE
C
C INPUT:
C TENSION COEFFICIENT                                                    T
C INFLATION PRESSUR COEFFICIENT                                          CPI
C EITHER THE SLOPE OF THE UNIFORM SHEAR PROFOLE                          AA
C OR THE MACHING PARAMETER FOR A POWER LAW PROFILE                       EB
C
C OUTPUT:
C THE LOCAL VELOCITY AT THE SURFACE OF THE BUILDING                      VC
C THE LOCAL PRESSURE COEFFICIENT                                         CP
C THE LOCAL CURVATURE
C THE LOCAL ANGLE BETWEEN THE BUILDING AND THE CHORD                     SIN(TH)
C THE LOCAL CHORDWISE COORDINATE                                         X
C THE LOCAL LENGTHWISE COORDINATE                                        S/L
C THE SHAPE OF THE BUILDING                                              YI, XI
C THE LENGTH OF THE BUILDING MEMBRANE                                    L
C THE CURRENT PROFILE SLOPE TO MATCH BUILDING HEIGHT (OPTION 2)          C/A
C
C ALL ITERATIONS ARE PRINTED. THE LAST ONE IS THE SOLUTION. UNLESS NO CONVERGE-
C NCE HAS BEEN ACHIEVED AFTER NL ITERATIONS.
C
      1       DOUBLE PRECISION A,B,WKAREA,D
      2       DIMENSION B(50,1)
      3       DIMENSION  WKAREA(50)
      4       DIMENSION  XI(50),YI(50),X(50),Y(50),ALF(50),DS(50),CP(50),VC(50),
             1 XN(50),YN(50),D(50),VX(50,50),VY(50,50),SS(50),A(50,50),DDY(50)
             2,VVX(50),VVY(50),VV(50),VXF(50)
      5       DIMENSION SL(50)
      6       PI=3.14159265E6
      7       BB=.3158
      8       NL=20
      9       DO 1234 IP=1,4
     10       READ  1235,T,CPI,AA
     11  1235 FORMAT(3F10.5)
     12       R=T/CPI
     13       RM=-SQRT(R*R-.25)
     C7 DATA FOR SUBROUTINE  LEQT2F (SOLVES SET OF LINEAR EQUATIONS)*********
     14       N=17
     15       M=1
     16       IA=50
     17       IDGT=5
     18       YM=0.
     19       NP1=N+1
     20       NM=N/2+1
C
C CHOICE OF POINTS, X COORDINATE
C
     21       NM5=N-5
     22       A1=.25/(1.5**NM5-1.)
     23       DO 1101 I=1,NM5
     24       XI(I)=A1*(1.5**(I-1)-1.)
     25  1101 CONTINUE
     26       XD=(.5-XI(NM5))/6.
     27       DO 1102 I=NM5,N
     28  1102 XI(I+1)=XI(NM5)+(I-NM5+1)*XD
     29       DO 1100 I=1,NP1
```

```
      XI(I)=XI(I)-.5
      YY=R*R      -XI(I)**2
C
C CALCULATION OF INITIAL SHAPE, Y COORDINATE
C
      YI(I)=SQRT(YY)+RM
1100  CONTINUE
      DO 1 MM=1,NL
      AL=0.
      PRINT1001
1001  FORMAT('1',T15,'X',T35,'Y',T55,'VC',T75,'CP',T95,'YI(NEW)',
     1 T115,'XI'//)
      DO 40 I=1,N
      DO 40 J=1,N
      VX(I,J)=0.
40    VY(I,J)=0.
C
C CALCULATION OF SURFACE ELEMENTS AND ONSET FLOW PROFILE
C
      DO 12 I=1,N
      X(I)=(XI(I)+XI(I+1))*.5
      Y(I)=(YI(I)+YI(I+1))*.5
      DX=XI(I+1)-XI(I)
      DY=YI(I+1)-YI(I)
      DS(I)=SQRT(DX*DX+DY*DY)
      AL=AL+2.*DS(I)
      SL(I)=AL/2.-DS(I)/2.
      ALF(I)=ATAN2(DY,DX)
      XN(I)=-SIN(ALF(I))
      YN(I)=COS(ALF(I))
      VXF(I)=1.     +ABS(Y(I))*AA
      D(I)=-XN(I)*VXF(I)
      B(I,1)=D(I)
12    CONTINUE
C
C CALCULATION OF THE COEFFICIENTS OF INFLUENCE
C
      DO 100 I=1,N
      DO 100 J=1,N
      DO 50 K=1,2
      INDX=-2*K+3
      DO 50 L=1,2
      INDY=-2*L+3
      S=INDX*SIN(ALF(J))
      C=INDY*COS(ALF(J))
      IF(INDY.EQ.-1) GO TO 3
      IF(INDX.EQ.-1) GO TO 3
      IF(I.NE.J) GO TO 3
      VXE=0.
      VYE=2.*PI
      GO TO 4
C
C TRANSFORMATION TO ELEMENT COORDINATES
C
3     XX=X(I)-X(J)*INDY
      YY=Y(I)-Y(J)*INDX
      XE=XX*C+YY*S
      YE=-XX*S+YY*C
      AN=(XE+.5*DS(J))**2+YE*YE
      AD=(XE-.5*DS(J))**2+YE*YE
```

```
      BN=YE*DS(J)
      BD=XE*XE+YE*YE-(.5*DS(J))**2
      VXE=ALOG(AN/AD)
      VYE=2.*ATAN2(BN,BD)
C
C TRANSFORMATION BACK TO BODY COORDINATES
C
    4 VX(I,J)=(VXE*C-VYE*S)*INDY +VX(I,J)
      VY(I,J)=(VXE*S+VYE*C)*INDY +VY(I,J)
   50 CONTINUE
      A(I,J)      =XN(I)*VX(I,J)+YN(I)*VY(I,J)
  100 CONTINUE
  300 CALL LEQTIF(A,M,N,IA,B,IDGT,WKAREA,IER)
C
C CALCULATION OF VELOCITIES AND CP
C
      DO 30 I=1,N
   30  SS(I)=B(I,1)
      DO 20 I=1,N
      VVX(I)=0.
   20 VVY(I)=0.
      DO 22 I=1,N
      DO 21 J=1,N
      VVX(I)=VVX(I)+VX(I,J)*SS(J)
   21 VVY(I)=VVY(I)+VY(I,J)*SS(J)
   22 VV(I)=SQRT((VVX(I)+VXF(I))**2+VVY(I)**2)
      DO 103 I=1,N
      CP(I)=1.-VV(I)**2
C
C CALCULATION OF THE  SHAPE FROM CP
C
      DDY(I)=(CP(I)-CPI)/T
  103 CONTINUE
      CALL ANTGL(N,X,DDY,YC)
C ***********************************************YC(I)=SIN (TH)
      DO 102 I=1,N
      YC(I)= YC(I)    -YC(N)
      YI(I+1)=YI(I)+(XI(I+1)-XI(I))/SQRT(1.-YC(I)**2)*YC(I)
  102 CONTINUE
      IF(AL.LT.1.0000001) GO TO 83
      CPIL=CPI/SQRT(AL-1.)
   83 DO 80 I=1,N
   80 PRINT 1000,X(I),Y(I),VV(I),CP(I),YI(I),XI(I)
 1000 FORMAT(6(10X,F10.5))
      PRINT 81,YI(NP1),XI(NP1)
   81 FORMAT(80X,2(10X,F10.5))
      PRINT 1002 ,IER ,IDGT
 1002 FORMAT(//3X,'IER=',I5/3X,'IDGT=',I5)
      PRINT 1003,T,CPI,AL
 1003 FORMAT(//3X,'CT=',F10.5,10X,'CPI=',F10.5,10X,'L(OLD)=',F10.5)
      PRINT 1004,AA, CPIL,MM
 1004 FORMAT(' - C/A=',F10.5,5X,'  CPI/SQRT(E)=',F10.5,40X,'ITR/ NO.=',I2)
      PRINT 1005
 1005 FORMAT (//T15,'S/L',T35,'CP    ',T52,'CURVATURE',T75,'SIN(TH)'/)
      DO 82 I=1,N
      SOL=SL(I)/AL
   82 PRINT 1000,SOL,CP(I),DDY(I),YC(I)
      EPS=ABS(YM-YI(NP1))
      IF(EPS.LE.0.00001) GO TO 999
      YM=YI(NP1)
```

```
C
C ADJUSTMENT OF THE SLOPE OF THE UNIFORM SHEAR PROFILE (OPTION 2)
C FOR OPTION 1 REMOVE THE FOLLOWING STATEMENT
C
      AA=BB/YM
      IF(YM.GT.1.) GO TO 999
1     CONTINUE
999   CALL PLOTI(XI,YI,NP1,90)
1234  CONTINUE
      STOP
      END


      SUBROUTINE ANTGL(N,X,Y,SF)
C
C THE SUBROUTINE INTEGRATES USING A QUADRATIC SPLINE WITH SMOOTHING
C
      DIMENSION X(50),Y(50),SF(50),AAA(50),BBB(50),CCC(50)
      NM1=N-1
      DO 70 I=2,NM1
      FF=X(I)-X(I+1)
      QQ=X(I)**2-X(I+1)**2
      PP=X(I+1)*X(I)**2-X(I)*X(I+1)**2
      DET=FF*X(I-1)**2-QQ*X(I-1)+PP
      AAA(I)=(Y(I-1)*FF-X(I-1)*(Y(I)-Y(I+1))
     1+Y(I)*X(I+1)-Y(I+1)*X(I))/DET
      BBB(I)=((Y(I)-Y(I+1))*X(I-1)**2-Y(I-1)*QQ
     1+Y(I+1)*X(I)**2-Y(I)*X(I+1)**2)/DET
      CCC(I)=((X(I)*Y(I+1)-X(I+1)*Y(I))*X(I-1)**2
     1-X(I-1)*(Y(I+1)*X(I)**2-Y(I)*X(I+1)**2)
     2+Y(I-1)*PP)/DET
70    CONTINUE
      AAA(1)=AAA(2)
      BBB(1)=BBB(2)
      CCC(1)=CCC(2)
      AAA(N)=AAA(N-1)
      BBB(N)=BBB(N-1)
      CCC(N)=CCC(N-1)
      SF(1)=0.
      DO 71 I=1,NM1
      DF=(AAA(I)+AAA(I+1))*(X(I+1)**3-X(I)**3)/6.
     1-(BBB(I)+BBB(I+1))*(X(I)**2-X(I+1)**2)/4.
     1-(CCC(I)+CCC(I+1))*(X(I)-X(I+1))/2.
      SF(I+1)=SF(I)+DF
71    CONTINUE
      RETURN
      END

      $DATA
*EXTENSION* PSEUDO VARIABLE DIMENSIONING ASSUMED FOR ARRAY WKAREA
*EXTENSION* PSEUDO VARIABLE DIMENSIONING ASSUMED FOR ARRAY B
*EXTENSION* PSEUDO VARIABLE DIMENSIONING ASSUMED FOR ARRAY A
*EXTENSION* PSEUDO VARIABLE DIMENSIONING ASSUMED FOR ARRAY EQUIL
*EXTENSION* PSEUDO VARIABLE DIMENSIONING ASSUMED FOR ARRAY IPVT
*EXTENSION* PSEUDO VARIABLE DIMENSIONING ASSUMED FOR ARRAY LU
*EXTENSION* PSEUDO VARIABLE DIMENSIONING ASSUMED FOR ARRAY A
*EXTENSION* PSEUDO VARIABLE DIMENSIONING ASSUMED FOR ARRAY X
*EXTENSION* PSEUDO VARIABLE DIMENSIONING ASSUMED FOR ARRAY IPVT
*EXTENSION* PSEUDO VARIABLE DIMENSIONING ASSUMED FOR ARRAY B
```

X	Y	VC	CP	YI(NEW)	XI
-0.49951	0.00022	0.42227	0.82169	0.00000	-0.50000
-0.49830	0.00078	0.50214	0.74786	0.00048	-0.49903
-0.49648	0.00161	0.56232	0.68379	0.00120	-0.49757
-0.49375	0.00284	0.61658	0.61982	0.00228	-0.49539
-0.48955	0.00468	0.66978	0.55140	0.00390	-0.49211
-0.48351	0.00740	0.72434	0.47534	0.00631	-0.48720
-0.47429	0.01140	0.78182	0.38875	0.00989	-0.47982
-0.46047	0.01723	0.84359	0.28835	0.01516	-0.46876
-0.43973	0.02558	0.91062	0.17077	0.02287	-0.45218
-0.40863	0.03724	0.98348	0.03277	0.03392	-0.42725
-0.36197	0.05286	1.06134	-0.12643	0.04932	-0.38997
-0.30615	0.06906	1.13136	-0.27997	0.06966	-0.33398
-0.25049	0.08235	1.18277	-0.39895	0.08653	-0.27832
-0.19482	0.09287	1.22083	-0.49043	0.10004	-0.22265
-0.13916	0.10070	1.24792	-0.55730	0.11017	-0.16699
-0.08350	0.10590	1.26539	-0.60121	0.11693	-0.11133
-0.02783	0.10848	1.27396	-0.62298	0.12031	-0.05566
				0.12031	0.00000

ERR= 0
IDET= 5

CT= 2.40000 CPI= 2.00000 L(OLD)= 1.03138
C/A= 0.00000 CPI/SQRT(E)= 11.29013 ITR NO.= 1

S/L	CP	CURVATURE	SIN(TH)
0.00052	0.82169	-0.49096	0.44427
0.00181	0.74786	-0.52173	0.44382
0.00375	0.68379	-0.54842	0.44315
0.00666	0.61982	-0.57507	0.44212
0.01101	0.55140	-0.60358	0.44014
0.01753	0.47534	-0.63528	0.43663
0.02727	0.38875	-0.67135	0.43074
0.04181	0.28835	-0.71319	0.42122
0.06389	0.17077	-0.76218	0.40594
0.09570	0.03277	-0.81968	0.38131
0.14341	-0.12643	-0.88601	0.34146
0.19979	-0.27997	-0.94999	0.29014
0.25529	-0.39895	-0.99956	0.23582
0.31023	-0.49043	-1.03768	0.17907
0.36475	-0.55730	-1.06554	0.12049
0.41897	-0.60121	-1.08384	0.06063
0.47301	-0.62298	-1.09291	0.00000

X	Y	VC	CP	YI(NEW)	XI
-0.49951	0.00041	0.19102	0.96351	0.00000	-0.50000
-0.49830	0.00142	0.25075	0.93713	0.00081	-0.49903
-0.49648	0.00294	0.30599	0.90637	0.00203	-0.49757
-0.49375	0.00522	0.36156	0.86928	0.00385	-0.49535
-0.48965	0.00863	0.42155	0.82229	0.00658	-0.49211
-0.48251	0.01371	0.48933	0.76056	0.01067	-0.48720
-0.47429	0.02125	0.56834	0.67699	0.01675	-0.47982
-0.46047	0.03237	0.66379	0.55938	0.02576	-0.46876
-0.43973	0.04857	0.78332	0.38641	0.03900	-0.45218
-0.40863	0.07171	0.93852	0.11918	0.05818	-0.42729
-0.36197	0.10356	1.14678	-0.31509	0.08531	-0.38997
-0.30615	0.13735	1.37405	-0.88801	0.12191	-0.33398
-0.25049	0.16546	1.58299	-1.50587	0.15293	-0.27832
-0.19482	0.18759	1.76305	-2.10835	0.17816	-0.22265
-0.13916	0.20345	1.89796	-2.60225	0.19723	-0.16699
-0.08350	0.21299	1.96804	-2.87319	0.20995	-0.11133
-0.02783	0.21614	1.93904	-2.75988	0.21625	-0.05566
				0.21625	0.00000

ITER= 0
IDGT= 5

CT= 2.40000 CPI= 2.00000 L(OLD)= 1.11713
A= 1.46108 CPI/SQRT(E)= 5.84387 ITR NO.=10

S/L	CP	CURVATURE	SIN(TH)
0.00057	0.96351	-0.43187	0.64098
0.00198	0.93713	-0.44286	0.64093
0.00411	0.90637	-0.45568	0.64089
0.00729	0.86928	-0.47113	0.64050
0.01206	0.82229	-0.49071	0.63907
0.01920	0.76056	-0.51643	0.63635
0.02986	0.67699	-0.55125	0.63162
0.04574	0.55938	-0.60026	0.62371
0.06929	0.38641	-0.67233	0.61053
0.10400	0.11918	-0.78368	0.58791
0.15458	-0.31509	-0.96462	0.54720
0.21303	-0.88801	-1.20333	0.48675
0.26890	-1.50587	-1.46078	0.41267
0.32258	-2.10835	-1.71181	0.32425
0.37447	-2.60225	-1.91760	0.22292
0.42510	-2.87319	-2.03050	0.11245
0.47509	-2.75988	-1.98328	0.00000

X	Y	VC	CP	YI(NEW)	XI
-0.49951	0.00041	0.19095	0.96354	0.00000	-0.50000
-0.49830	0.00142	0.25059	0.93720	0.00081	-0.49903
-0.49648	0.00294	0.30577	0.90651	0.00202	-0.49757
-0.49375	0.00522	0.36137	0.86941	0.00384	-0.49535
-0.48965	0.00863	0.42139	0.82243	0.00656	-0.49211
-0.48351	0.01371	0.48904	0.76084	0.01065	-0.48720
-0.47429	0.02125	0.56806	0.67731	0.01674	-0.47932
-0.46047	0.03238	0.66356	0.55969	0.02575	-0.46876
-0.43973	0.04859	0.78312	0.38673	0.03899	-0.45218
-0.40863	0.07174	0.93835	0.11950	0.05817	-0.42729
-0.36197	0.10361	1.14666	-0.31482	0.08531	-0.39597
-0.30615	0.13742	1.37401	-0.88789	0.12192	-0.35398
-0.25049	0.16554	1.58306	-1.50607	0.15294	-0.32832
-0.19482	0.18769	1.76323	-2.10899	0.17817	-0.22268
-0.13916	0.20359	1.89826	-2.60339	0.19725	-0.16699
-0.08350	0.21310	1.96842	-2.87466	0.20999	-0.11133
-0.02783	0.21625	1.93940	-2.76126	0.21629	-0.05566
				0.21629	0.00000

IER= 0
IDGT= 5

CT= 2.40000 CPI= 2.00000 L(OLD)= 1.11723
C/A= 1.46032 CPI/SQRT(E)= 5.84121

ITR NO.=11

S/L	CP	CURVATURE	SIN(TH)
0.00057	0.96354	-0.43186	0.64016
0.00198	0.93720	-0.44283	0.63983
0.00410	0.90651	-0.45562	0.63946
0.00729	0.86941	-0.47108	0.63958
0.01206	0.82243	-0.49065	0.63924
0.01919	0.76084	-0.51632	0.63854
0.02985	0.67731	-0.55112	0.63717
0.04574	0.55969	-0.60013	0.63377
0.06930	0.38673	-0.67220	0.61060
0.10401	0.11950	-0.78354	0.58800
0.15459	-0.31482	-0.96451	0.54729
0.21305	-0.88789	-1.20329	0.48608
0.26891	-1.50607	-1.46086	0.41277
0.32259	-2.10899	-1.71208	0.32434
0.37448	-2.60339	-1.91808	0.22299
0.42511	-2.87466	-2.03111	0.11249
0.47509	-2.76126	-1.98386	0.00000

X	Y	VC	CP	YI(NEW)	XI
-0.49951	0.00040	0.19114	0.96347	0.00000	-0.50000
-0.49830	0.00142	0.25076	0.93712	0.00081	-0.49903
-0.49648	0.00293	0.30576	0.90651	0.00202	-0.49757
-0.49375	0.00520	0.36101	0.86967	0.00383	-0.49539
-0.48965	0.00851	0.42086	0.82288	0.00655	-0.49211
-0.48351	0.01369	0.48873	0.76115	0.01064	-0.48720
-0.47429	0.02124	0.56786	0.67753	0.01672	-0.47982
-0.46047	0.03237	0.66339	0.55991	0.02573	-0.46876
-0.43973	0.04858	0.78296	0.38697	0.03897	-0.45218
-0.40853	0.07174	0.93821	0.11976	0.05816	-0.42725
-0.36197	0.10361	1.14655	-0.31458	0.08529	-0.38997
-0.30615	0.13743	1.37394	-0.88770	0.12191	-0.33398
-0.25049	0.16556	1.58304	-1.50602	0.15294	-0.27832
-0.19482	0.18771	1.76328	-2.10916	0.17816	-0.22265
-0.13916	0.20362	1.89837	-2.60379	0.19725	-0.16699
-0.08350	0.21314	1.96856	-2.87522	0.20999	-0.11133
-0.02783	0.21629	1.93953	-2.76178	0.21629	-0.05566
				0.21629	0.00000

IER= 0
IDGT= 5

CT= 2.40000 CPI= 2.00000 L(OLD)= 1.11726
/A= 1.46009 CPI/SQRT(E)= 5.84052 ITR NO.=12

S/L	CP	CURVATURE	SIN(TH)
0.00057	0.96347	-0.43189	0.63915
0.00198	0.93712	-0.44287	0.63875
0.00410	0.90651	-0.45562	0.63862
0.00728	0.86967	-0.47097	0.63934
0.01205	0.82288	-0.49047	0.63919
0.01918	0.76115	-0.51619	0.63645
0.02985	0.67753	-0.55103	0.63168
0.04573	0.55991	-0.60004	0.62378
0.06929	0.38697	-0.67210	0.61063
0.10400	0.11976	-0.78343	0.58802
0.15459	-0.31458	-0.96441	0.54732
0.21305	-0.88770	-1.20321	0.48691
0.26891	-1.50602	-1.46084	0.41280
0.32260	-2.10916	-1.71215	0.32437
0.37449	-2.60379	-1.91825	0.22301
0.42511	-2.87522	-2.03134	0.11250
0.47509	-2.76178	-1.98408	0.00000

APPENDIX III

Design of the Spires

The spires are obstacles which are placed in a wind tunnel upstream of the model in one row across the tunnel to cause the boundary layer to be artificially thickened and assume a prescribed profile.

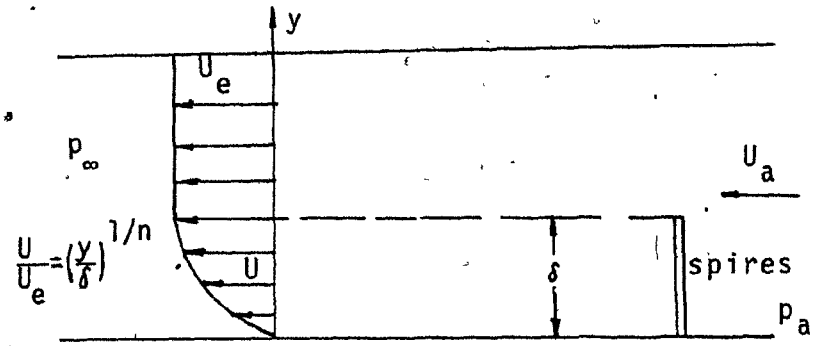

A power law boundary layer is needed with prescribed δ and n.

The height of the spires is equal to the boundary layer thickness δ. The spires are placed at a distance of at least 6δ from the model, since it takes this distance for the boundary layer to become fully developed (ref. 14). The spacing between the spires should be no more than $d = \frac{1}{2}\delta$ (ref. 13).

The calculation of the spires is based on the calculation of grids made of wires. The overall-pressure-drop coefficient K_1 across grids is now applied to spires:

$$K_1 = \frac{p_a - p_\infty}{\frac{1}{2}\rho U_a^2}$$

where p_a and U_a are the static pressure and the velocity upstream of the spires.

Applying the momentum equation to a layer of fluid at height y and using a local drag coefficient K which is a function of y

$$K_1 = (1 + K) \left(\frac{U}{U_a}\right)^2 - 1 \qquad \text{(III-1)}$$

K can be written in terms of the local solidity of the spires and a drag coefficient C_d of a two-dimensional flat plate with a width equal to the local width of the spire. The coefficient C_d equals 1.98 and is based of the average velocity of the flow between the spires, since this is the velocity which affects the wake behind the spires and therefore the drag.

$$K = \frac{1.98S}{(1-S)^2} \qquad \text{(III-2)}$$

where $S = W(y)/d$ is the local ratio of the solid area to the total area. $W(y)$ is the local width of the spire. For $y>\delta$ the flow is uniform: $U = U_e$ and $K = 0$, which reduces equation (III-1) to

$$1 + K = \left(\frac{U_e}{U}\right)^2 \qquad \text{(III-3)}$$

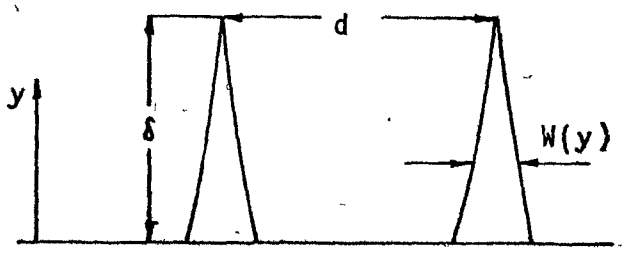

Using the velocity profile

$$\frac{U}{U_e} = \left(\frac{y}{\delta}\right)^{1/n}$$

and equations (III-2) and (III-3), S was calculated as a function of y, and by choosing d, W(y) was found.

It was found empirically (ref. 14) that in order to achieve a prescribed value 1/n, the design should be done with (1/n-.04).

As the upper part of the spires that are calculated is too narrow for practical application, the calculation is done for slightly higher spires of length δ' and then the extra length is chopped off.

The following data were taken as design values:

δ = 1.0 m 1/n = 0.16

d = 0.4 m δ' = 1.10 m

number of spires is 4.

Roughness No.	Power 1/n	U_τ [m/s] hot wire	U_τ [m/s] law of the wall	U_τ [m/s] velocity defect law	U_e [m/s]
1	0.13	0.33	0.24	0.23	7.9
2	0.24	0.37	0.34	0.36	7.5

Table 1: Experimental Wind Profile

Terrain	near open sea	flat open country	sparsely wooded country	wooded country	urban center
1/n	0.13	0.16	0.24	0.28	0.40
δ[m]	250	275	360	400	525
U_{10}/U_τ	15.9	12.1	6.15	4.65	1.98

Table 2: Natural Wind Data

(Based on ref. 7)

$\frac{h}{c}$	1/n	$\frac{C_{Ph}}{\sqrt{(\ell-c)/c}}$	experimental C_{Th}	theoretical C_{Th}	$\frac{C_{Th}(exp)}{C_{Th}(th)}$
0.186	0.13	6.99	2.075	1.95	1.06
		4.01	1.367	1.3	1.05
		6.23	1.871	1.75	1.06
		4.98	1.576	1.5	1.05
		2.07	0.925	0.92	1.005
0.186	0.24	18.8	4.86	4.3	1.13
		16.0	4.21	3.7	1.14
		14.4	3.91	3.4	1.15
0.246	0.24	15.1	4.45	3.55	1.25
		10.8	3.63	2.75	1.32

Table 3: Comparison between tension coefficient from thin aerofoil theory (ref. 6) and tension coefficient from present experiments based on U_h.

	$C_{p\tau}$ max	$C_{p\tau}$ min	$C_{T\tau}$
Experimental	35	-109	225
Theoretical, using matching method			
1	48.2	-115	220
2	44.5	-110	201
3	50	-116	218
4	58	-121	223
5	69	-138	182

Table 4: Comparison of five methods for matching a flow with a uniform vorticity to a wind velocity profile.
$(\ell-c)/c = 0.090$, $C_{p\tau} = 209$, $1/n = 0.24$

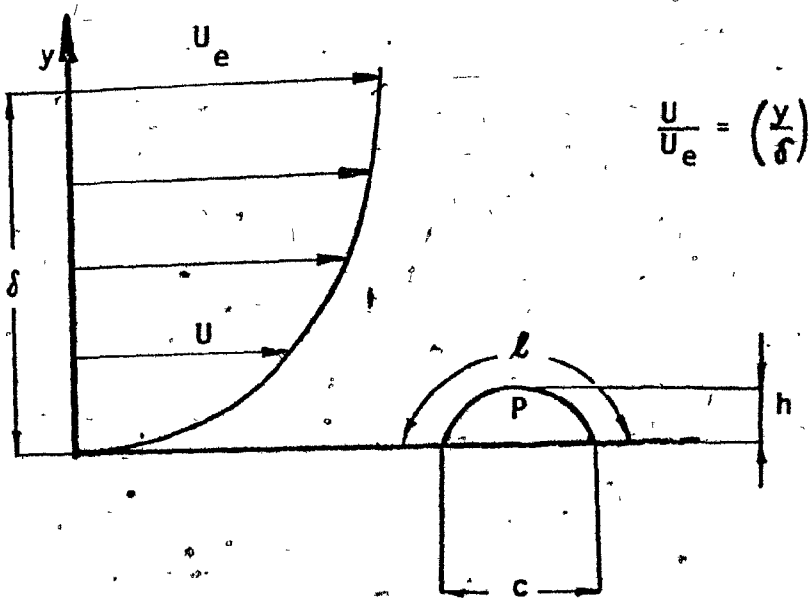

(a)

$$\frac{U}{U_e} = \left(\frac{y}{\delta}\right)^{1/n}$$

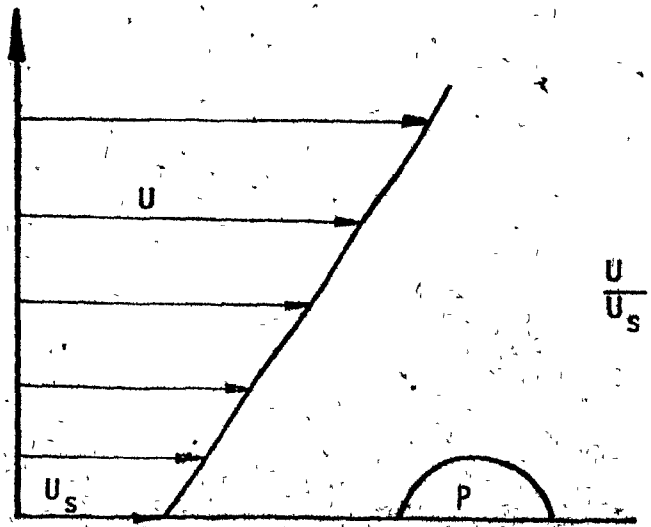

(b)

$$\frac{U}{U_s} = 1 + \frac{y}{a}$$

Fig. 1: Wind Profiles: (a) Actual (b) Idealized

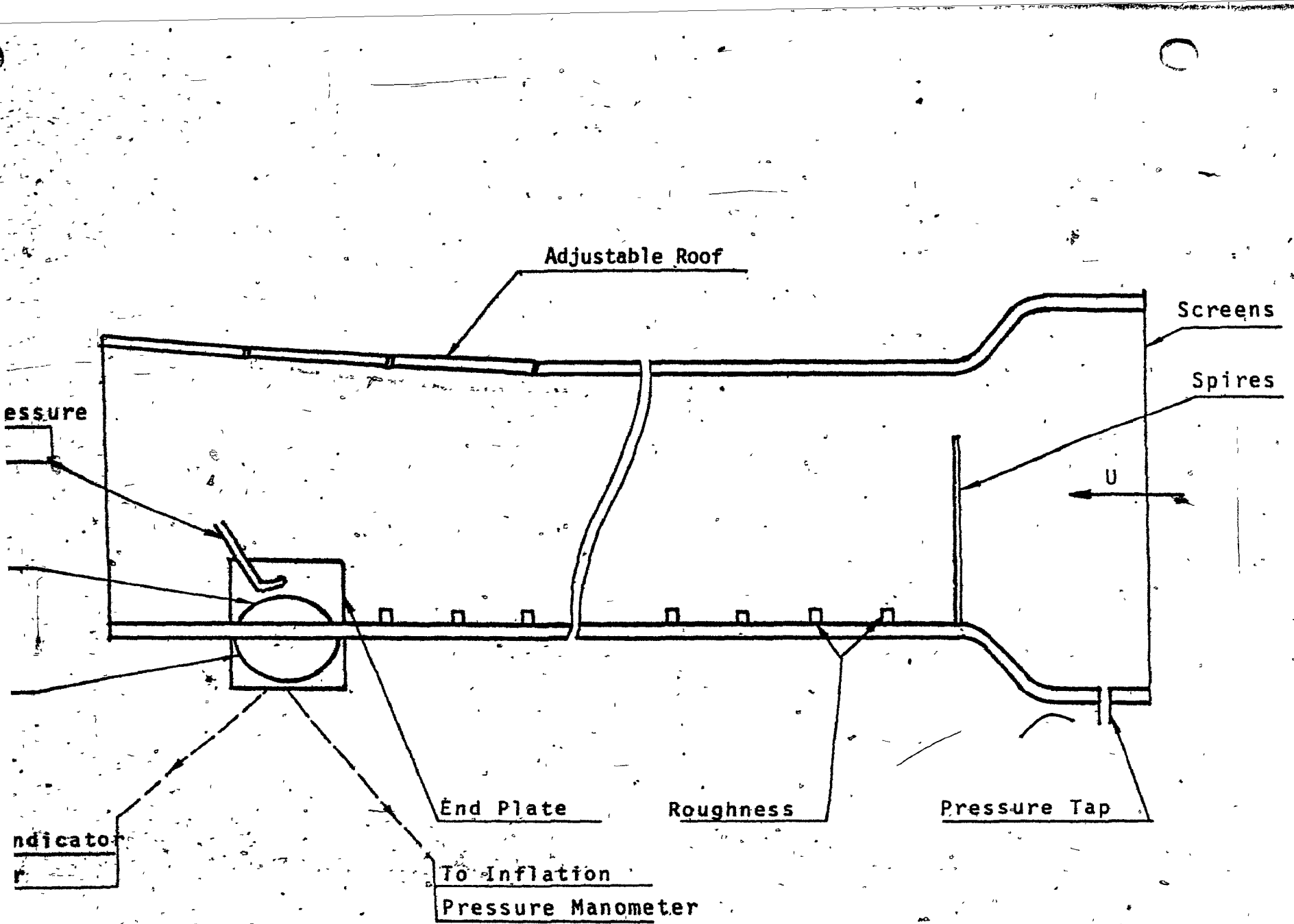

Fig. 2: Wind Tunnel Setup

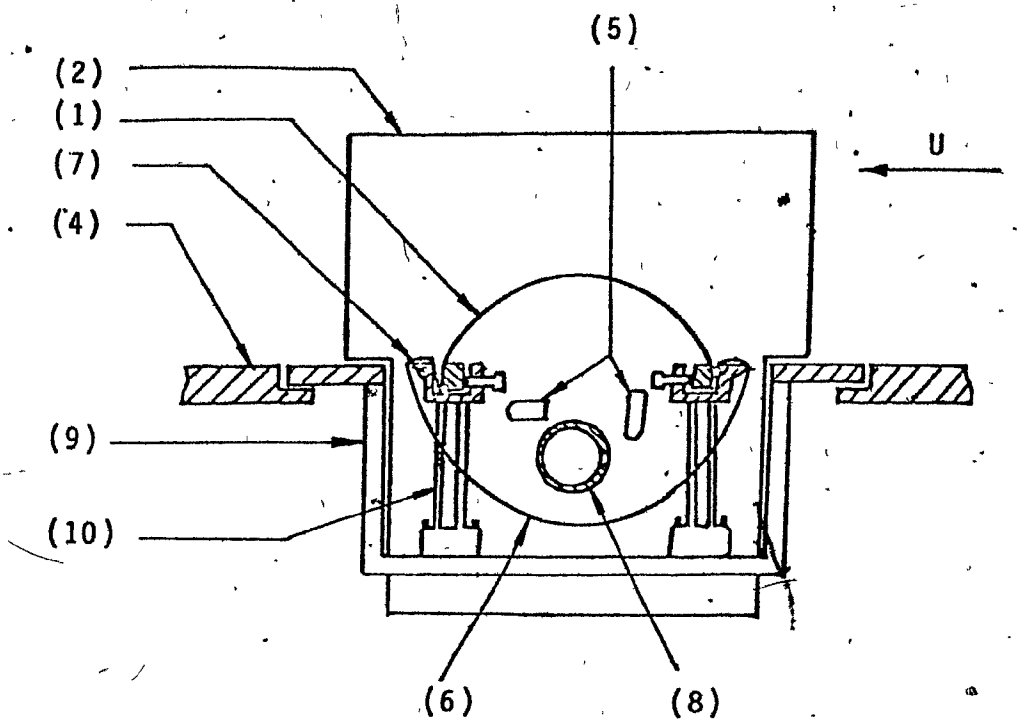

SECTION A-A

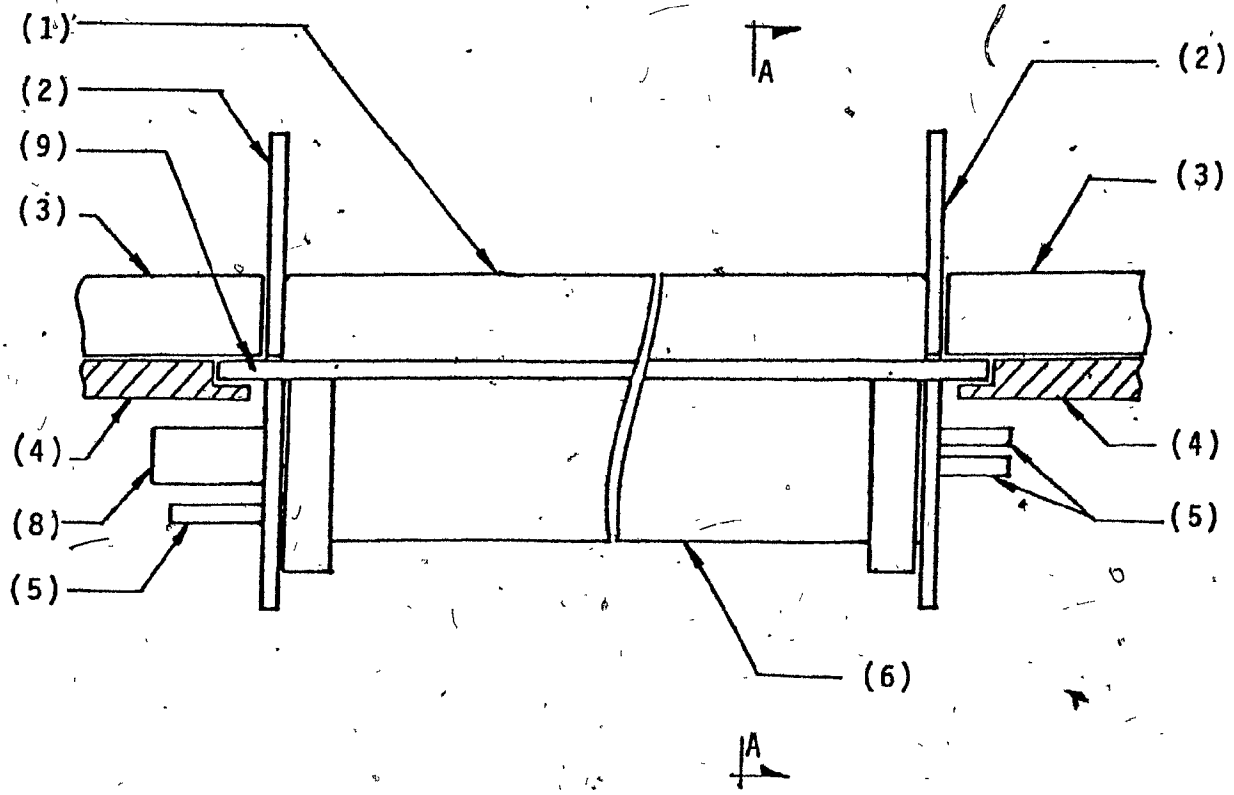

Fig. 3: The Model

(For part list see Fig. 3a)

Part Number	Part Name	Quantity
1	model	1
2	end-plate	2
3	rigid dummy	2
4	wind tunnel floor	1
5	pressure tubes	3
6	seal	1
7	clamp	2
8	inflation-air pipe	1
9	frame	1
10	flexure	4

Figure 3a: Part list

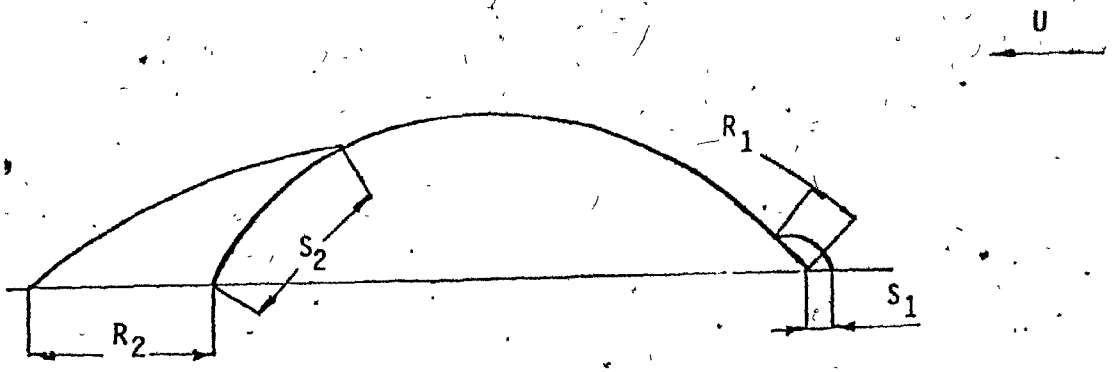

Fig. 4: Separation and Reattachment

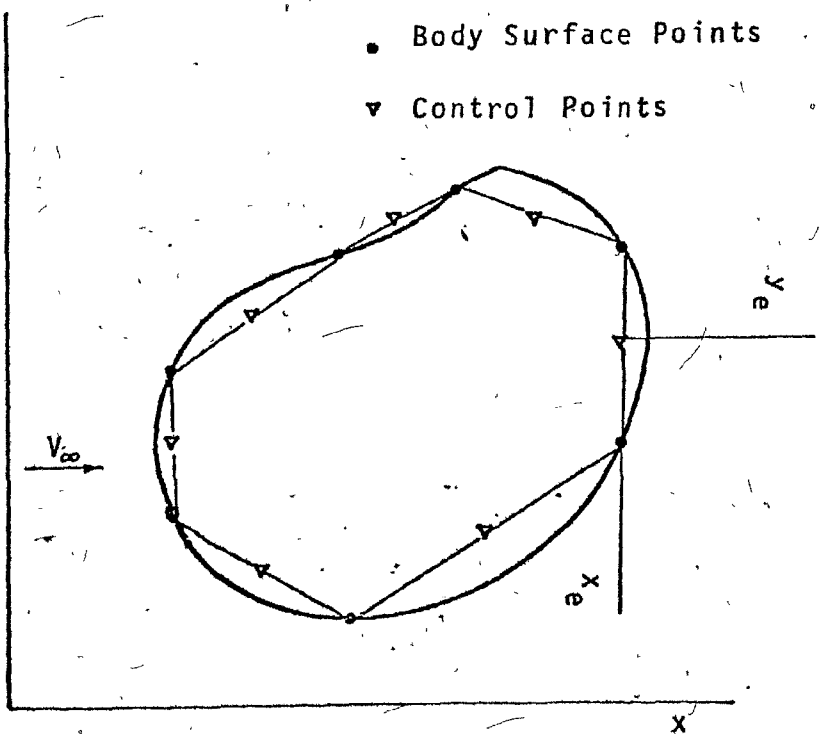

Fig. 5: Discretization of the Body

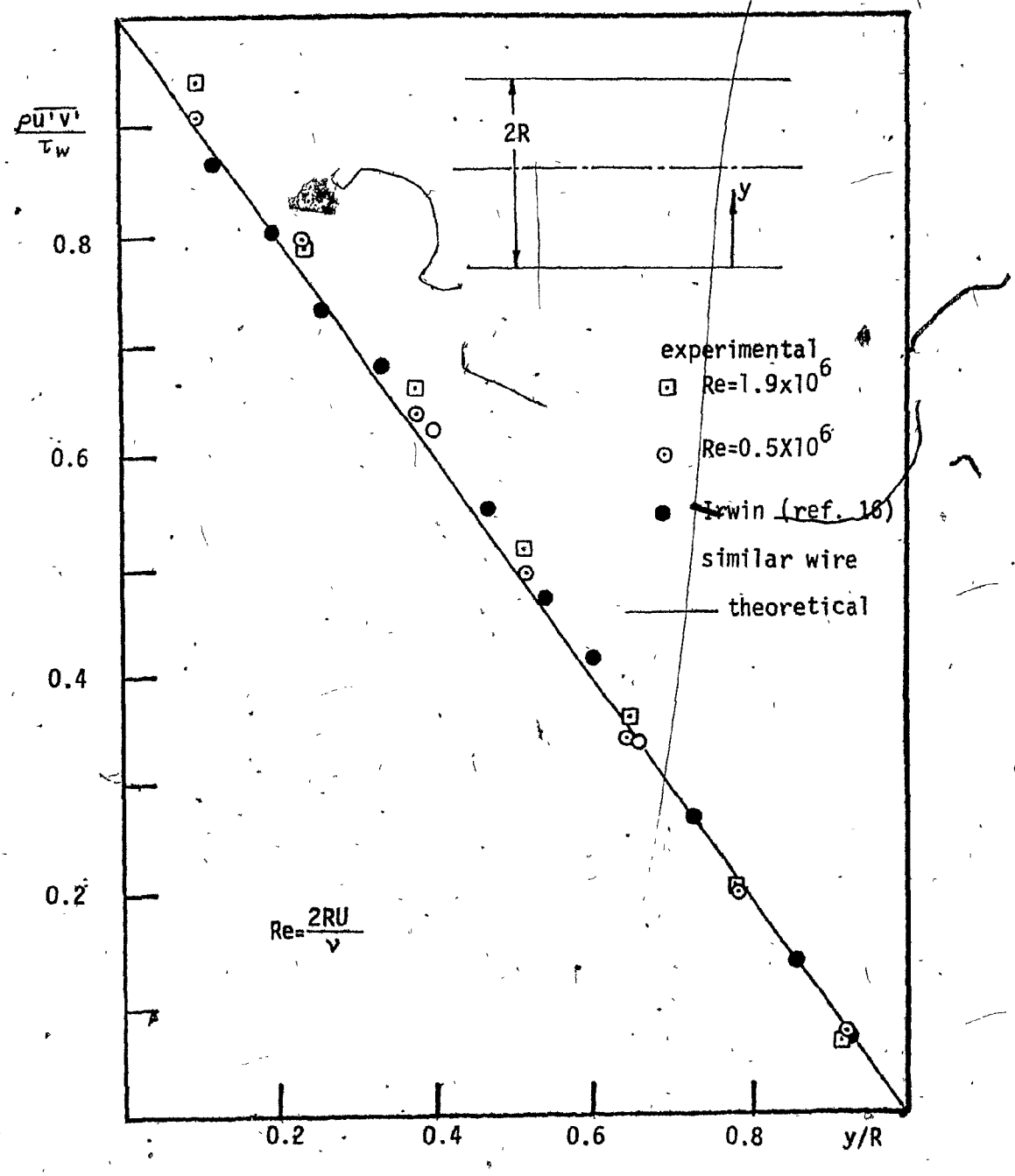

Fig. 6: Check of hot-wire system.
Turbulent flow in a smooth pipe.

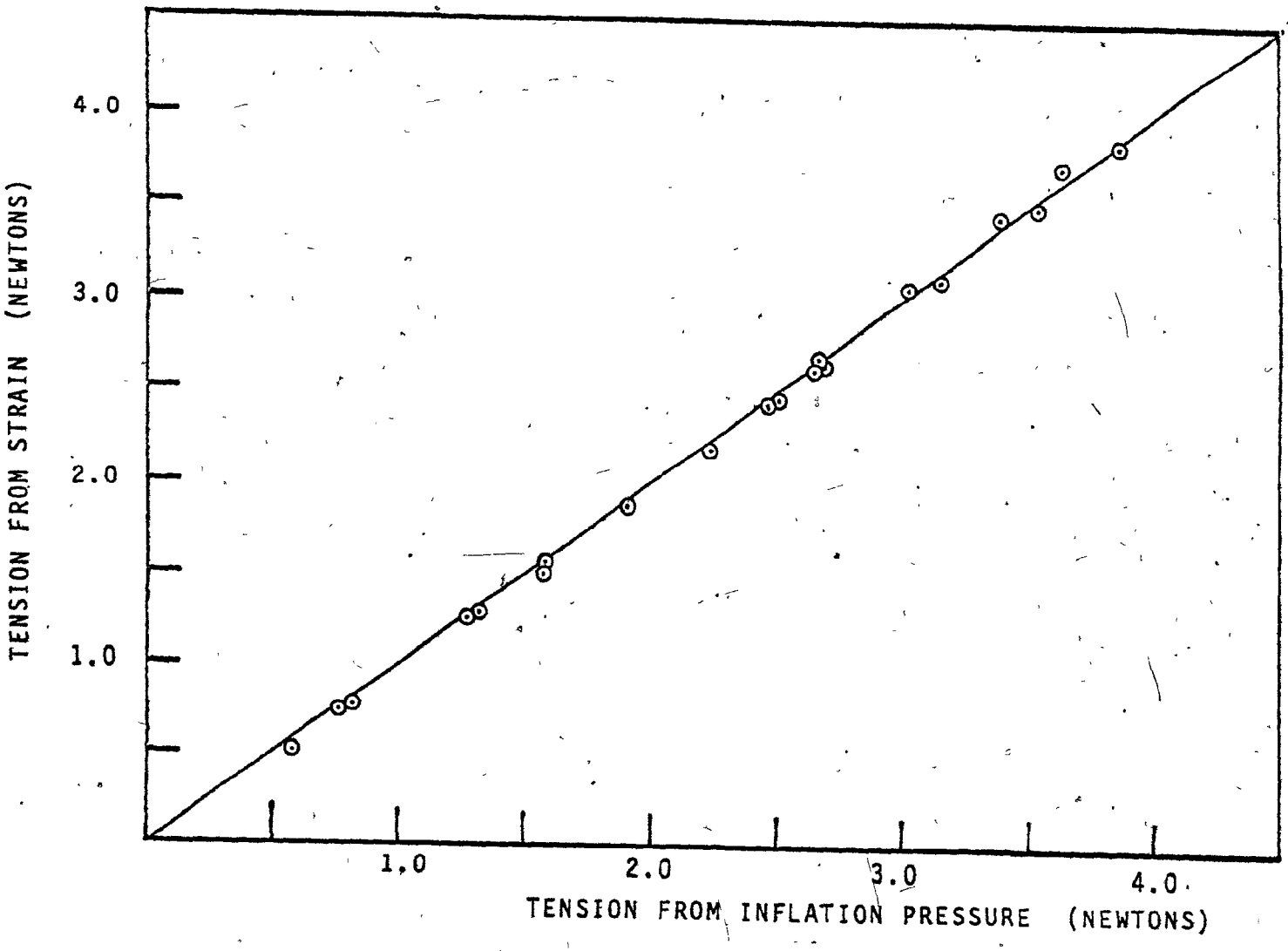

Fig. 7: Wind-off results

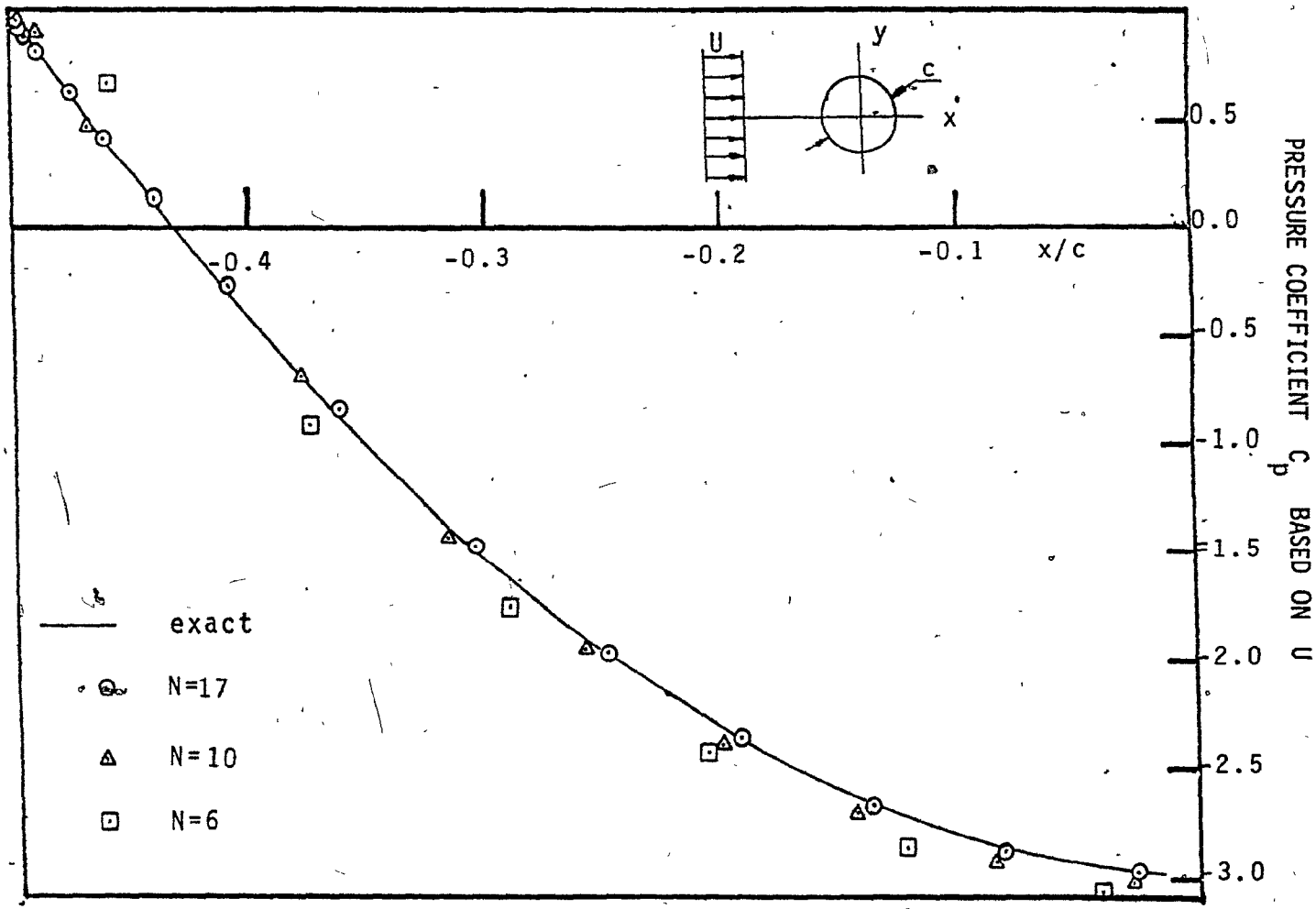

Fig. 8: Comparison between exact and numerical solution with N elements: Circular cylinder with diameter c in a uniform flow.

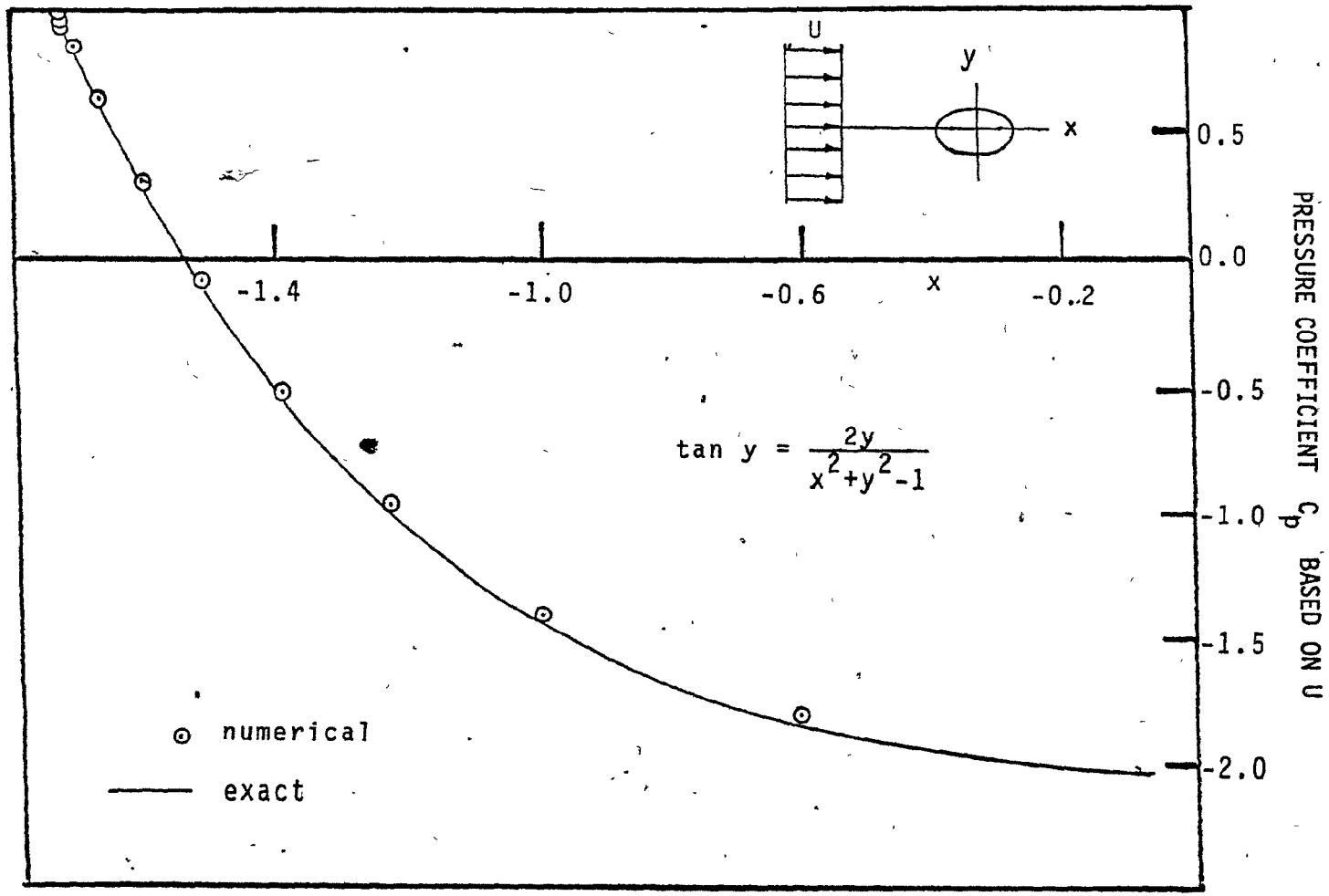

Fig.9: Comparison between exact and numerical solutions: Rankine Oval.

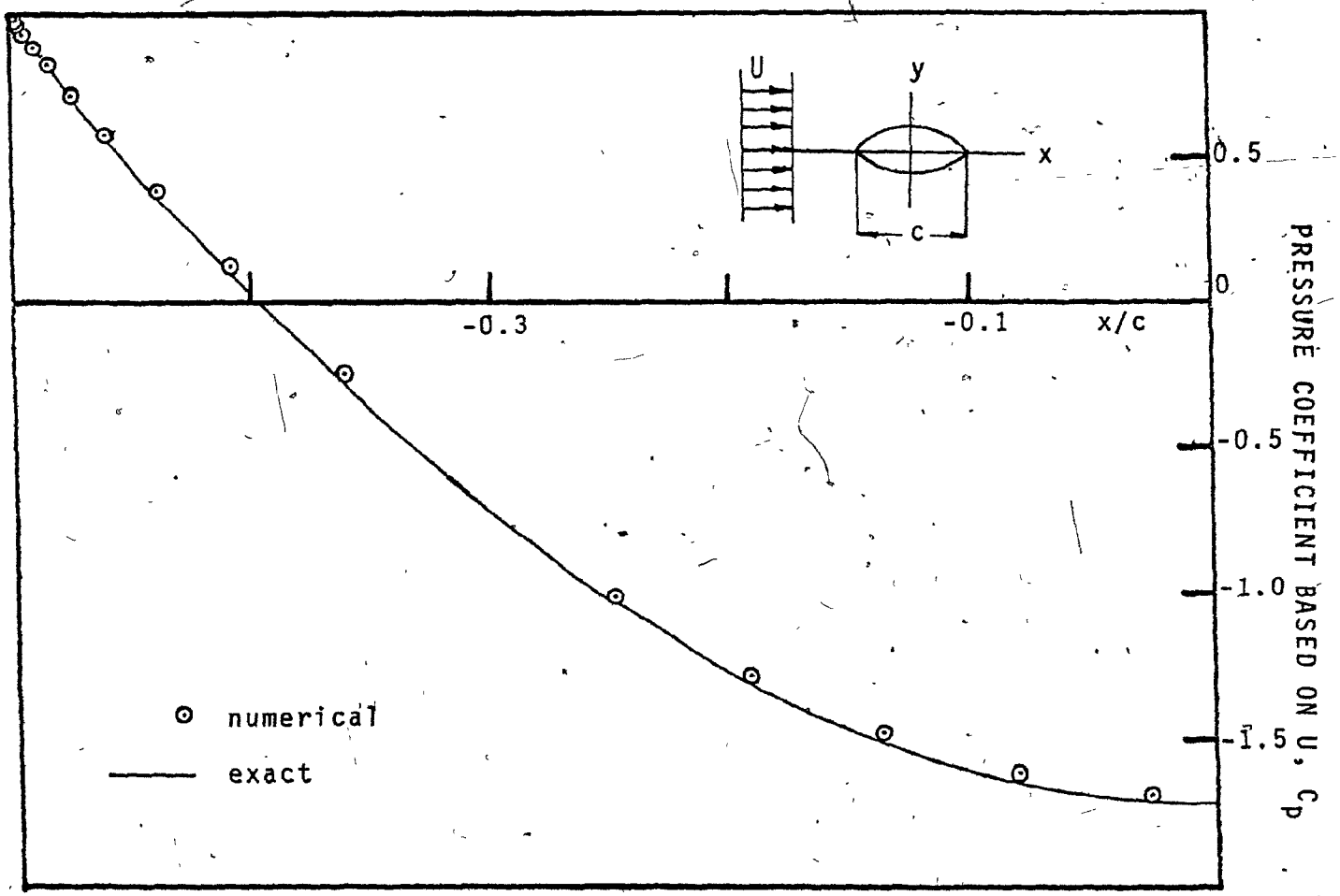

Fig. 10: Comparison between exact and numerical solutions. Lenticular aerofoil with chord length c in uniform flow

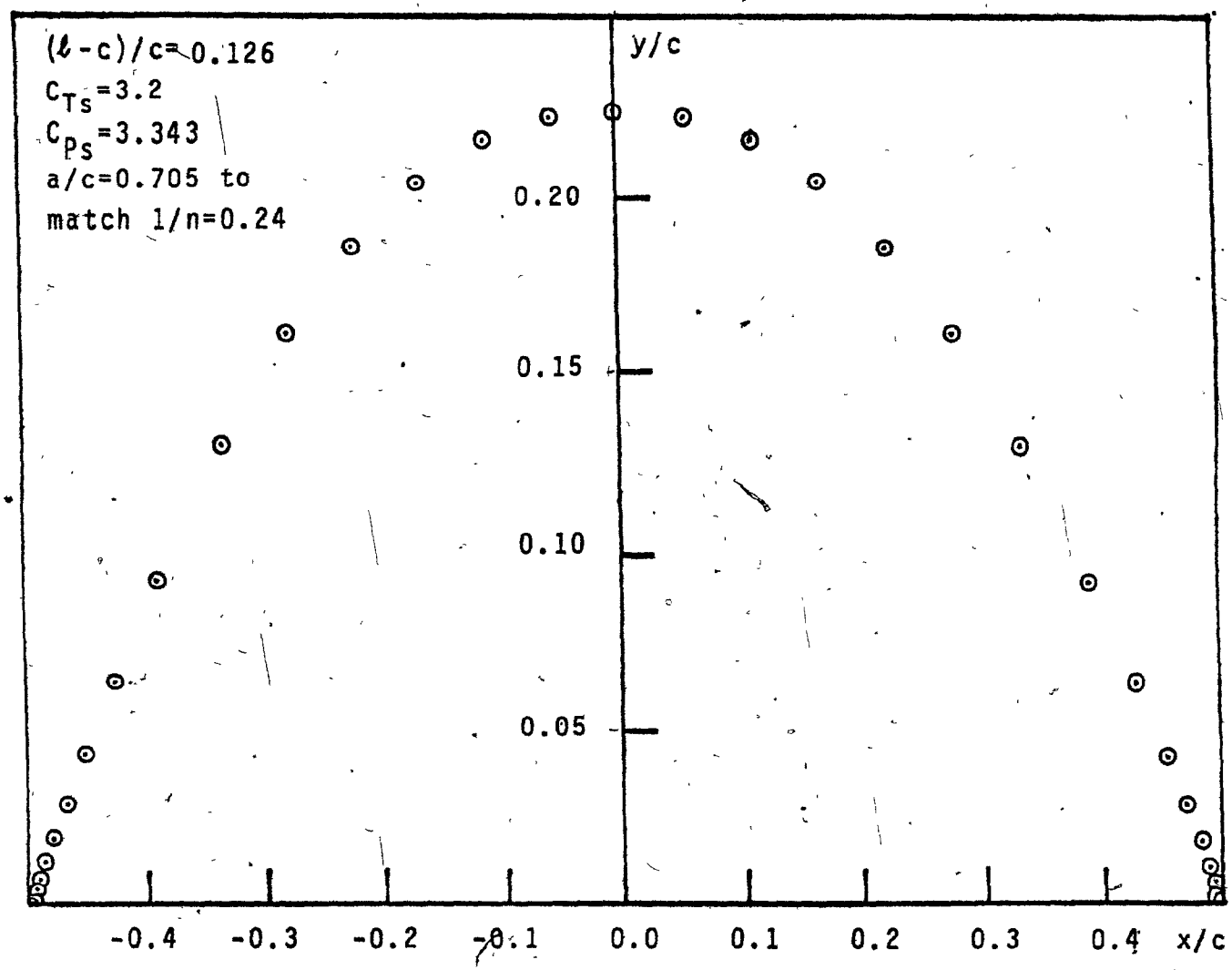

Fig. 11: Theoretical shape of the membrane

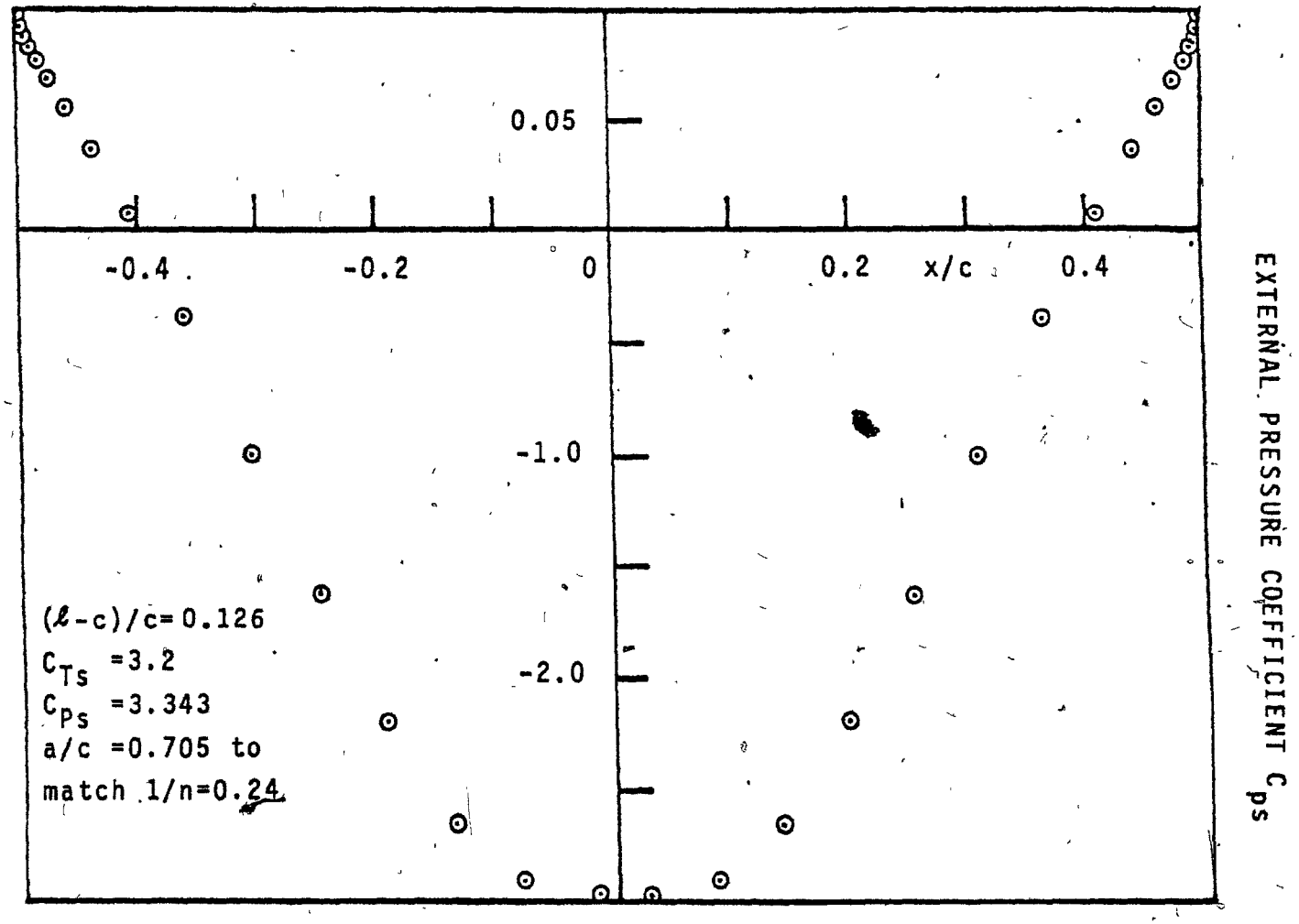

Fig. 12: Theoretical pressure distribution
(shape in Fig. 11)

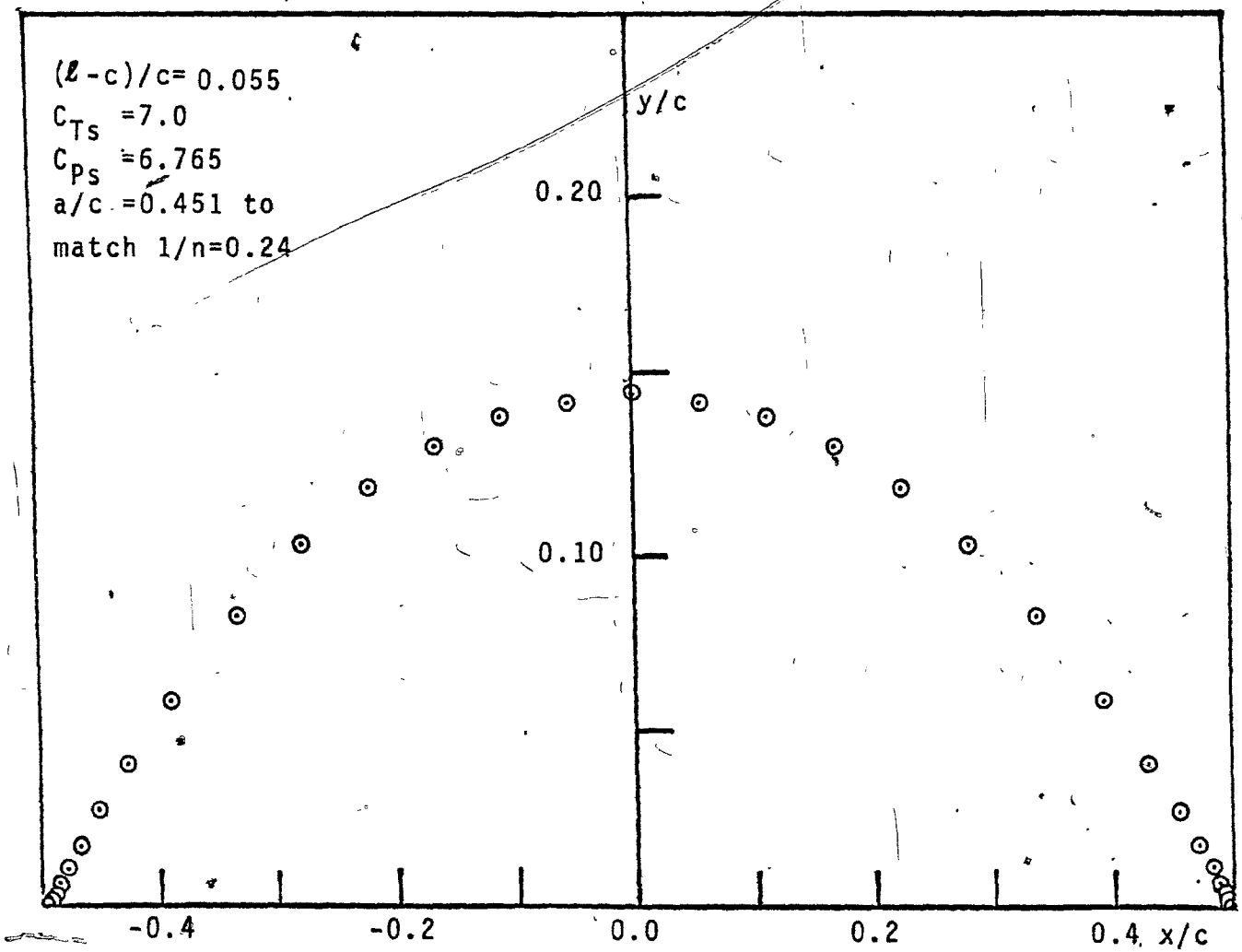

Fig. 13: Theoretical shape of the membrane

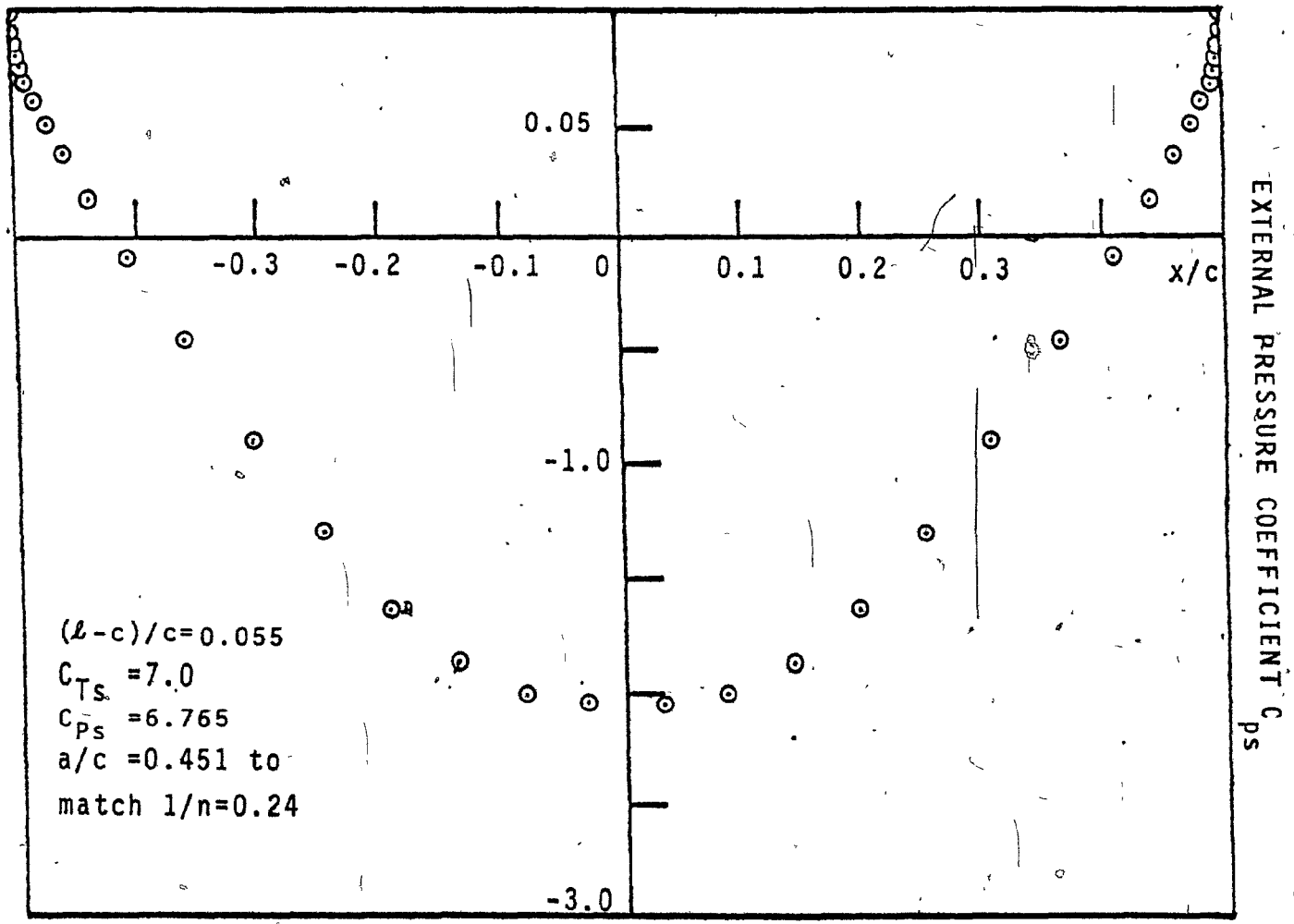

Fig. 14: Theoretical pressure distribution
(shape in Fig. 13)

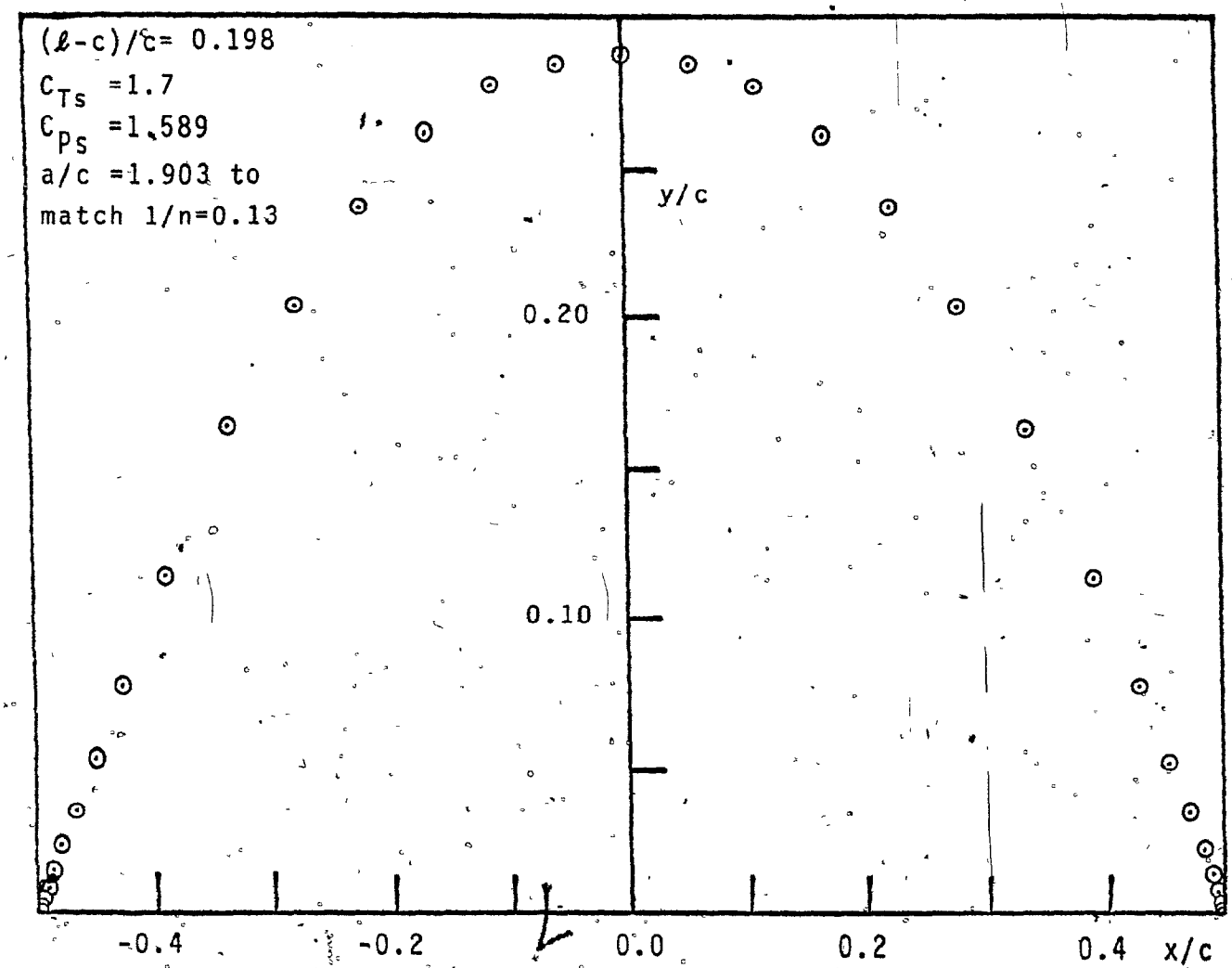

Fig. 15: Theoretical shape of the membrane

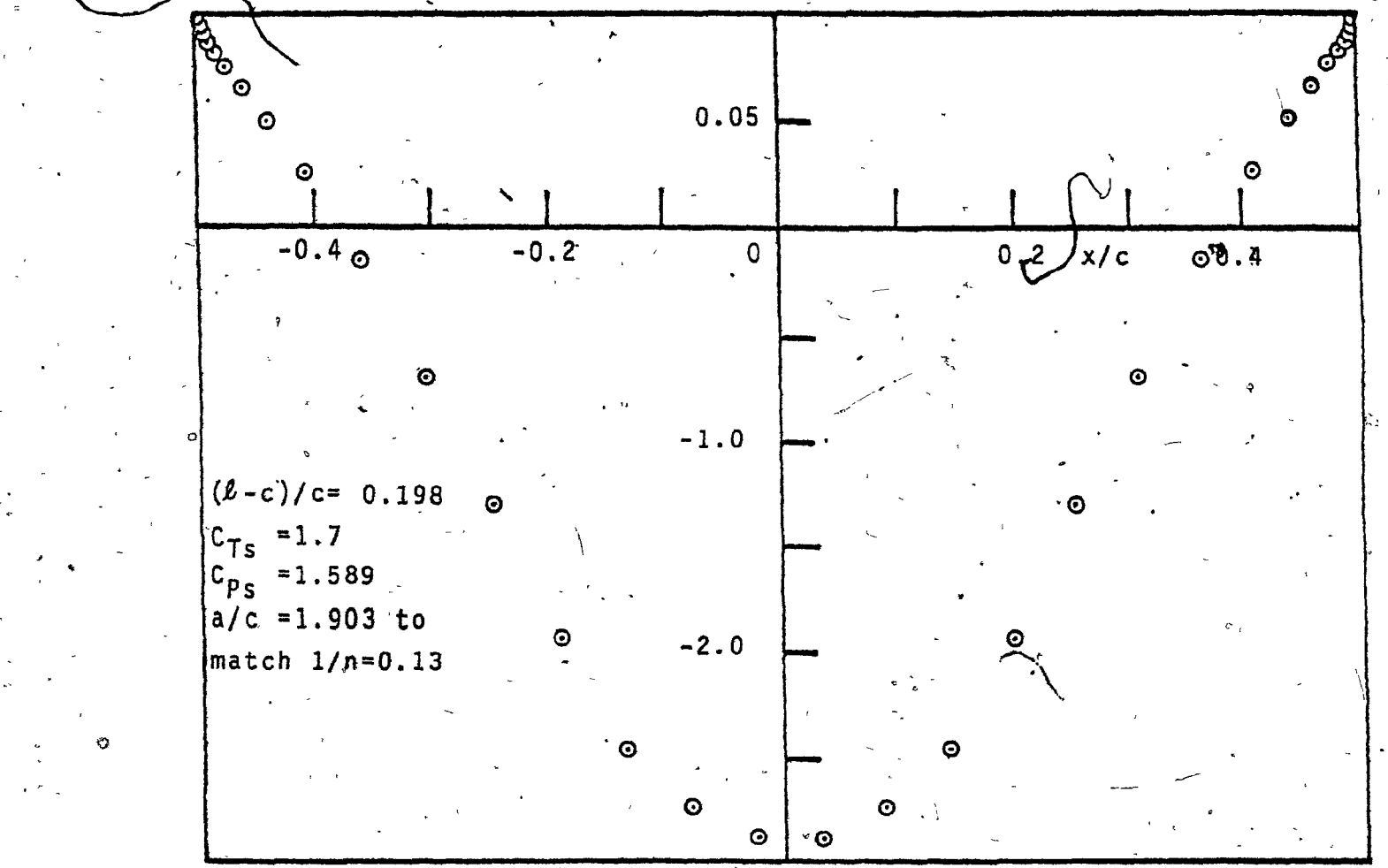

Fig. 16: Theoretical pressure distribution (shape in Fig. 15)

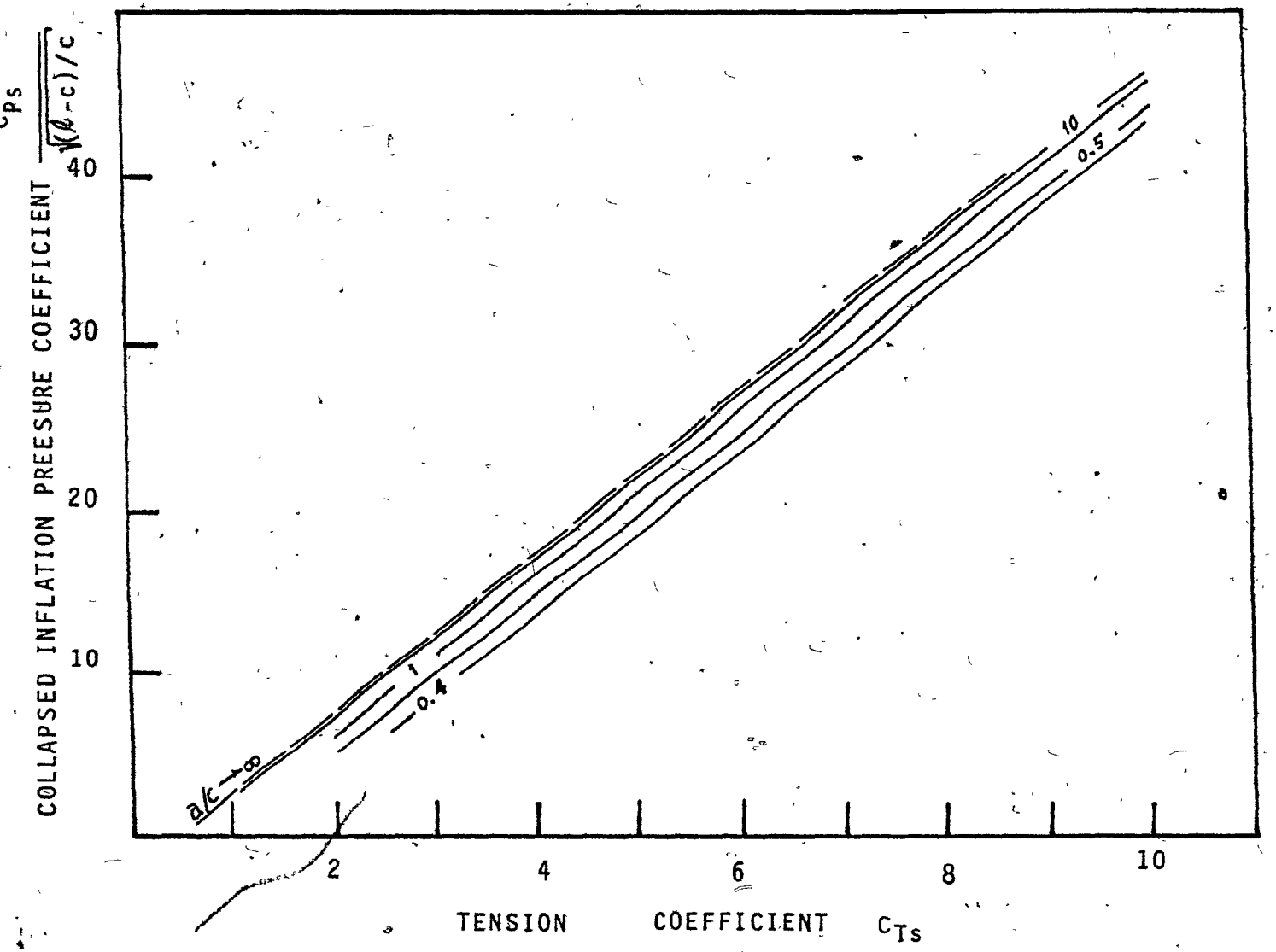

Fig. 17: Theoretical results for low buildings (h/c<0.1) for various upstream flows of constant vorticity U_s/a.

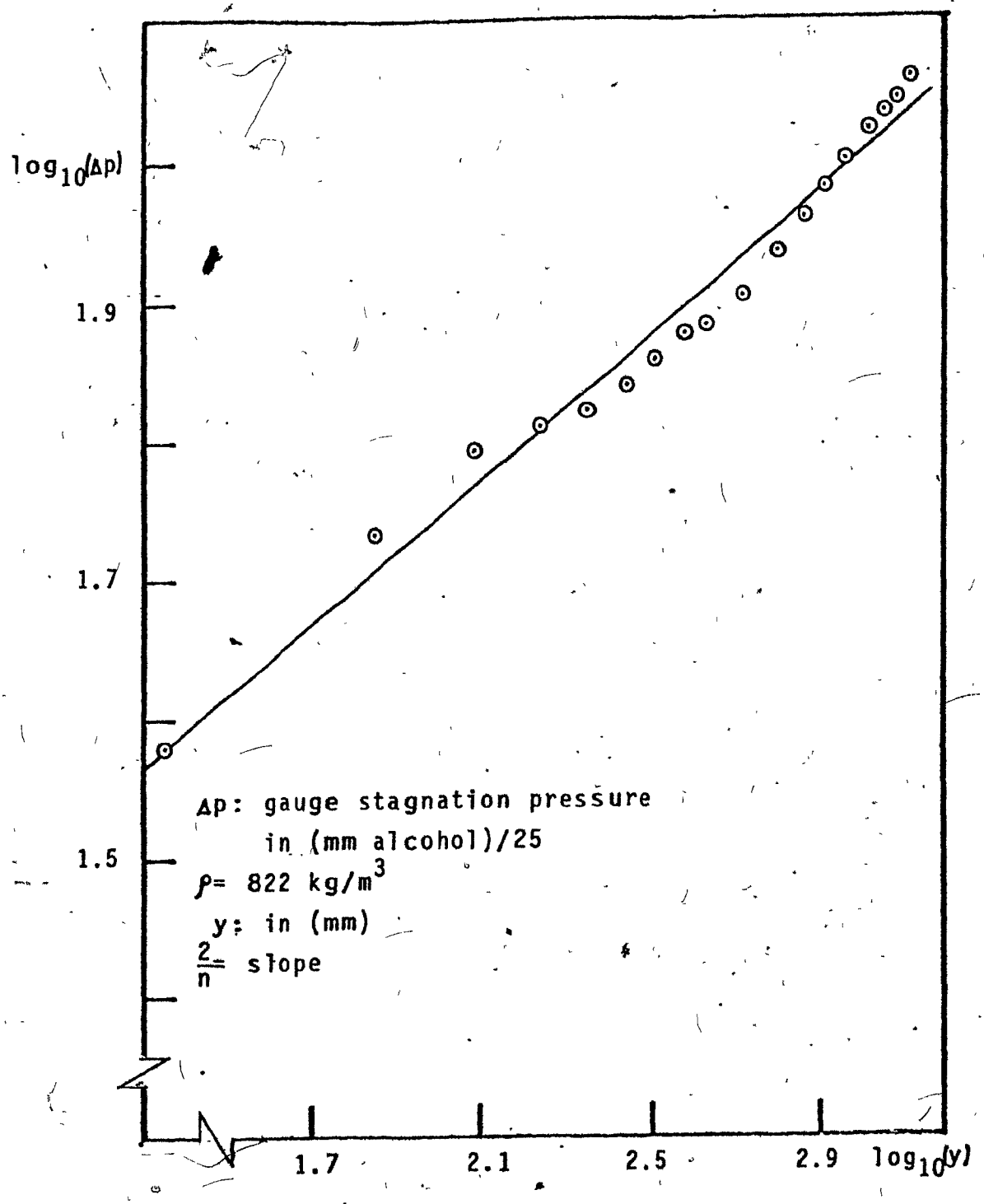

Fig. 18: Calculation of the power of the wind profile. 1/n=0.13 roughness 1.

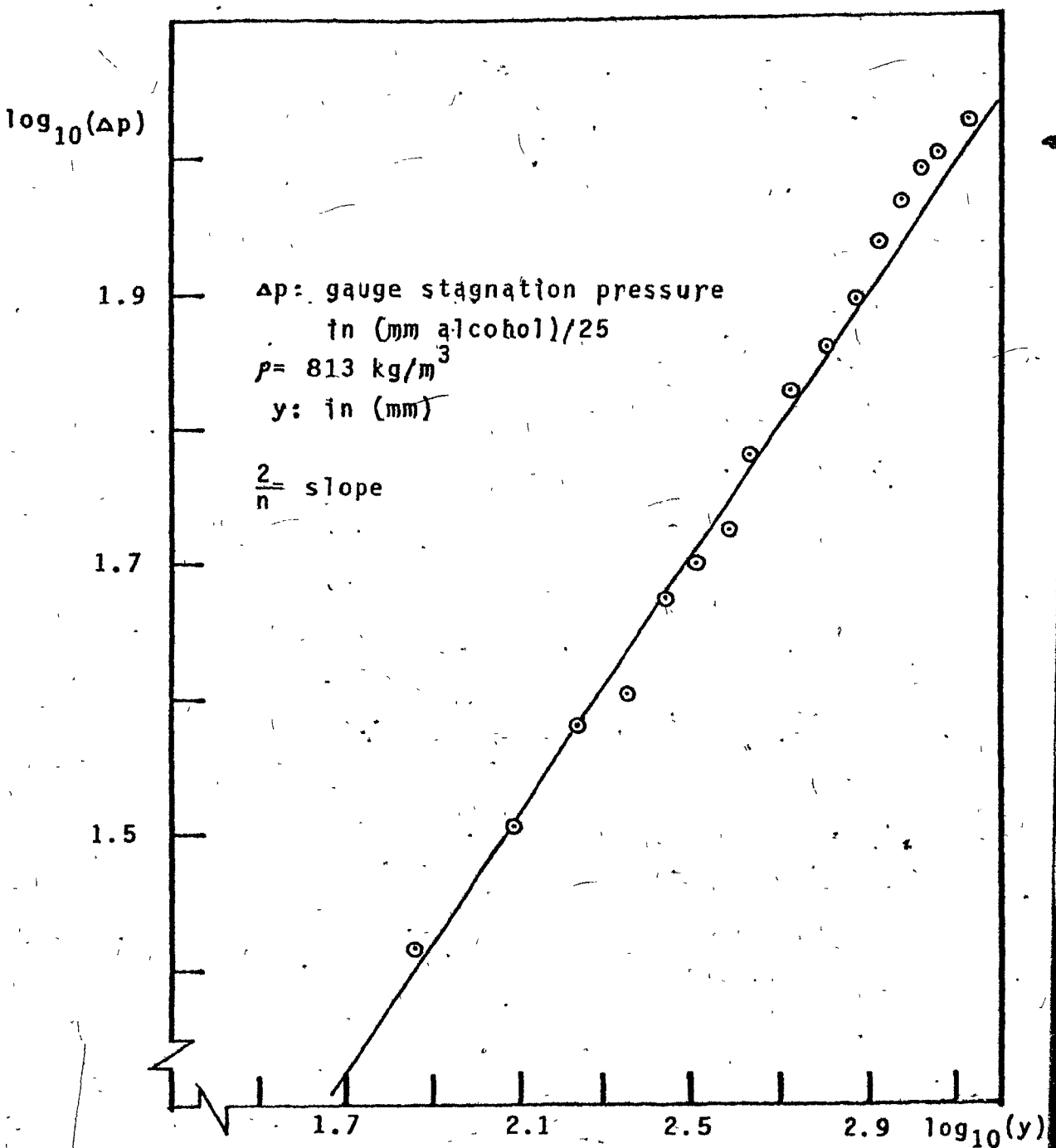

Fig. 19: Calculation of the power of the wind profile. 1/n=0.24 roughness 2.

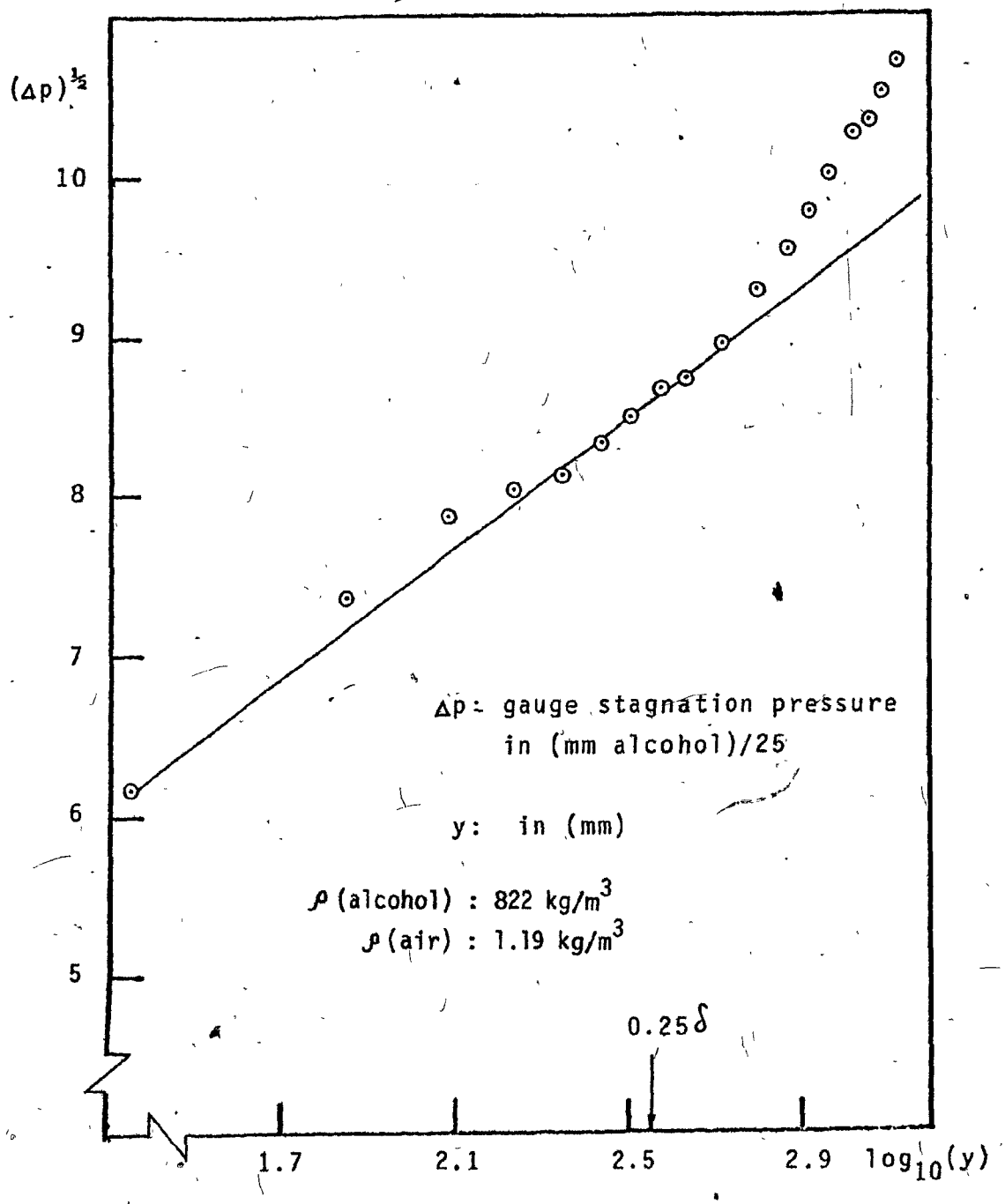

Fig. 20: Calculation of U_τ for 1/n=0.13 roughness 1.

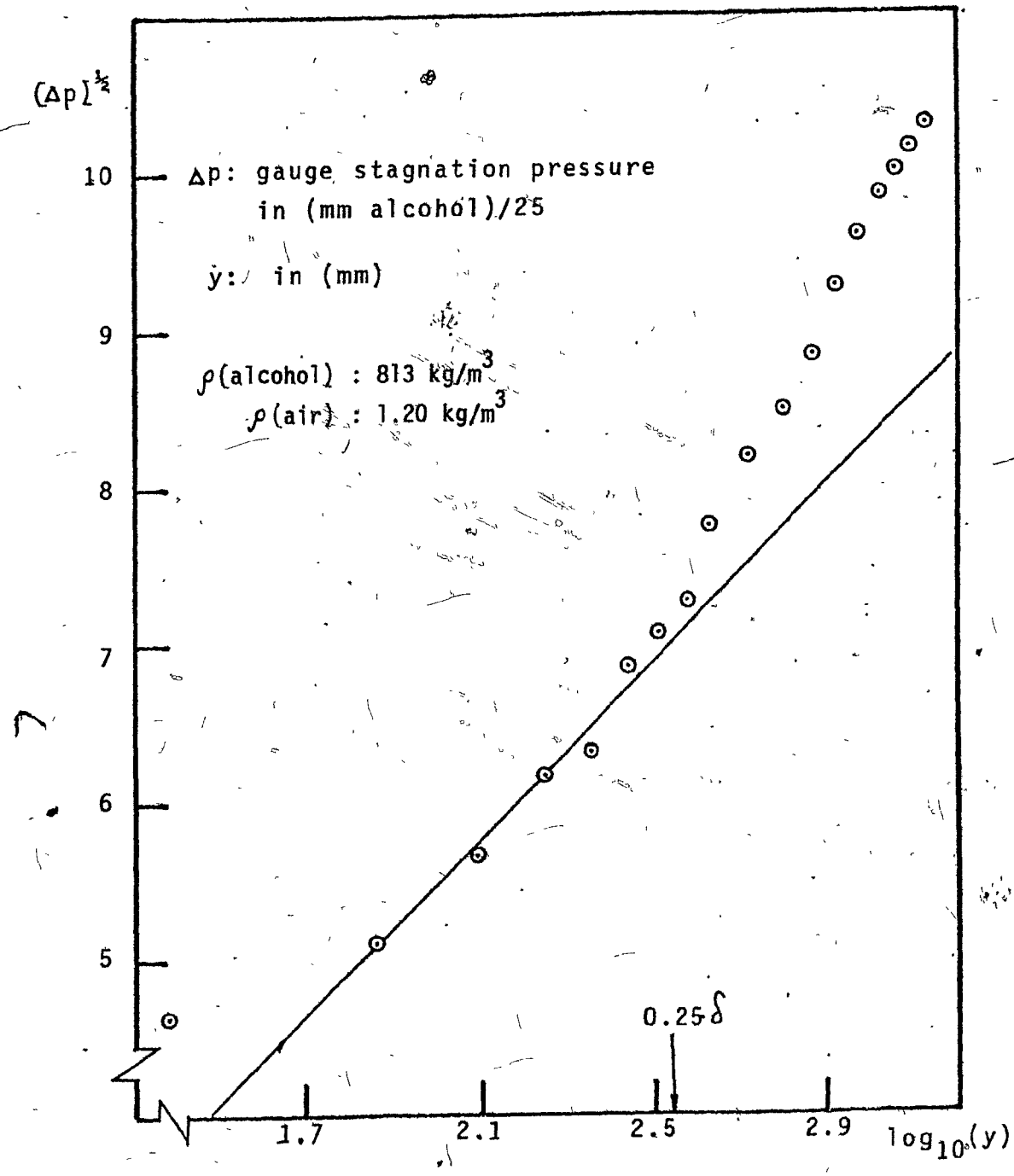

Fig. 21: Calculation of U_τ for 1/n=0.24 roughness 2.

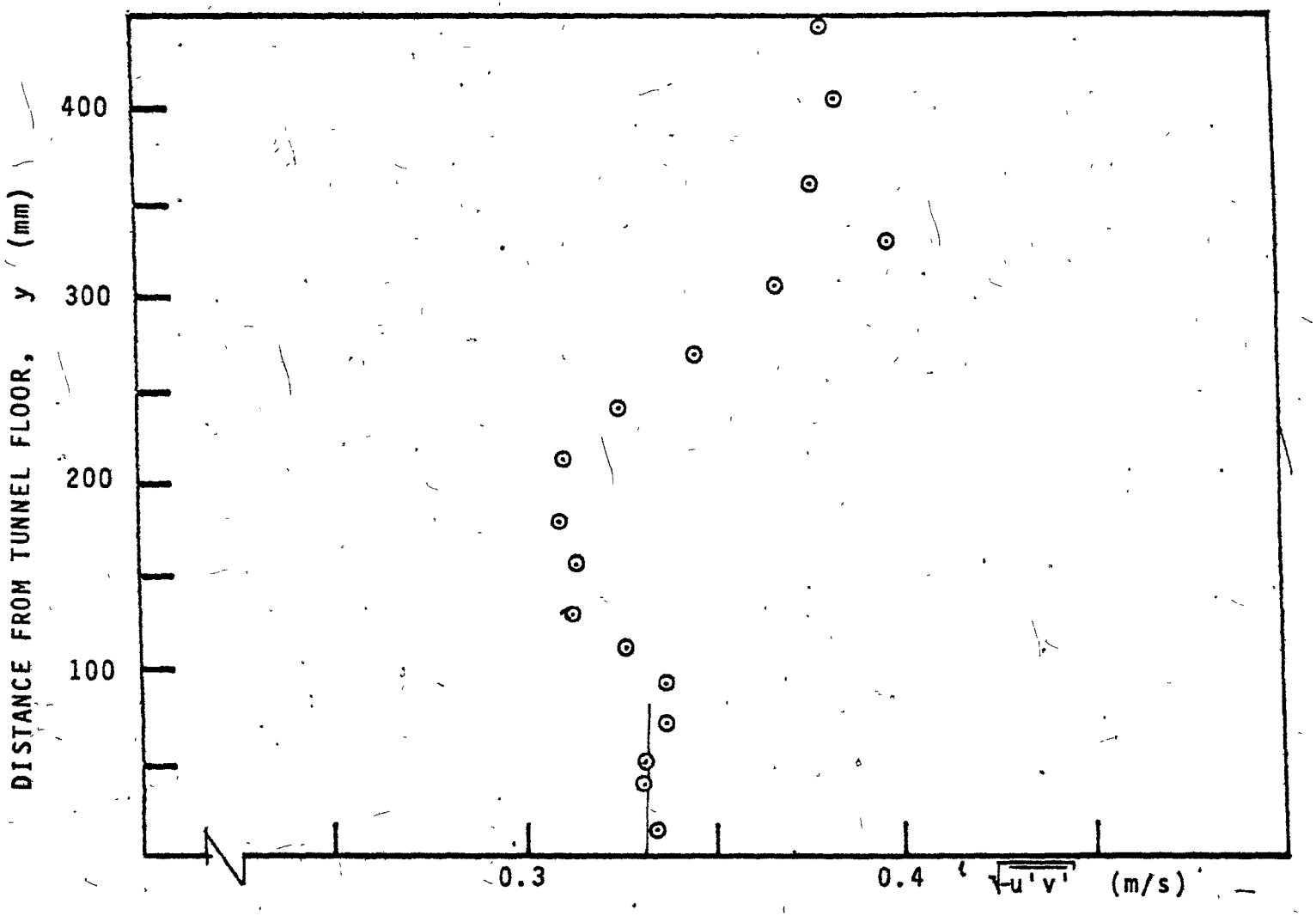

Fig. 22: Hot-wire results for U_τ. 1/n=0.13 roughness 1.

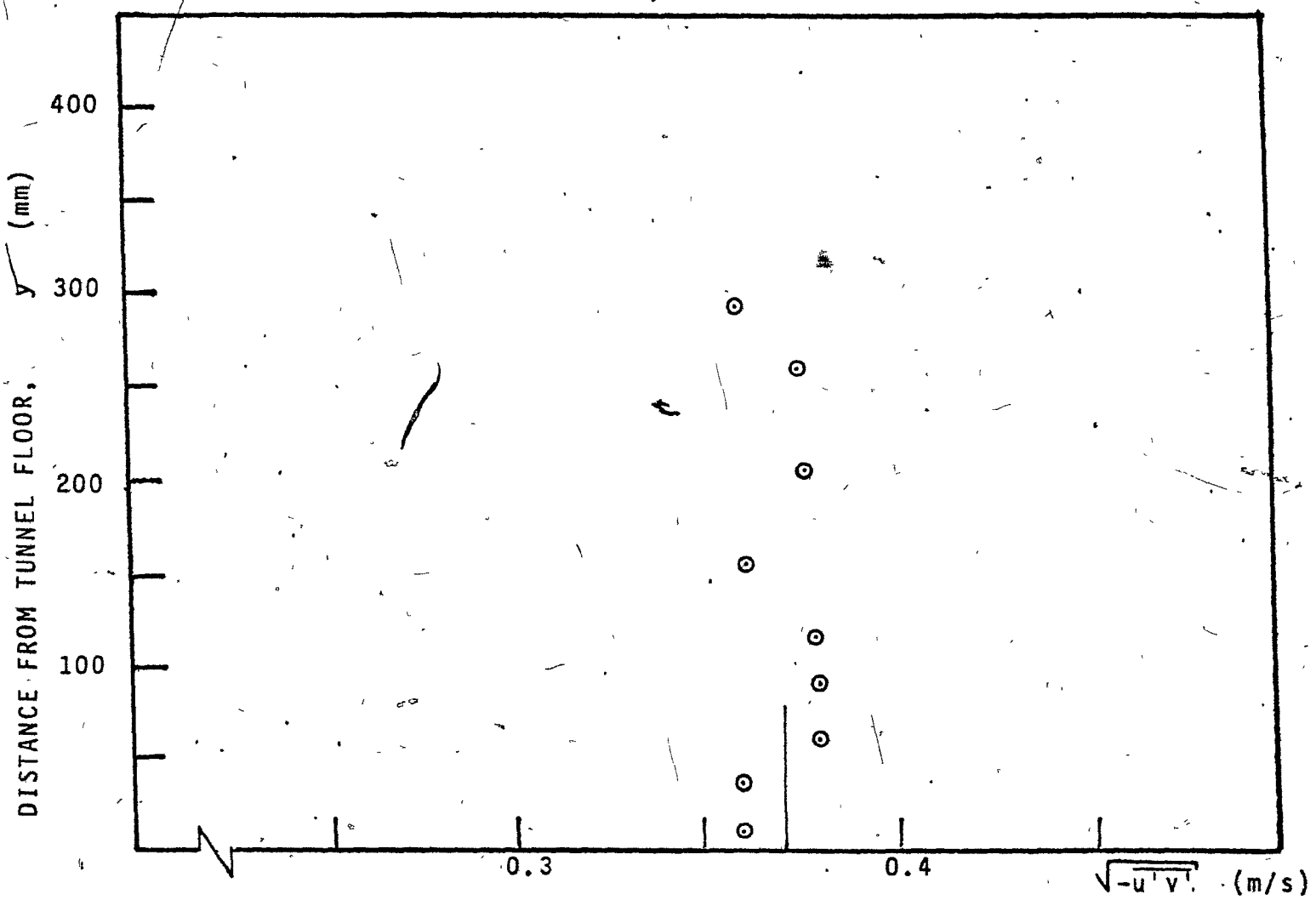

Fig. 23: Hot-wire results for U_τ. 1/n=0.24 roughness 2

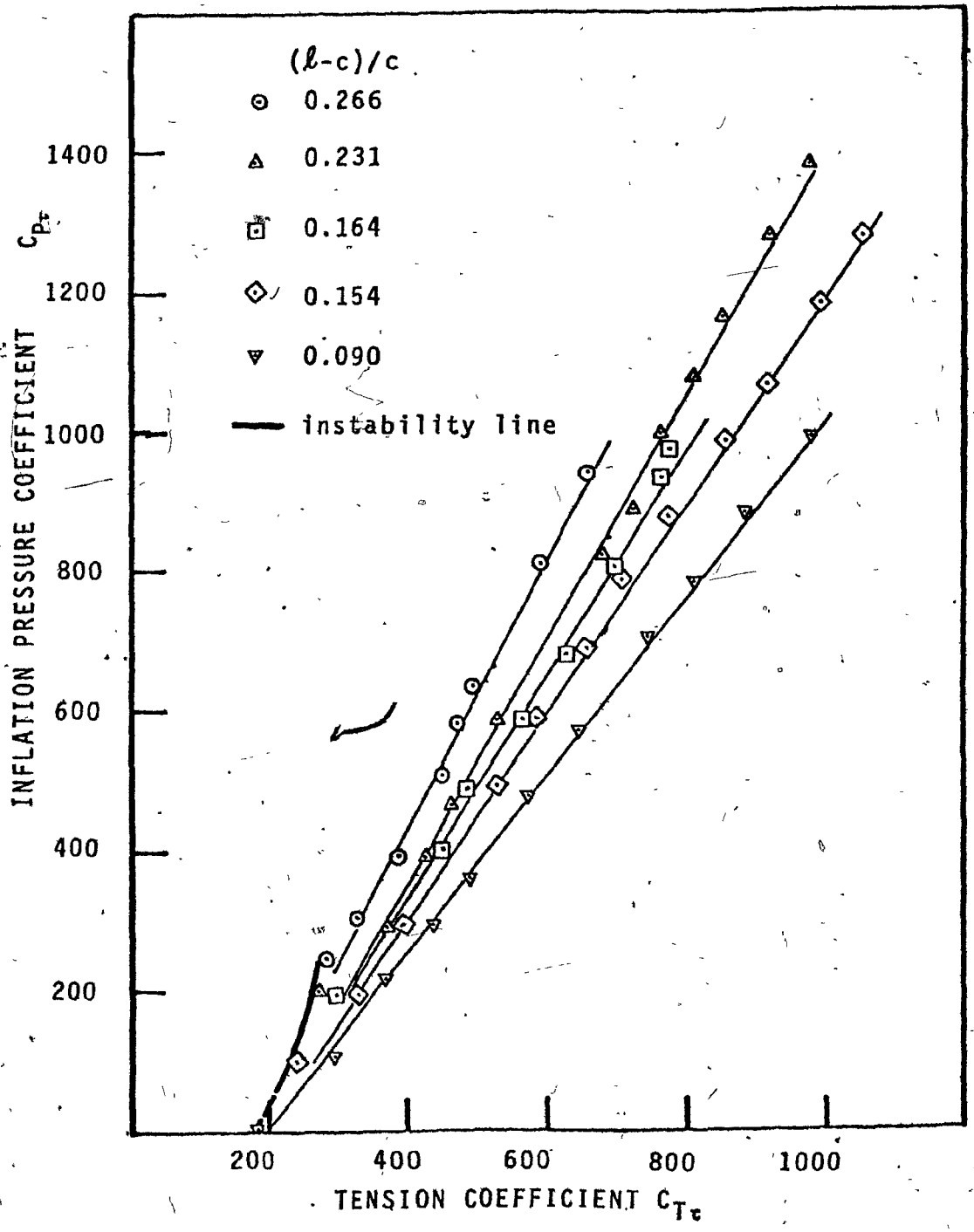

Fig. 24: Tension and inflation pressure.
Roughness 1 (1/n=0.13)

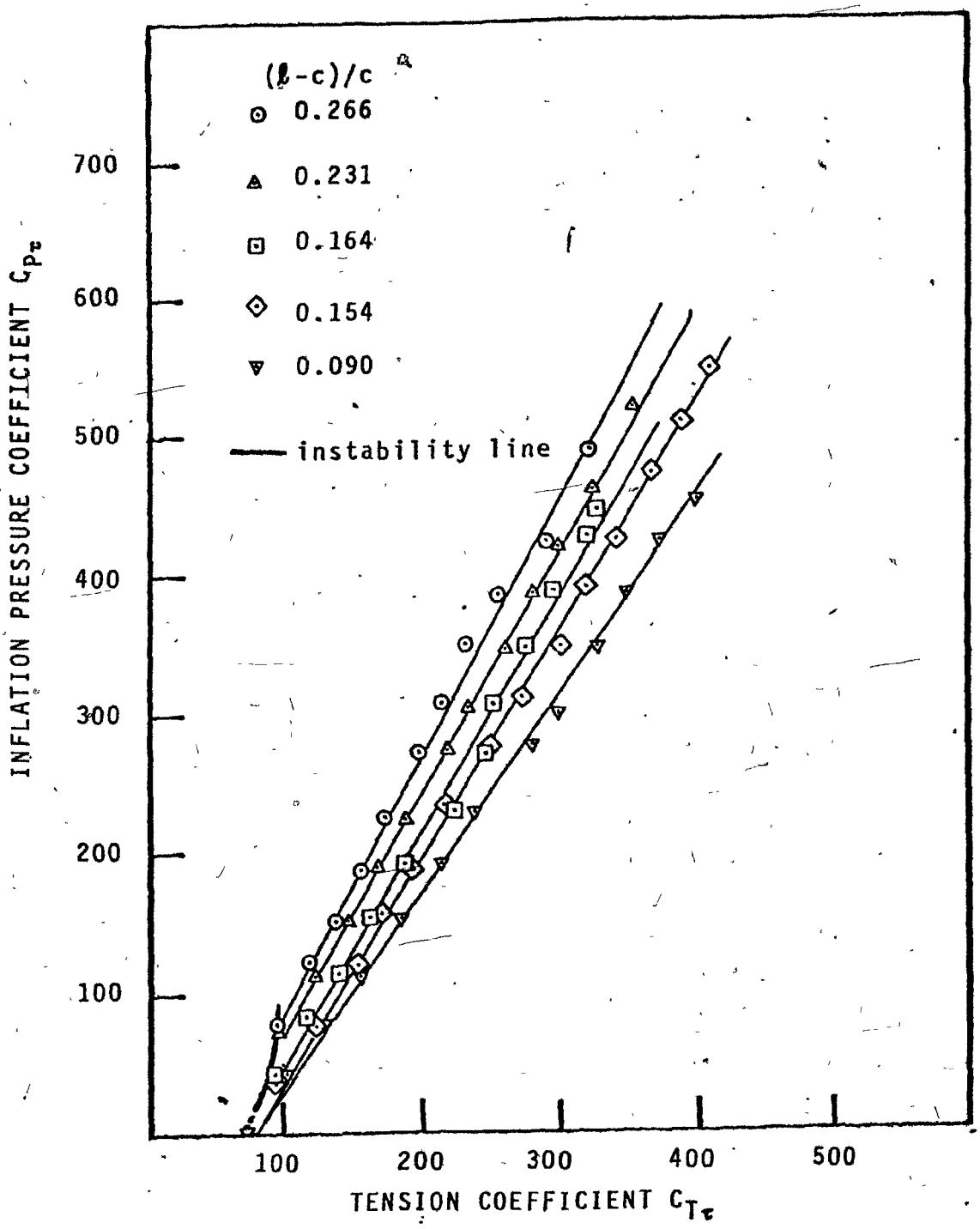

Fig. 25: Tension and inflation pressure.
Roughness 2 (1/n=0.24)

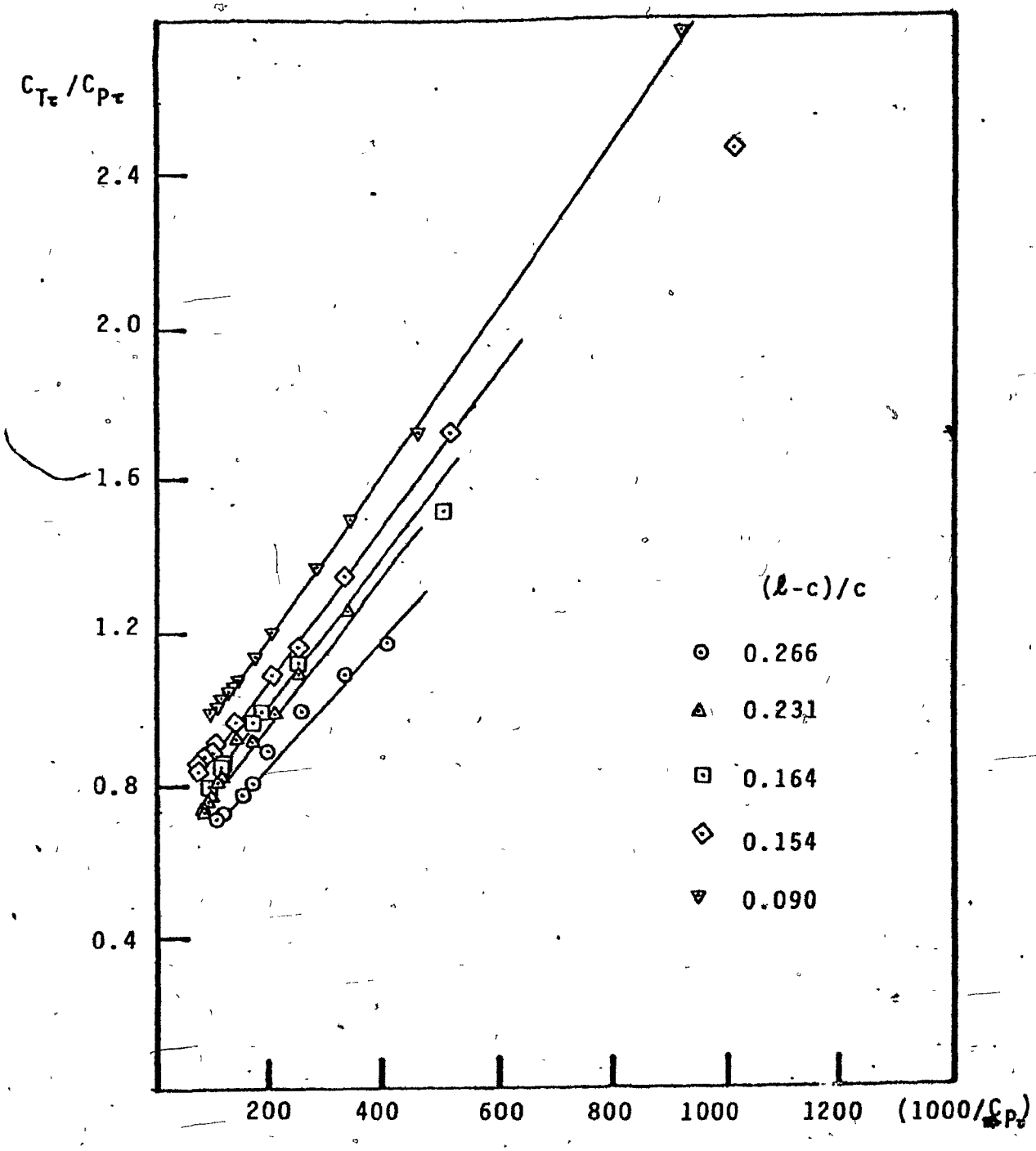

Fig. 26: An attempt to collapse parameters. 1/n=0.13

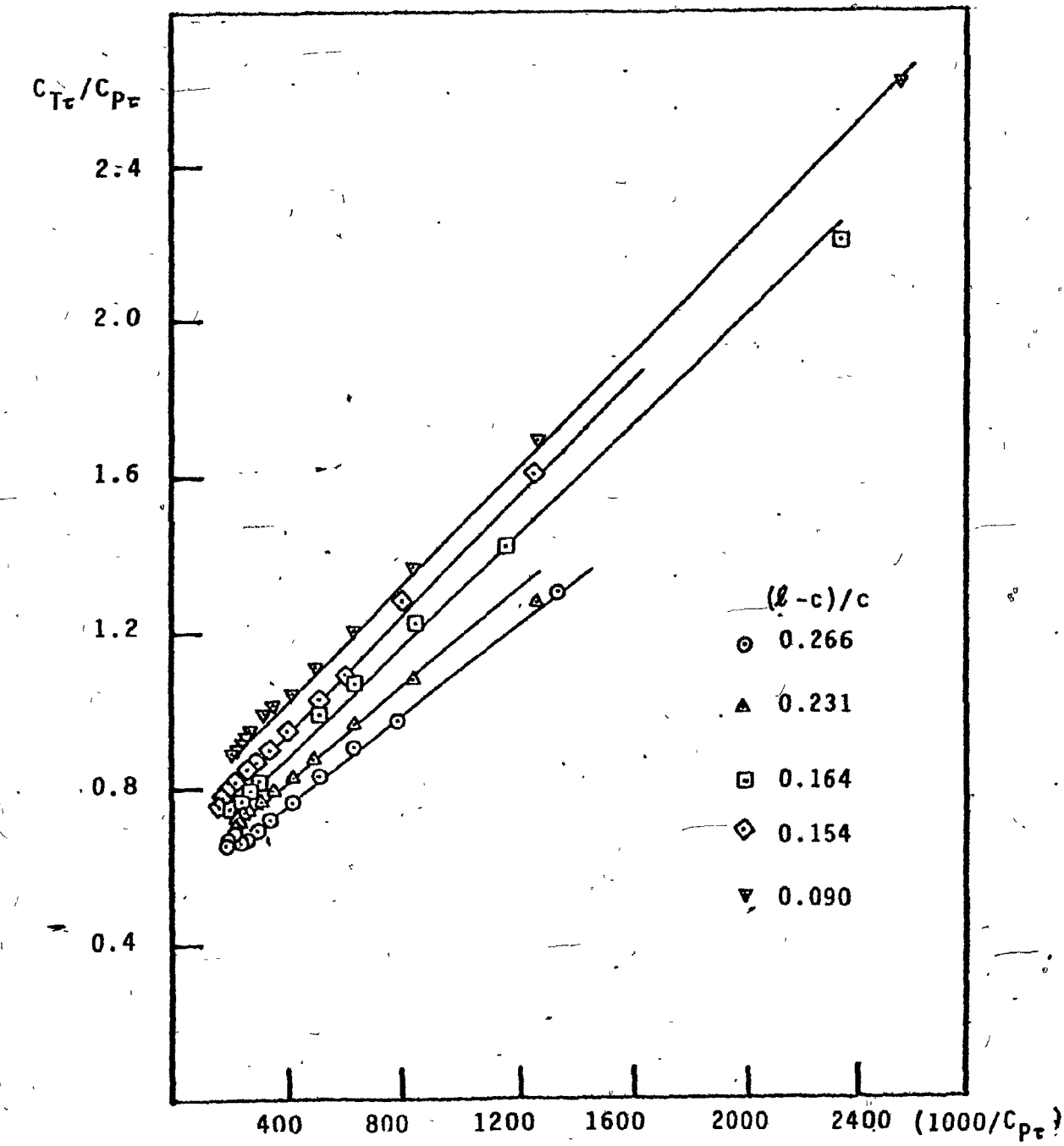

Fig. 27: An attempt to collapse parameters. 1/n=0-24

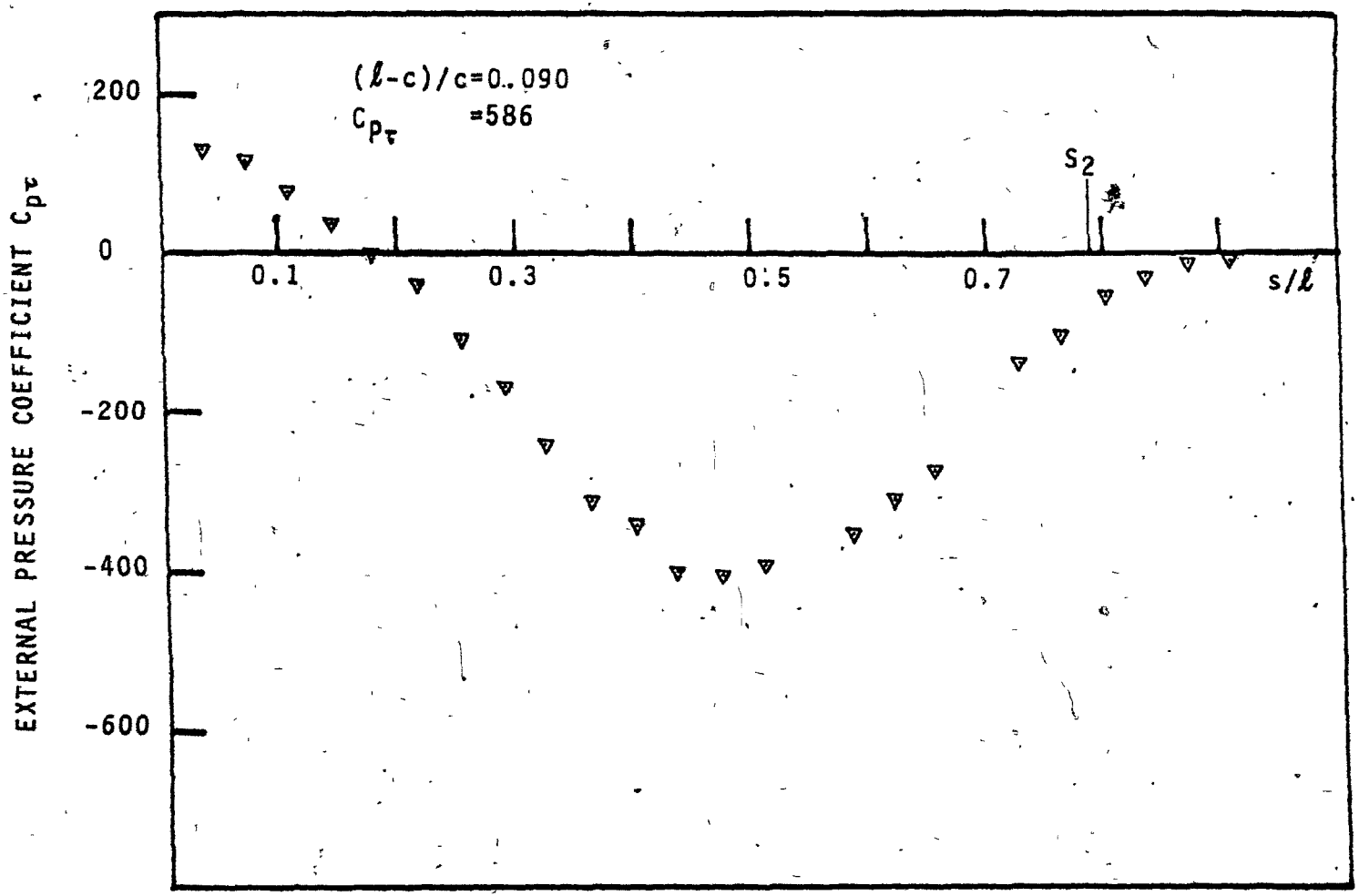

Fig. 28: External pressure distribution. Roughness 1 (1/n=0.13)

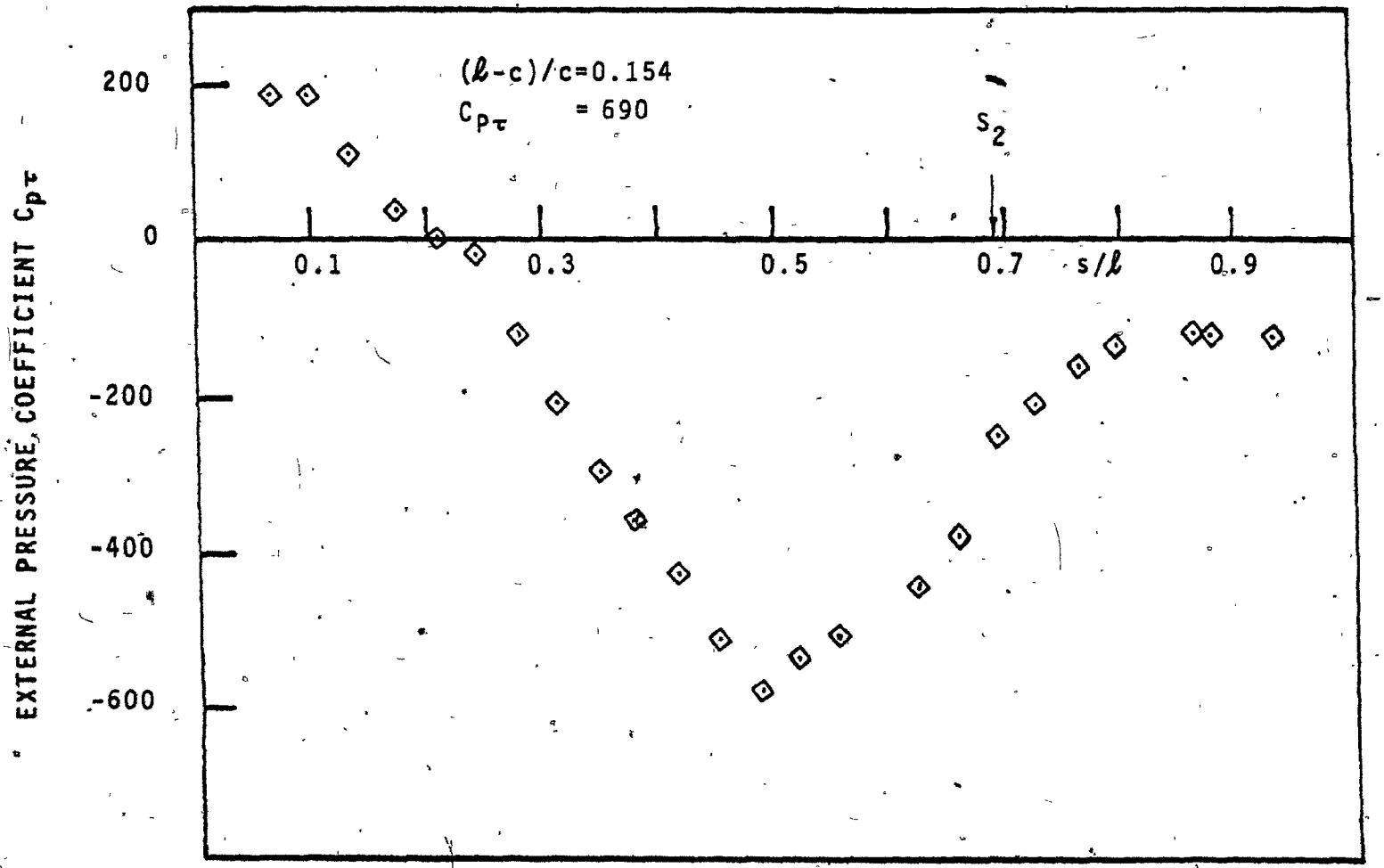

Fig. 29: External pressure distribution. Roughness 1 (1/n=0.13)

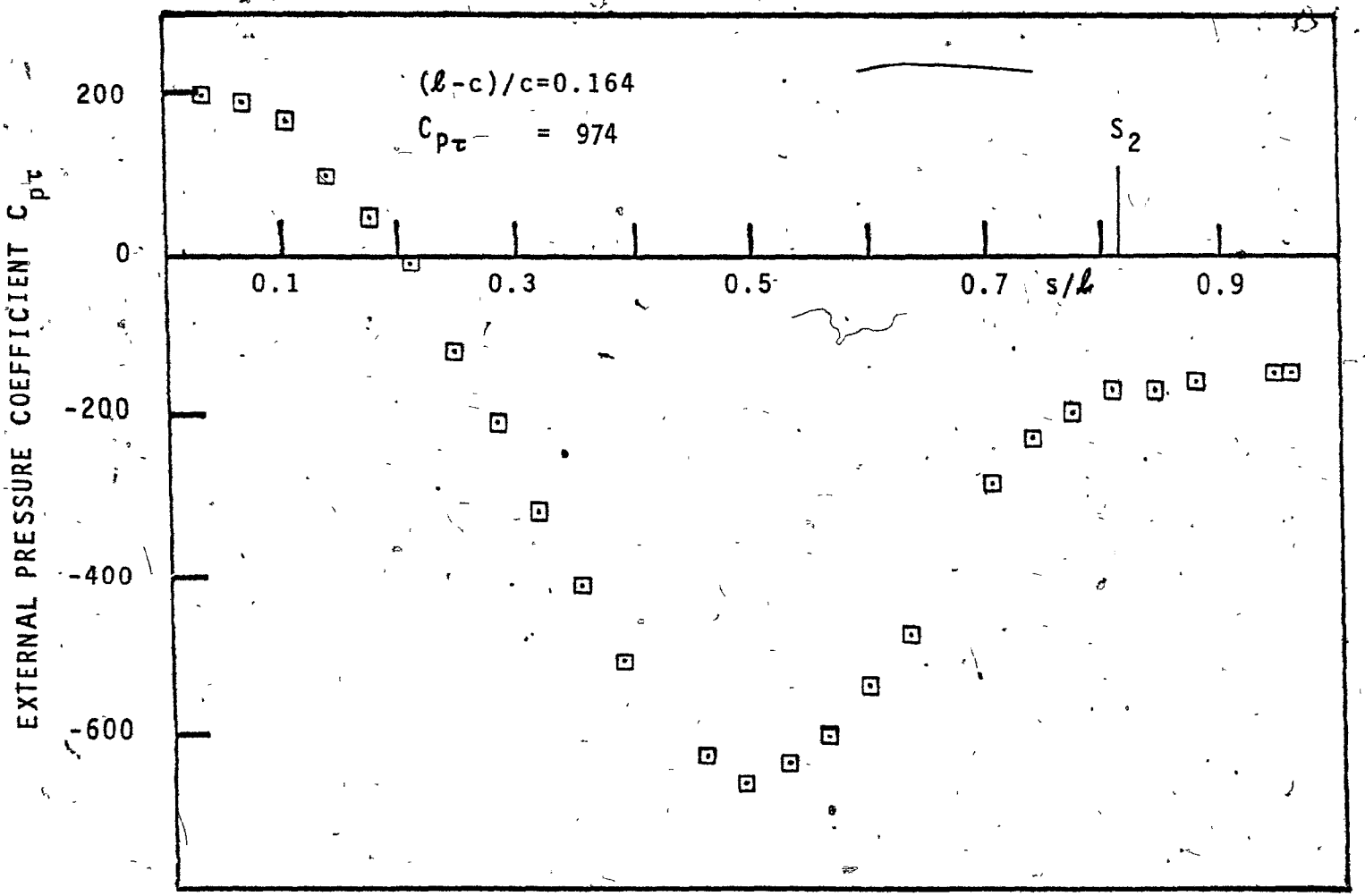

Fig. 30: External pressure distribution. Roughness 1 (1/n=0.13)

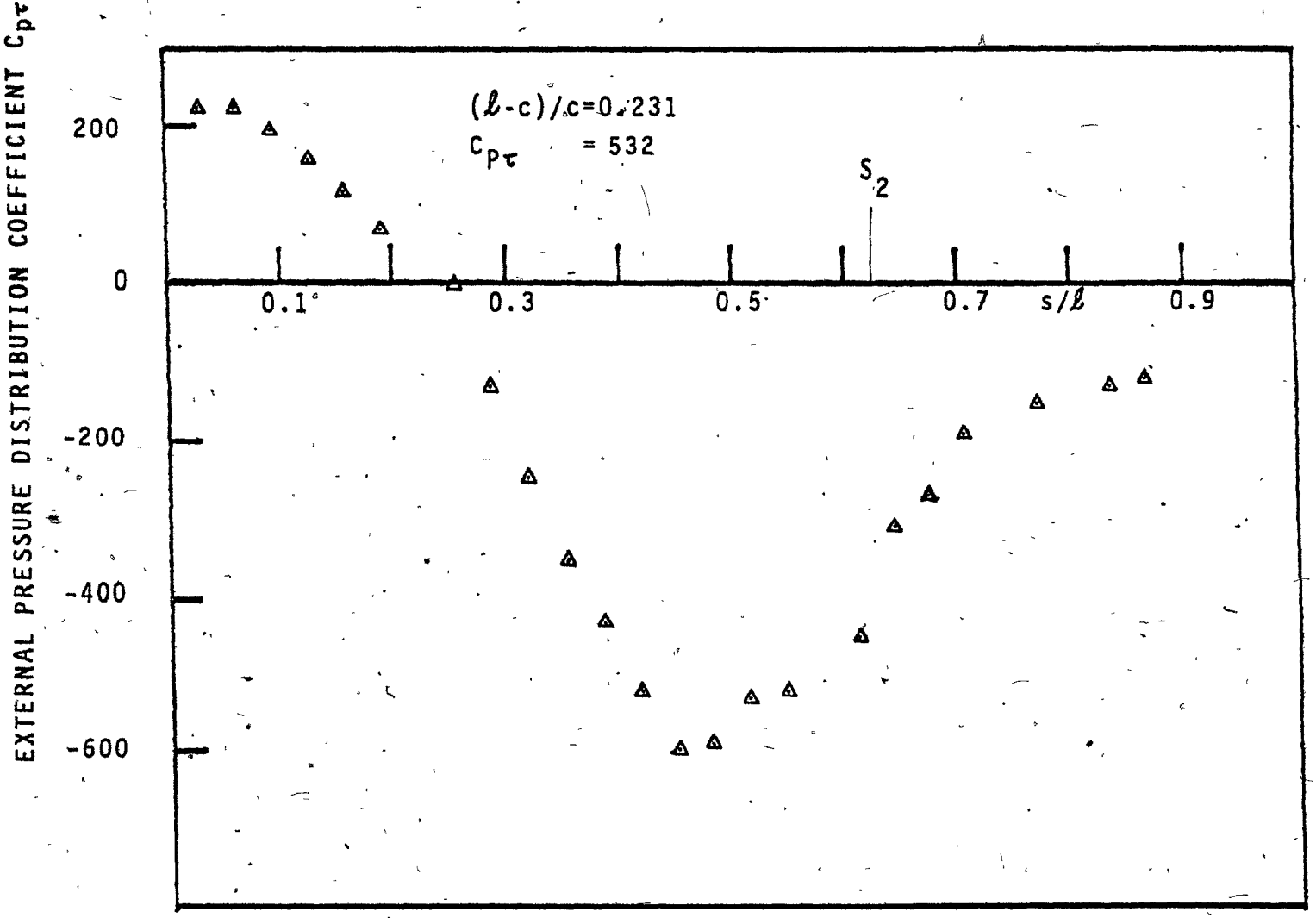

Fig. 31: External pressure distribution. Roughness 1 (1/n=0.13)

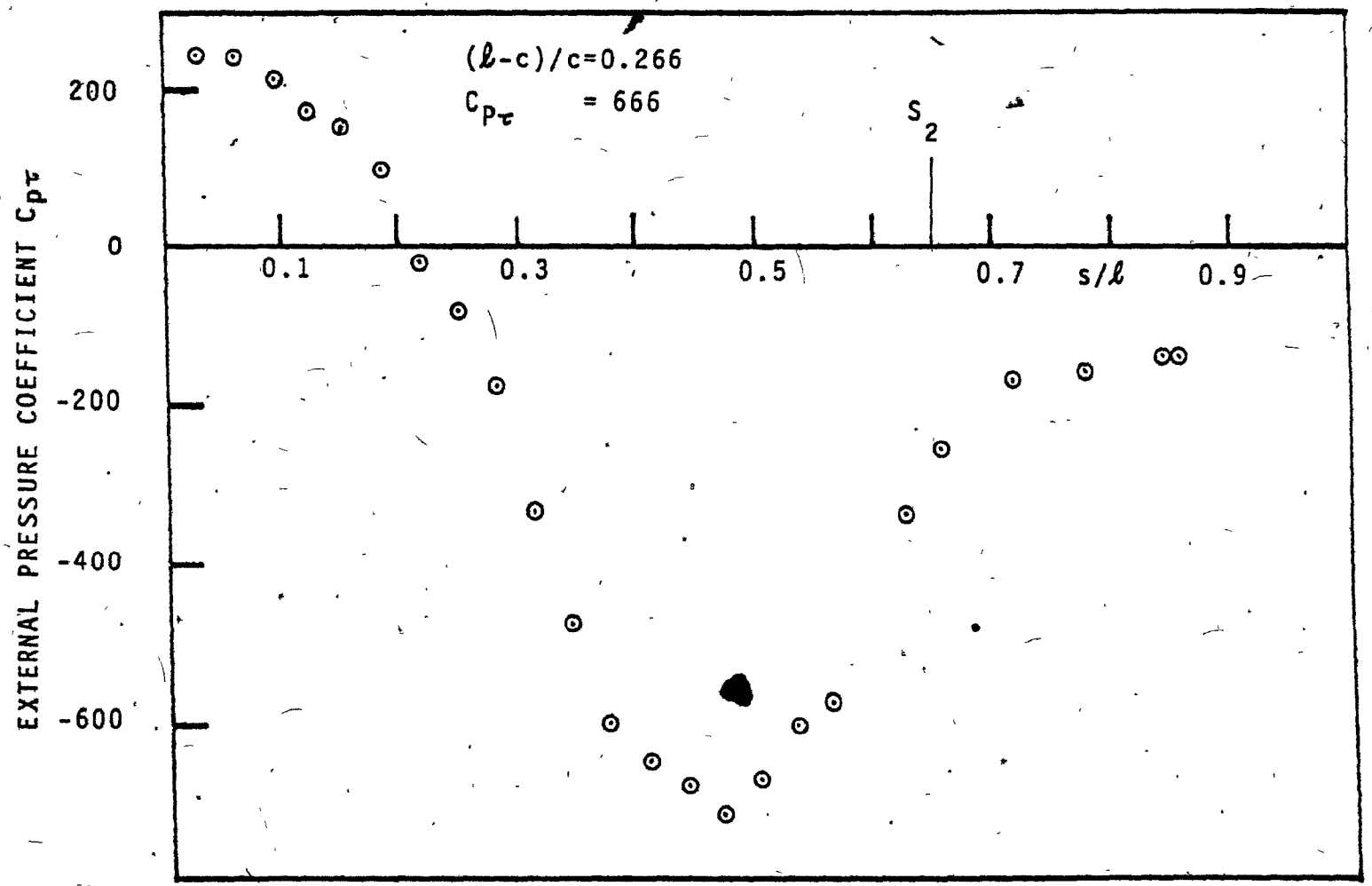

Fig. 32: External pressure distribution. Roughness 1 (1/n=0.13)

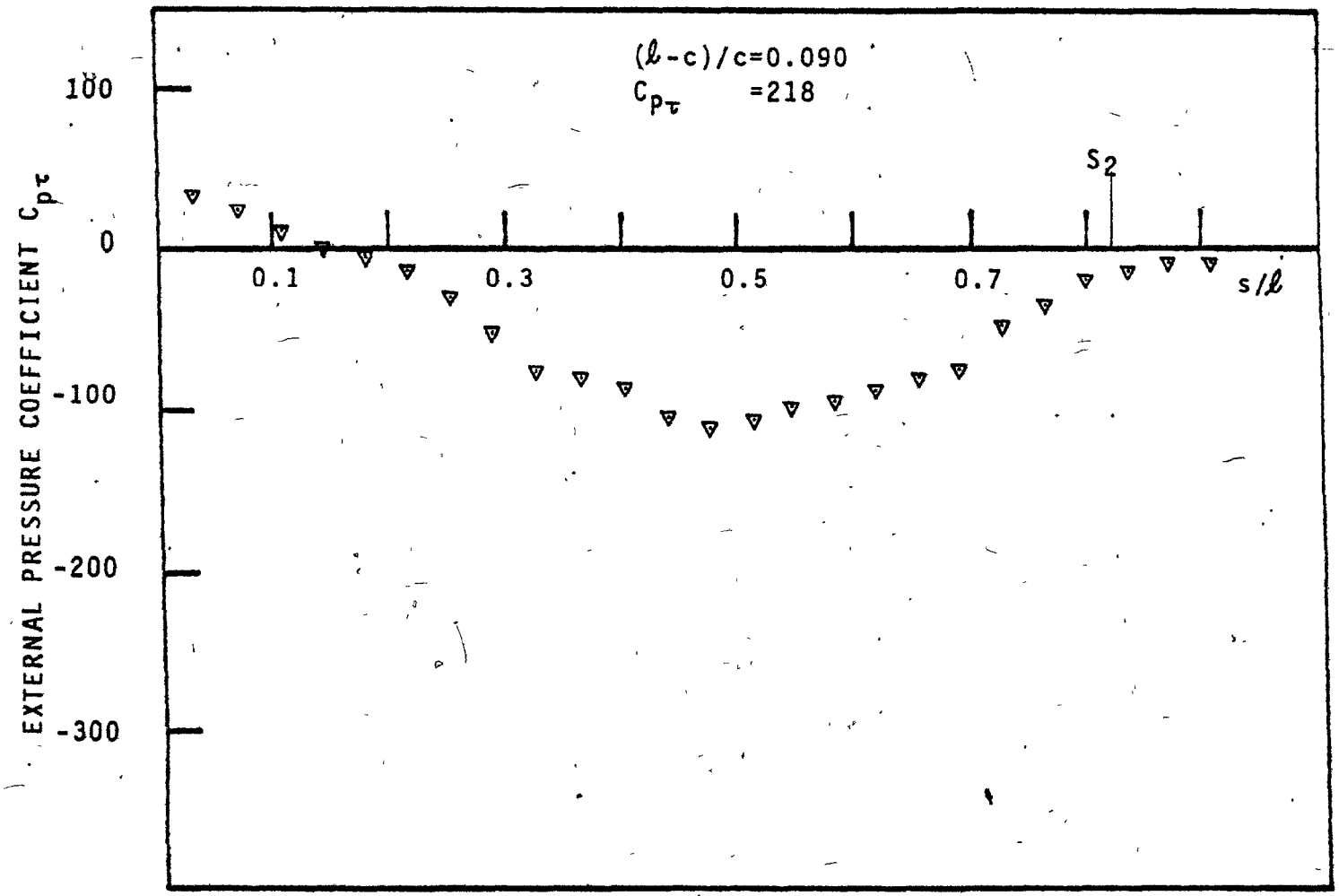

Fig. 33: External pressure distribution. Roughness 2 (1/n=0.24)

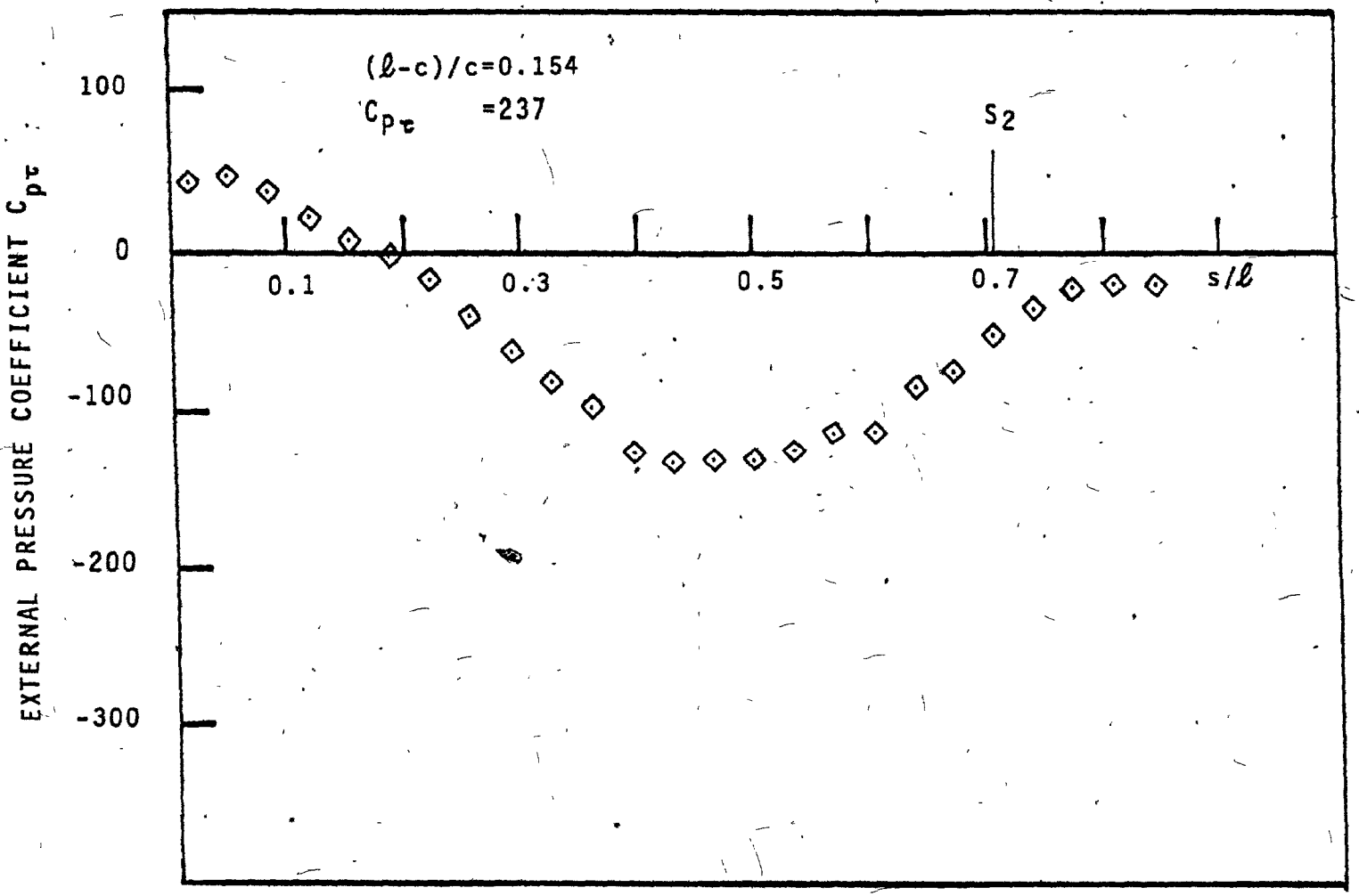

Fig. 34: External pressure distribution. Roughness 2 (1/n=0.24)

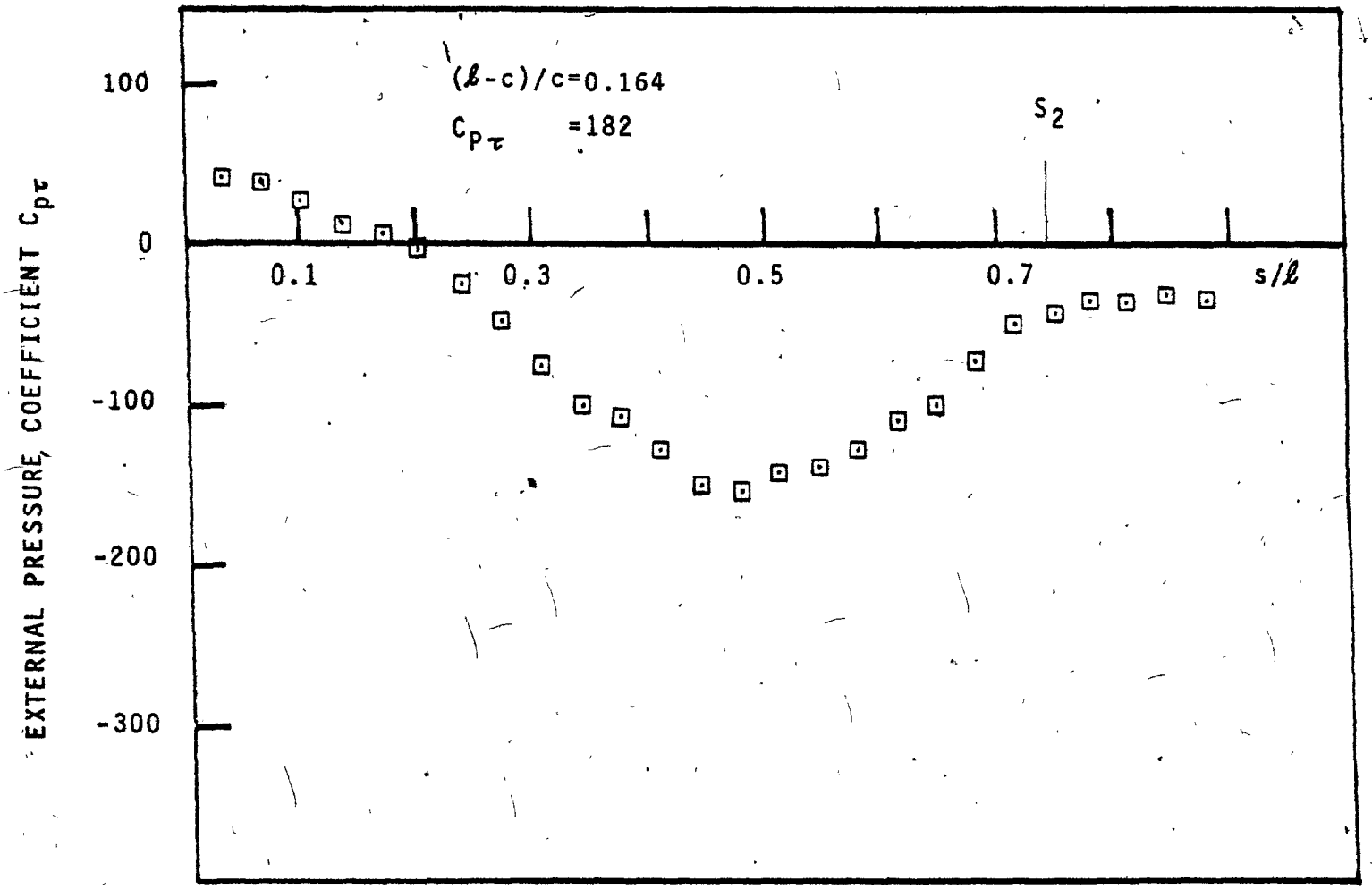

Fig. 35: External pressure distribution. Roughness 2 (1/n=0.24)

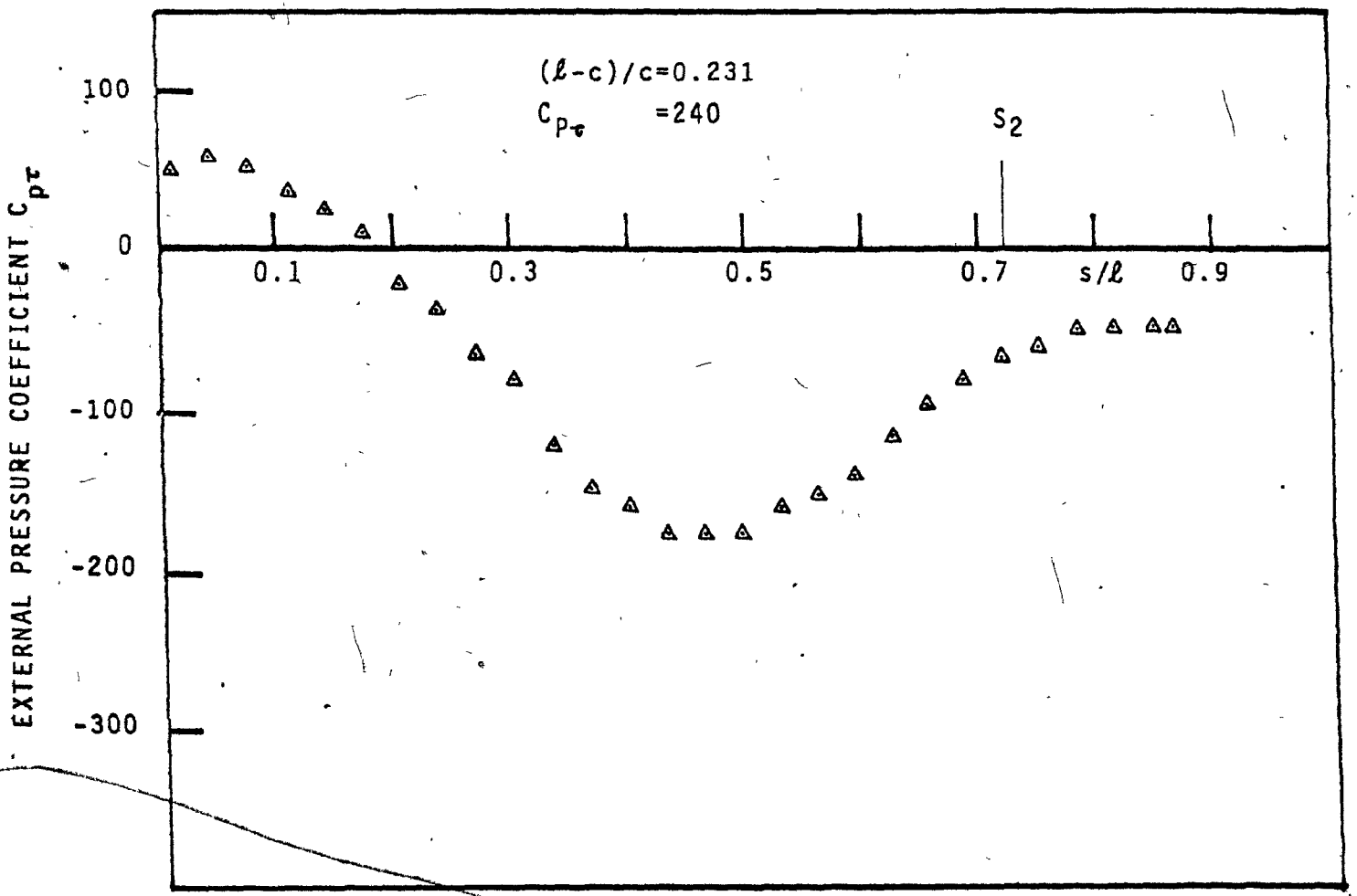

Fig. 36: External pressure distribution. Roughness 2 (1/n=0.24)

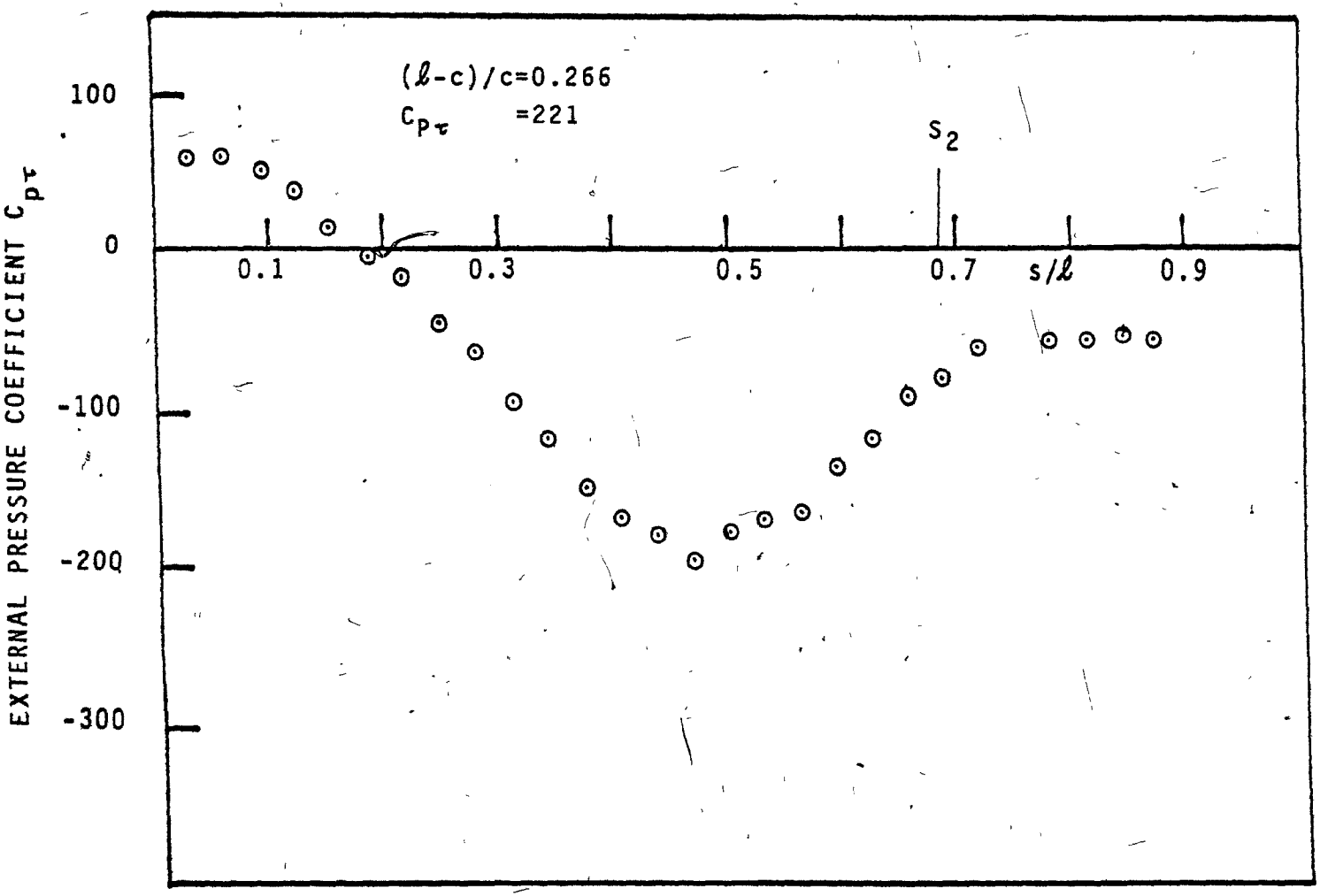

Fig. 37: External pressure distribution. Roughness 2 (1/n=0.24)

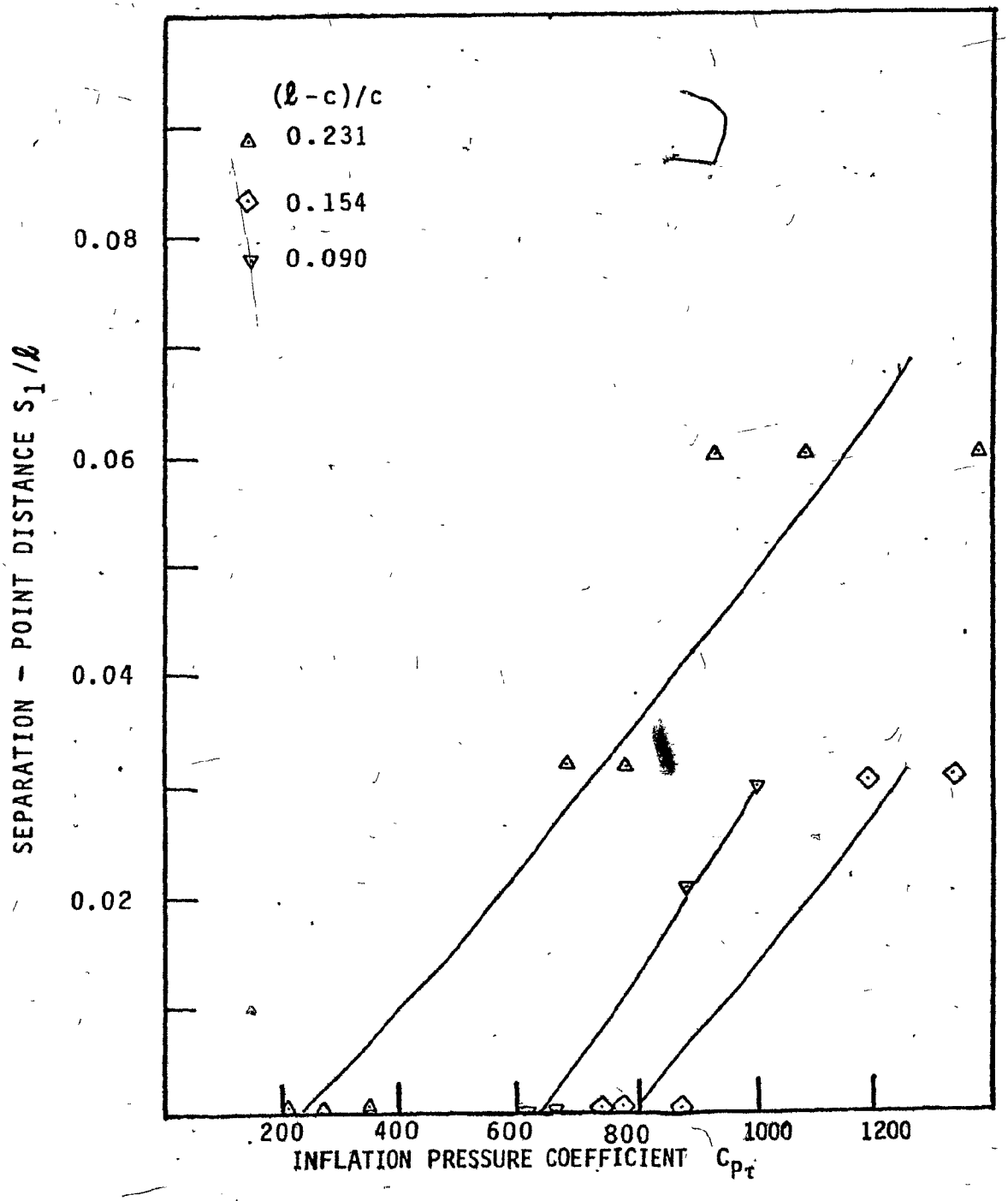

Fig. 38: Separation point S_1 (leading edge).
Roughness 1 (1/n=0.13)

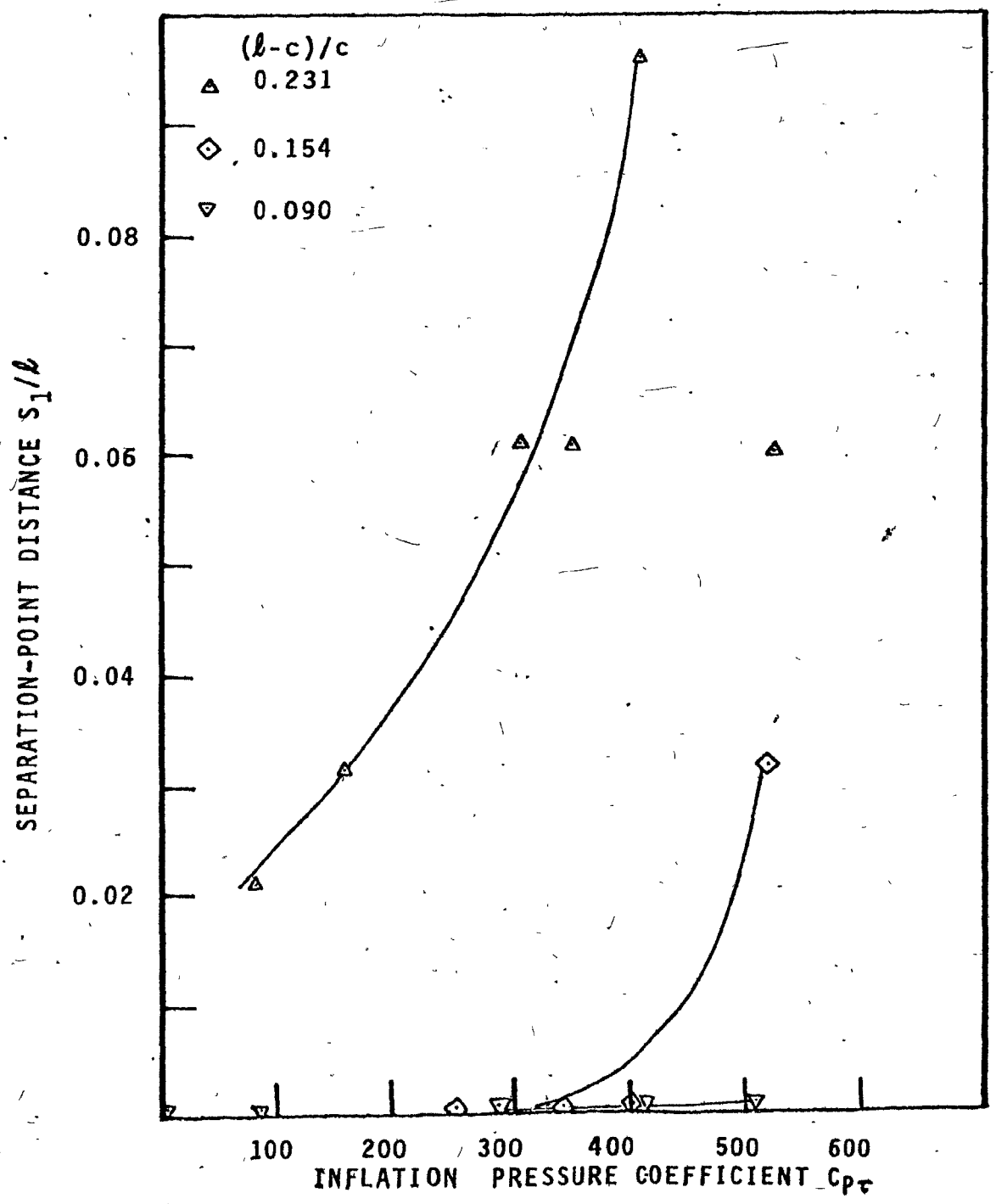

Fig. 39: Separation point S_1 (leading edge). Roughness 2 (1/n=0.24)

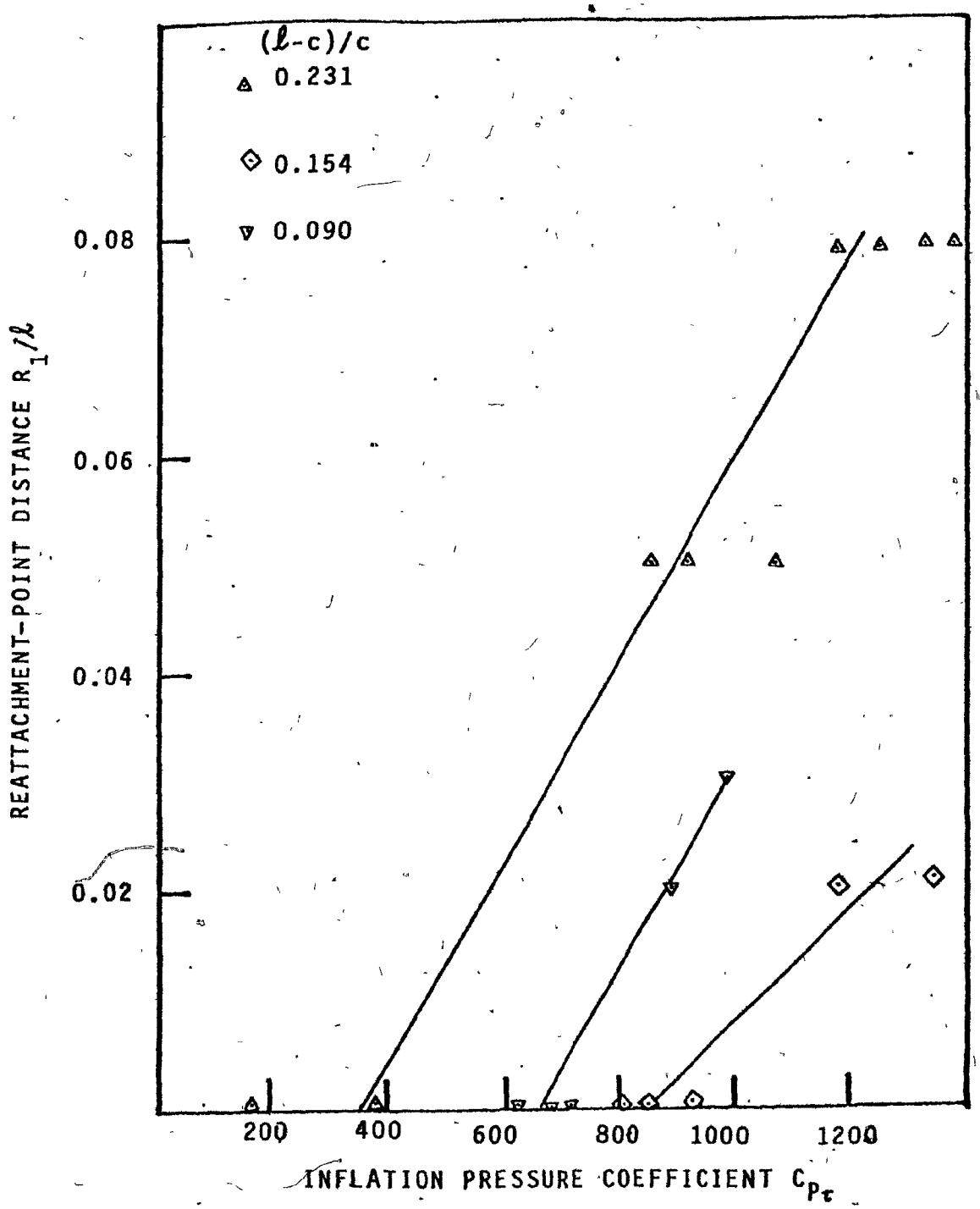

Fig. 40: Reattachment point R_1 (leading edge). Roughness 1 (1/n=0.13).

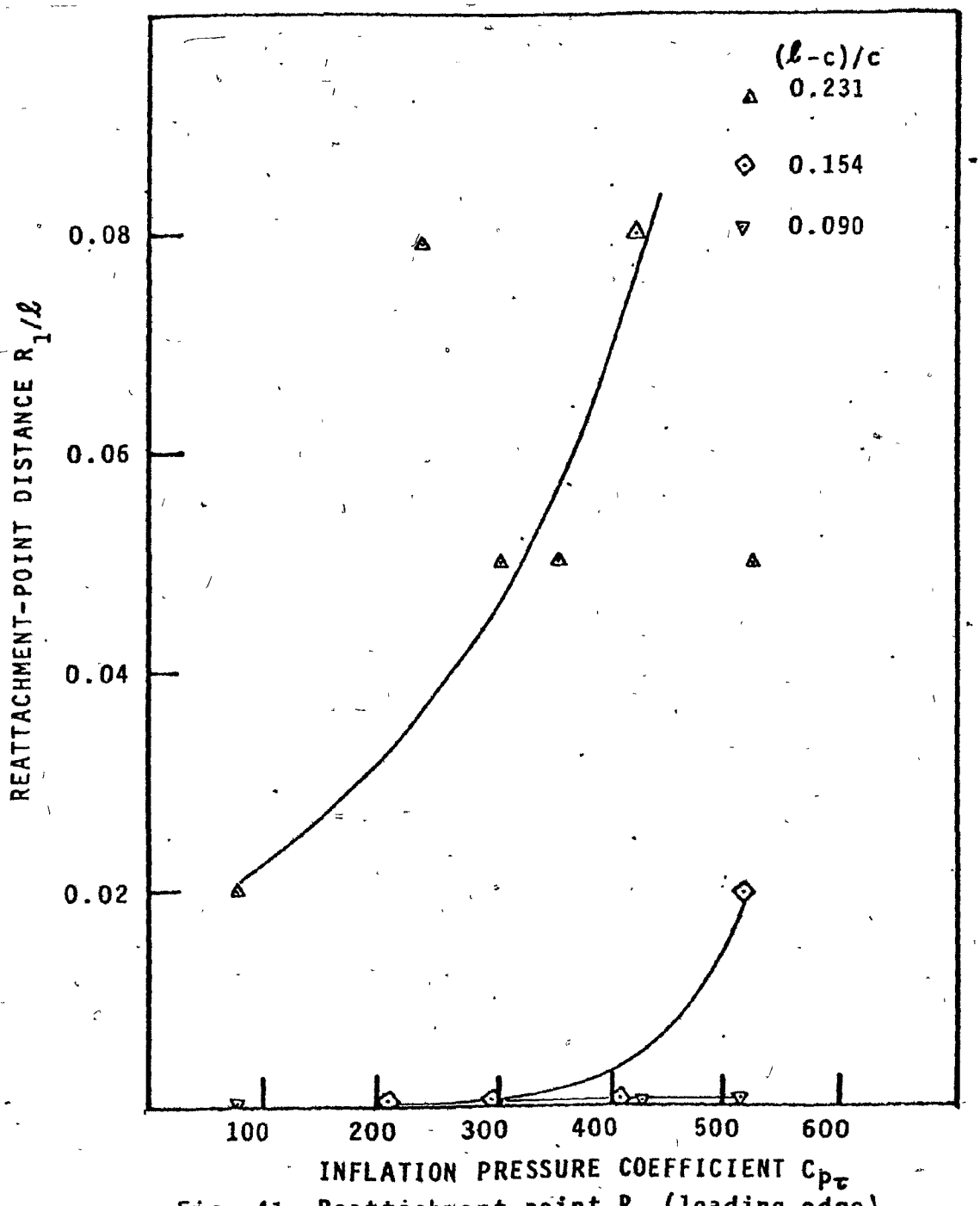

Fig. 41: Reattachment point R_1 (leading edge). Roughness 2 (1/n=0.24)

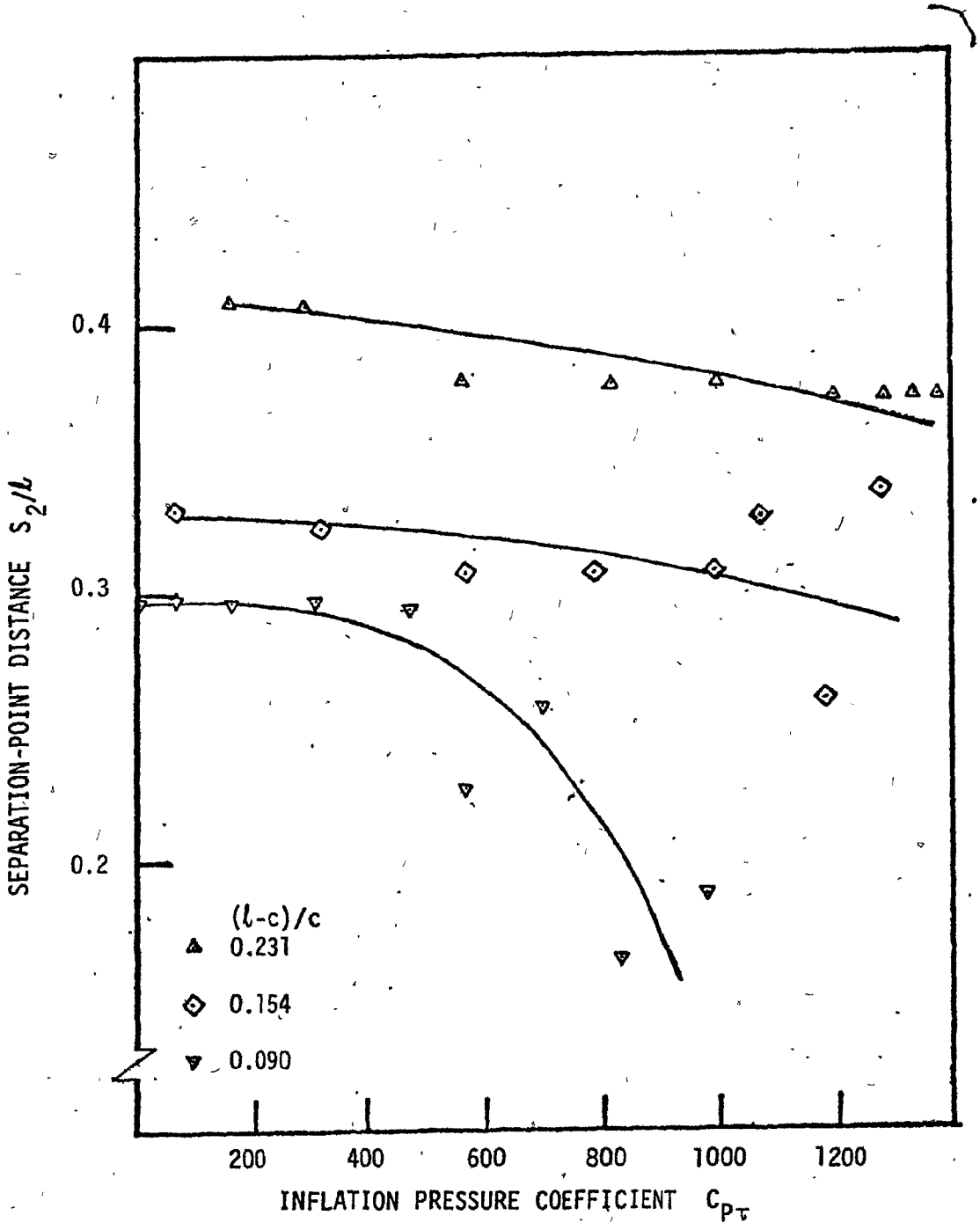

Fig. 42: Separation point S_2. Roughness 1 (1/n=0.13)

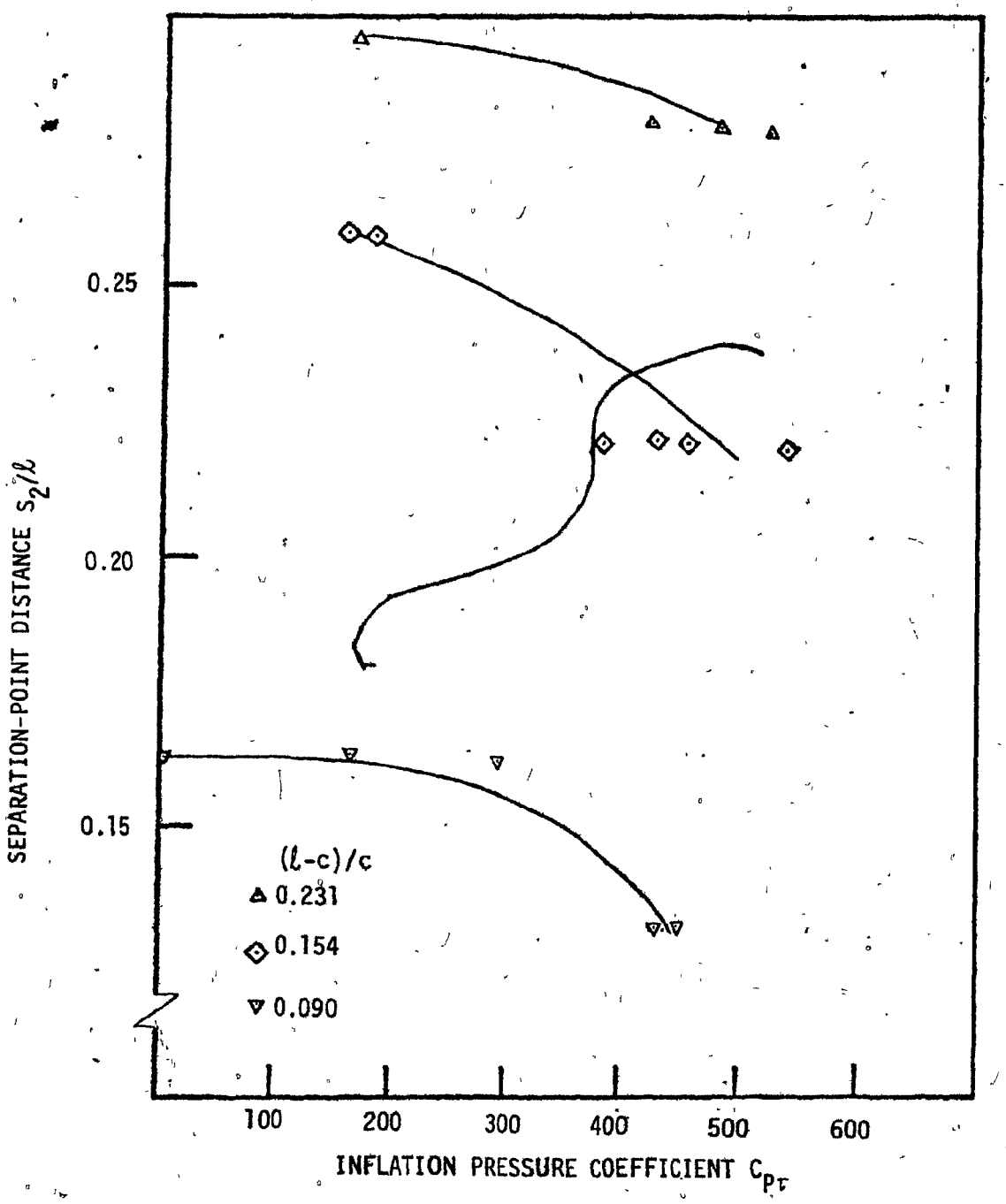

Fig. 43: Separation point S_2. Roughness 2 ($1/n = 0.24$)

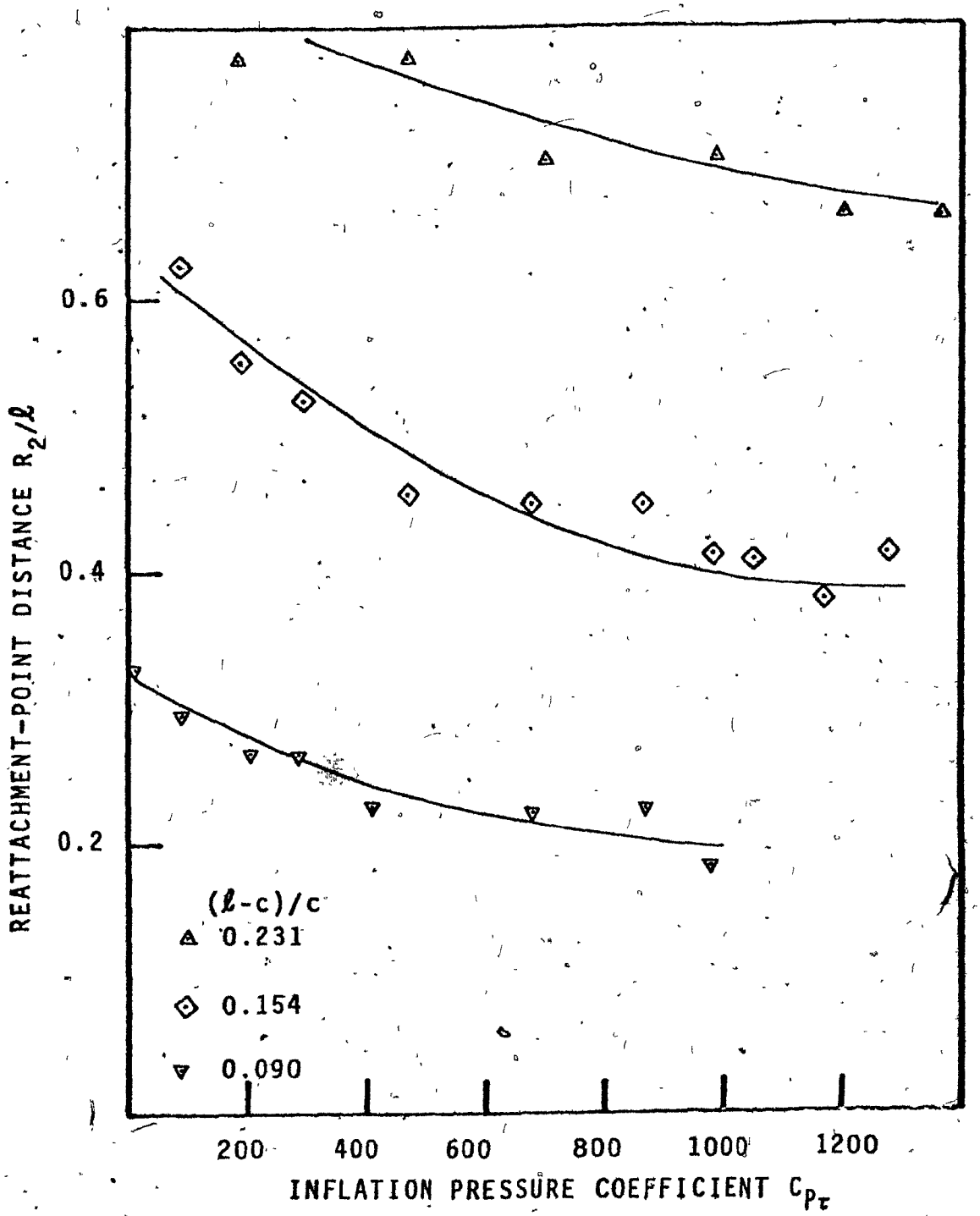

Fig. 44: Reattachment point R_2. Roughness 1 (1/n=0.13)

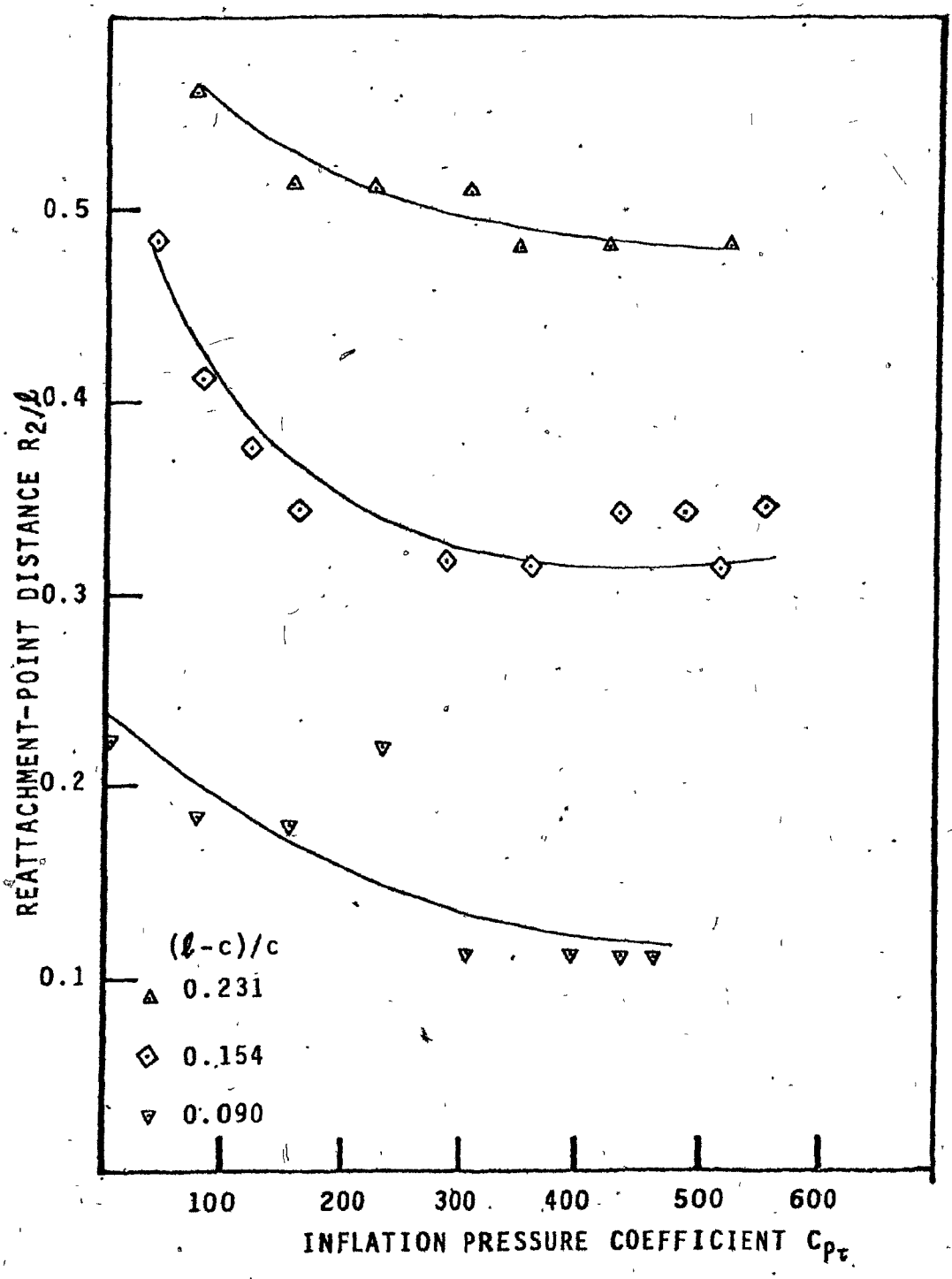

Fig. 45: Reattachment point R_2. Roughness 2 (1/n=0.24)

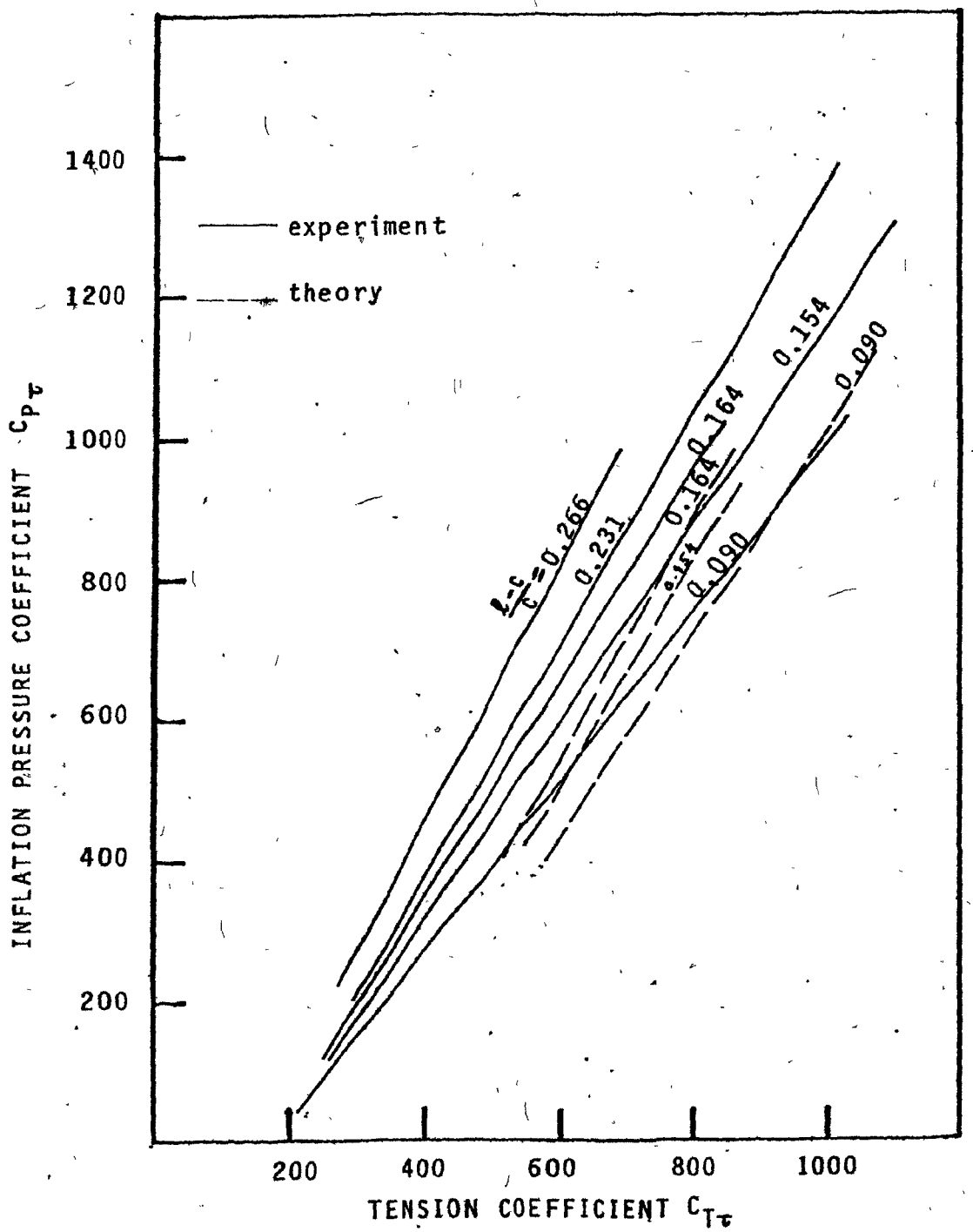

Fig. 46: Comparison between theory and experiment; Tension. Roughness 1 (1/n=0.13)

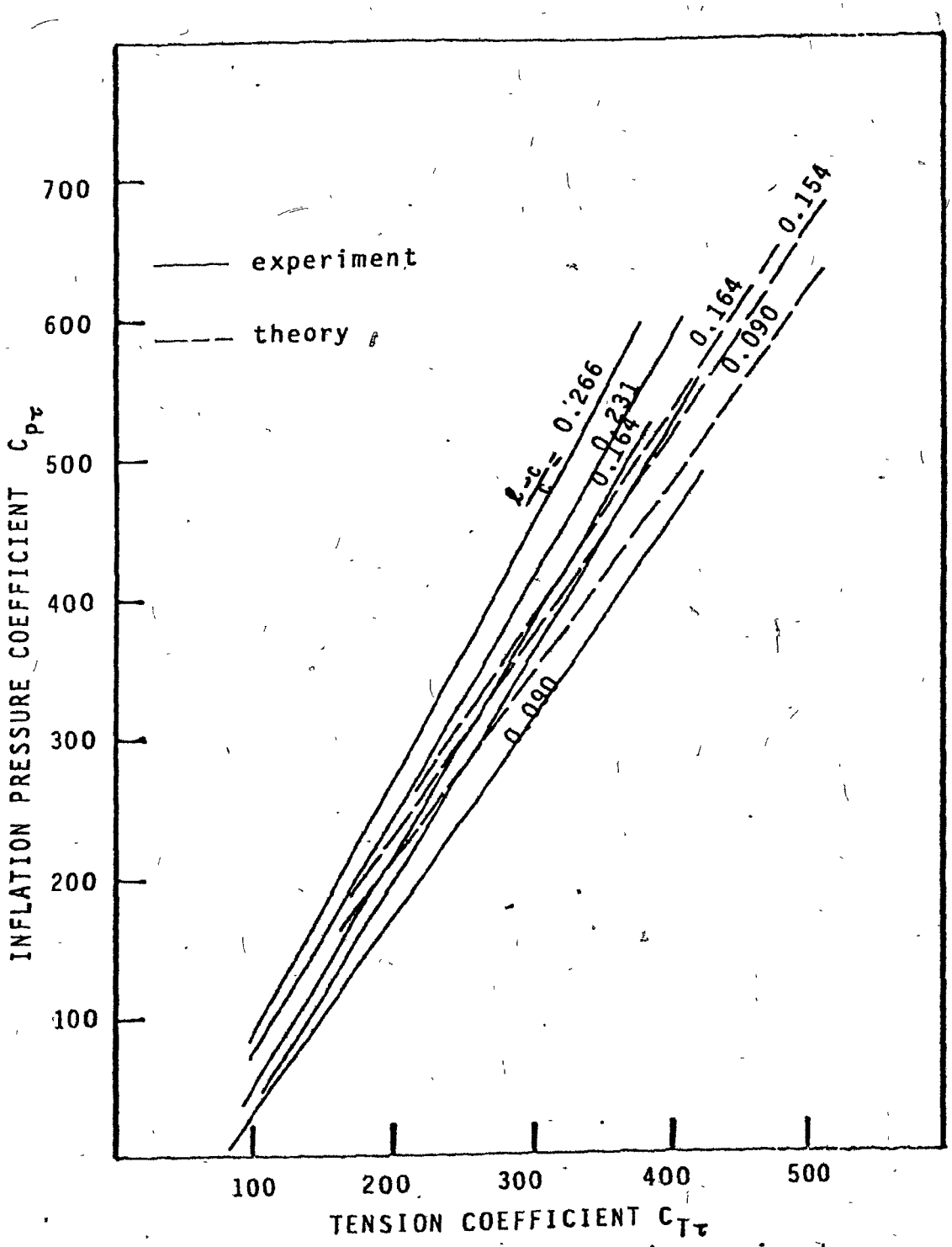

Fig. 47: Comparison between theory and experiment; Tension. Roughness 2 (1/n=0.24).

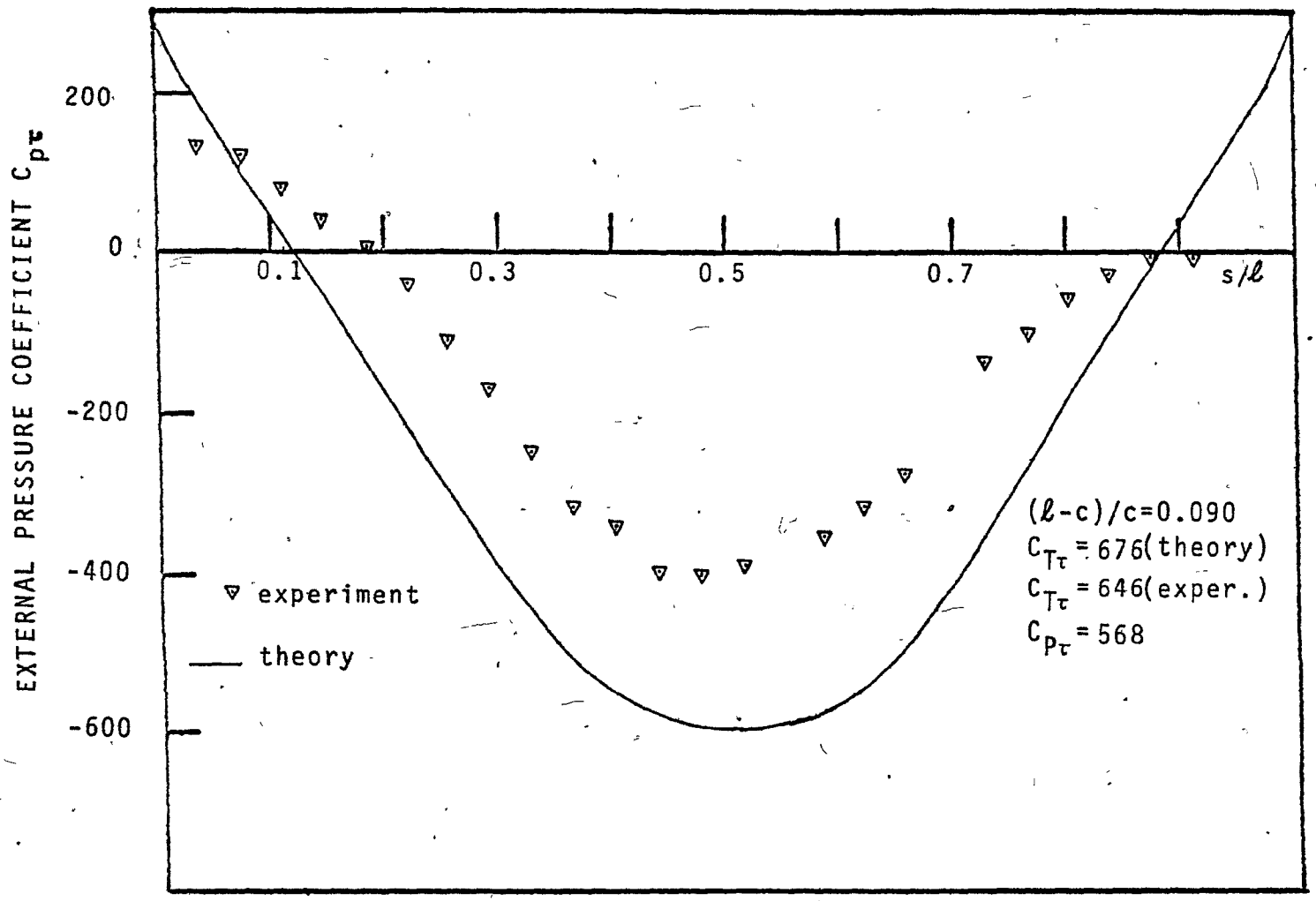

Fig. 48: Comparison between experiment and theory. Pressure distribution. Roughness 1.(1/n=0.13)

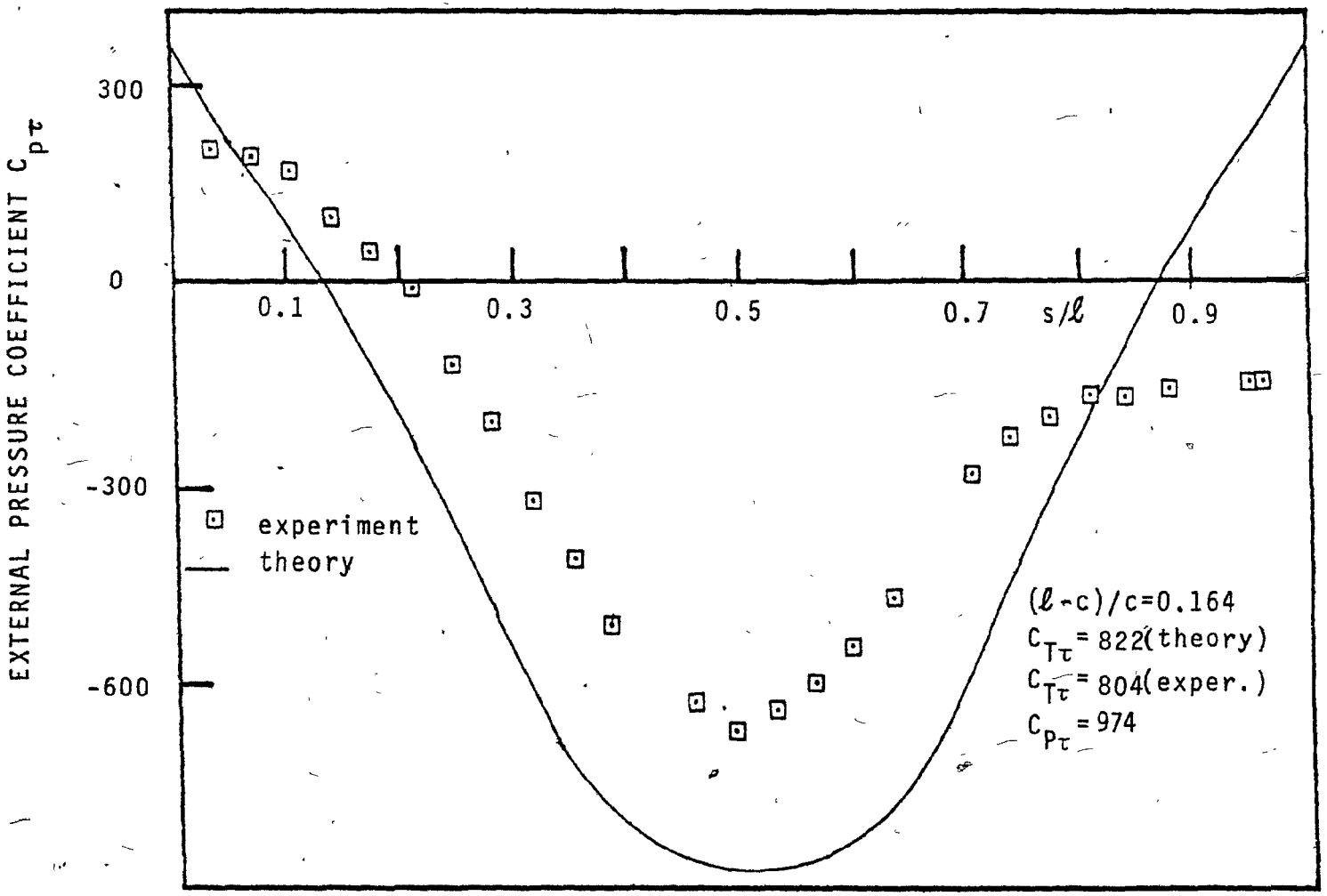

Fig. 49: Comparison between experiment and theory. Pressure distribution. Roughness 1 (1/n=0.13)

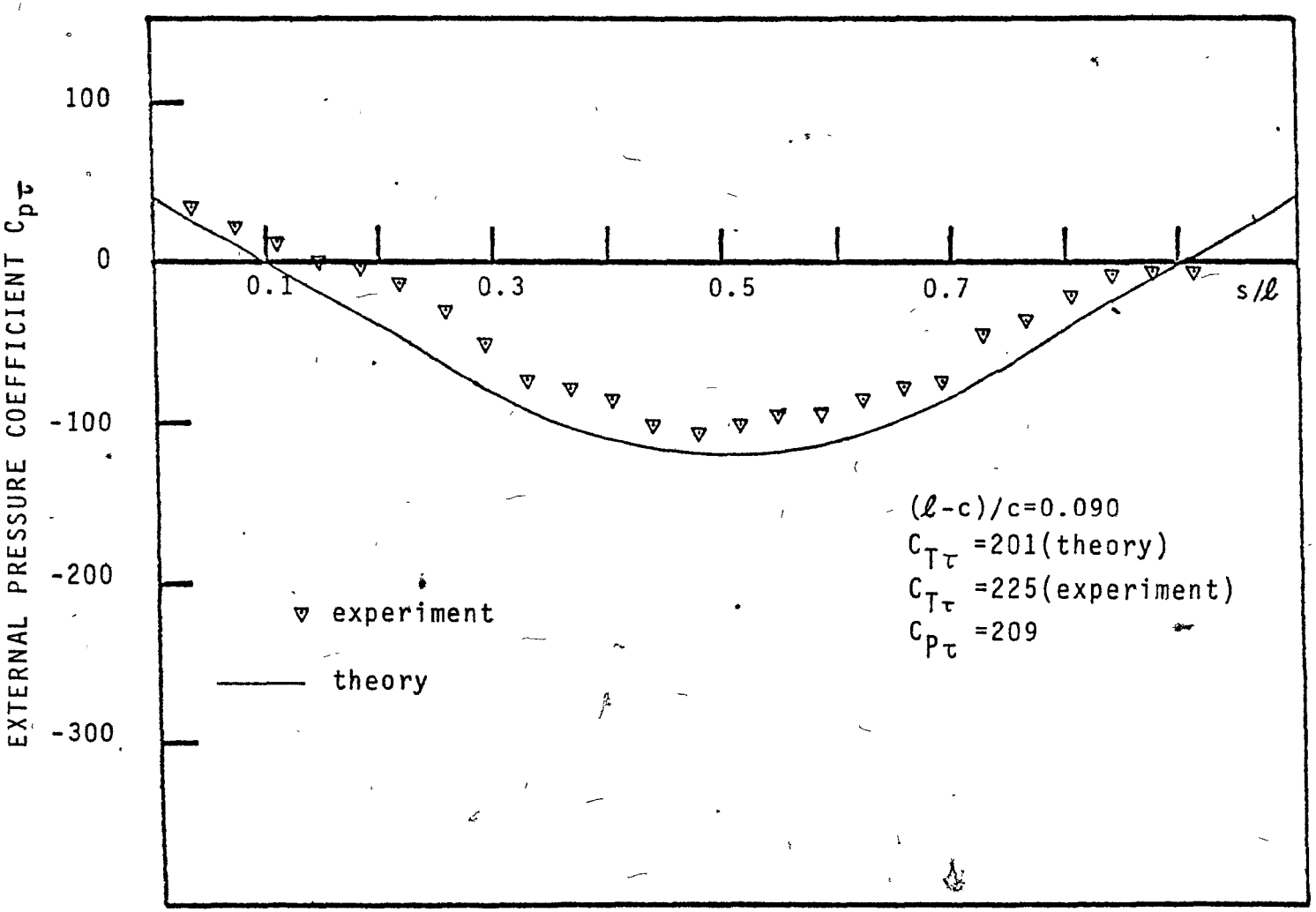

Fig. 50: Comparison between experiment and theory. Pressure distribution. Roughness 2 (1/n=0.24)

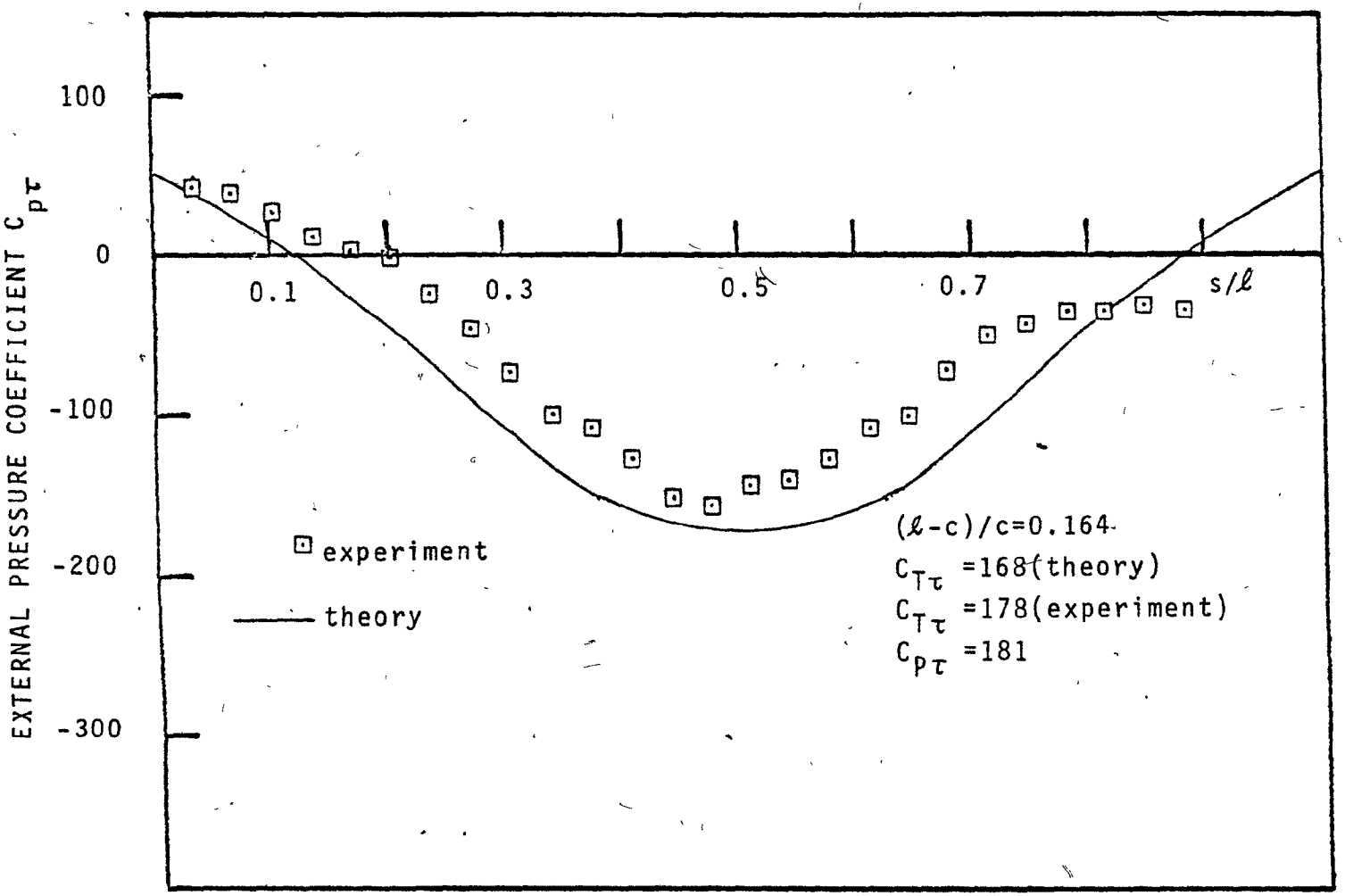

Fig. 51: Comparison between experiment and theory. Pressure distribution. Roughness 2 (1/n=0.24)

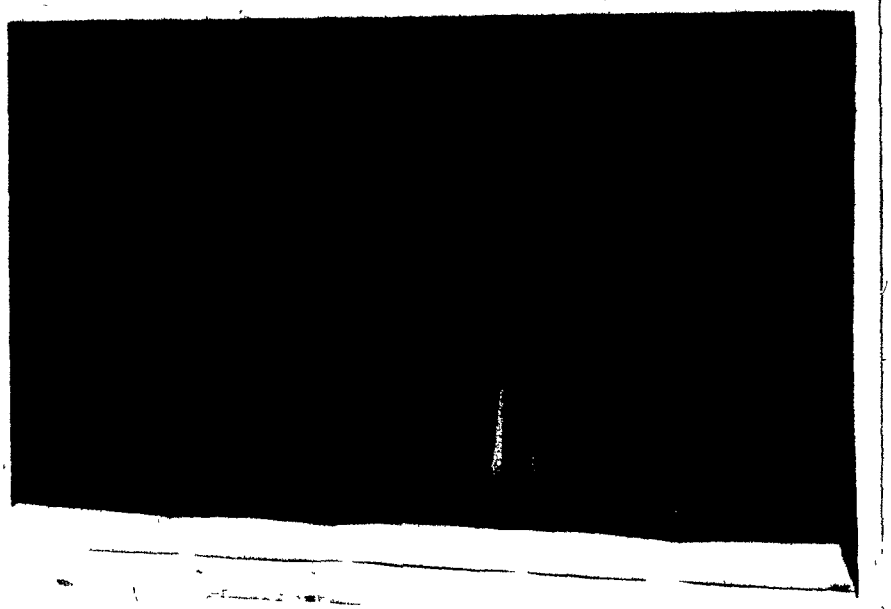

Plate 1: Spires and roughness 2

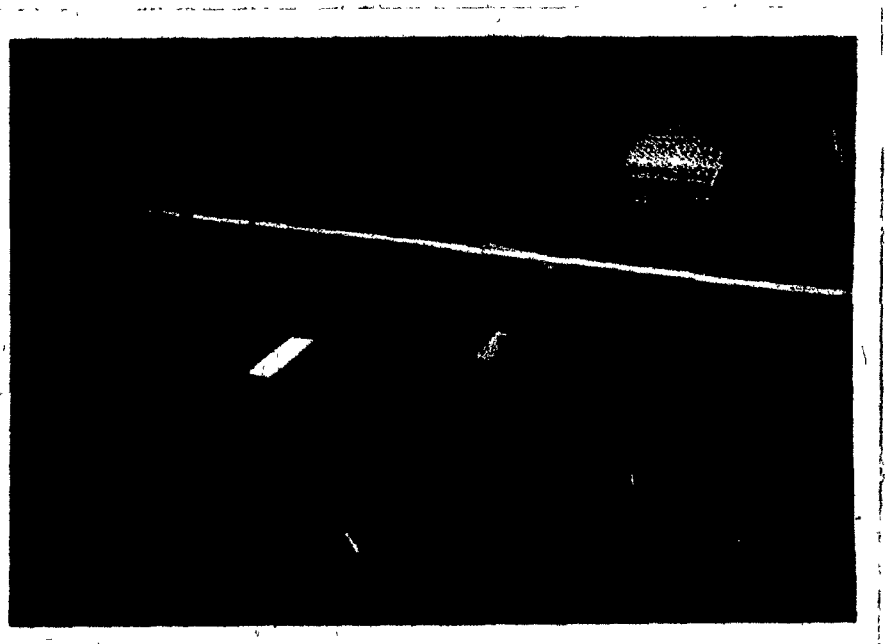

Plate 2: The model in the wind tunnel with the rigid dummies and roughness 1

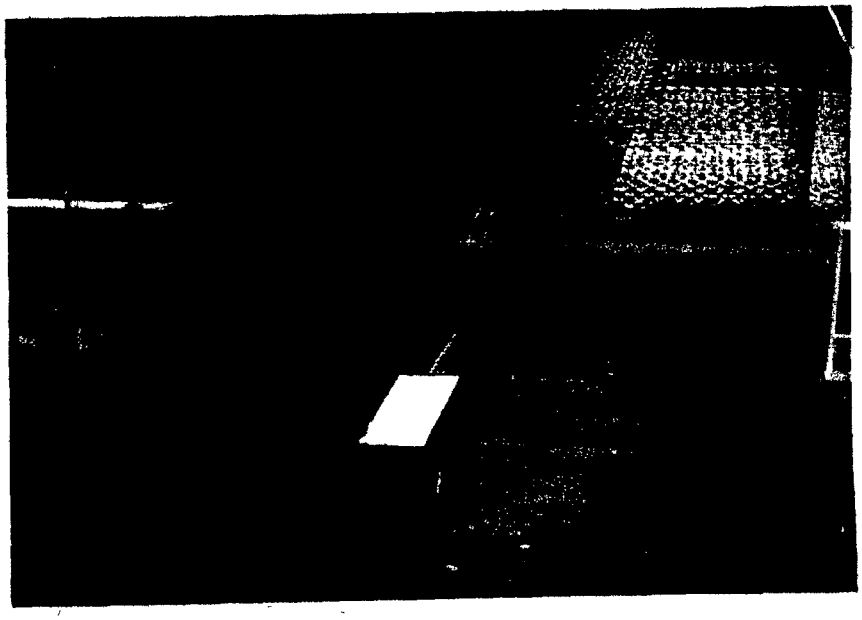

Plate 3: Model: span view

Plate 4: Model: side view

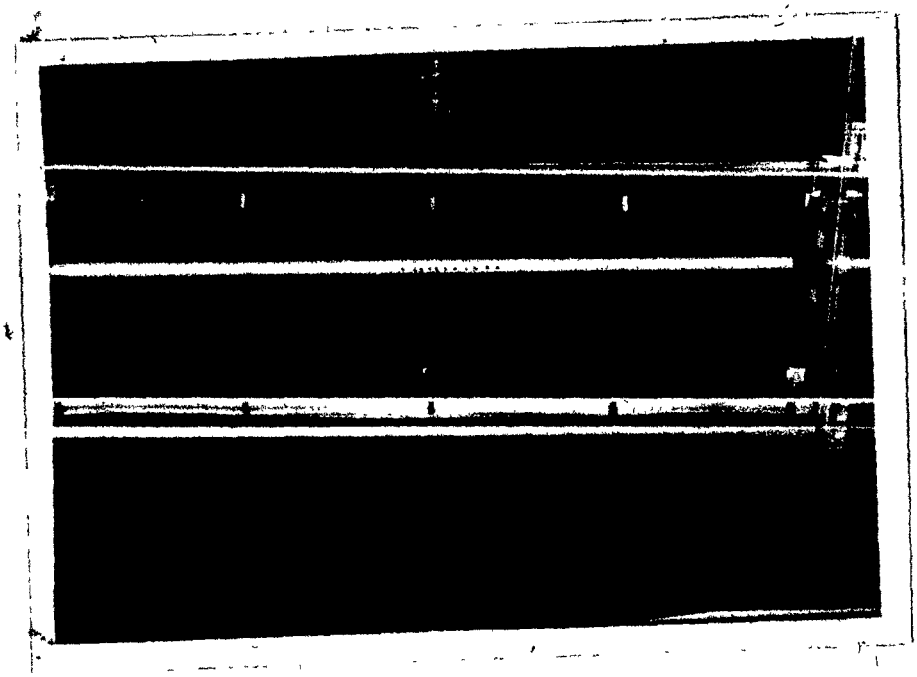

Plate 5: Model: interior.
Air-supply pipe, three pressure tubes, clamps and seal.